A STUDY OF THE MECHANISM OF BOILING HEAT TRANSFER

Thesis by

Max Edmund Ellion

In Partial Fulfillment of the Requirements

for the Degree of

Doctor of Philosophy

California Institute of Technology

Pasadena, California

1953

ACKNOWLEDMENTS

The author wishes to express his appreciation to Dr. R. H. Sabersky for helpful criticism, discussion, and encouragement during the development of this research. The author is indebted to Mr. K. S. MacDavid and Mr. M. B. Noel of the Jet Propulsion Laboratory for aid in setting up the apparatus for the experimental phase of the program and to the staff at the Jet Propulsion Laboratory. In particular the author wishes to thank Mr. F. Gunther also of the Jet Propulsion Laboratory for many valuable discussions he had on the the mechanism of bubble growth and collapse. Mr. N. Van De Verg was in charge of the section of the Laboratory in which this research was carried out and has supported the research with continued interest. The author also wishes to express his appreciation to Miss Evelyn Jordan for typing the manuscript.

ABSTRACT

PART I. AN EXPERIMENTAL STUDY OF PARTIAL AND COMPLETE FILM BOILING WITH FORCED CONVECTION

An apparatus was developed to investigate the regions of peak heat flux, partial film boiling, and complete film boiling. High-speed motion pictures and experimental data were taken to study the effects of liquid velocity, pressure, and temperature on the boiling heat transfer in subcooled-distilled-degassed water. The motion pictures showed the types of vapor formation which occur in each of the three regions and indicated that the heat transfer at the transition from nucleate boiling to partial film boiling was about 90 per cent of the peak heat flux.

PART II. A DETAILED PHOTOGRAPHIC STUDY OF NUCLEATE POOL BOILING

The dynamics of nucleate bubbles in aerated and degassed liquids was studied by means of high-speed motion picture cameras. A mechanism is proposed for the growth and collapse of nucleate bubbles which successfully predicts the effects of liquid properties and conditions on bubble dynamics.

The liquids chosen for this study were distilled water and carbon tetrachloride because of their widely different physical properties. The influence of surface tension on the bubble dynamics was investigated separately by adding a surface-tension depressor to the water. For a range of liquid temperature experimental data are presented including the size and lifetime of the bubbles as well as the peak heat flux values.

TABLE OF CONTENTS

PART I

PART II

PART II (Continued)

PART I

AN EXPERIMENTAL STUDY OF PARTIAL AND COMPLETE FILM BOILING WITH FORCED CONVECTION

SUMMARY

The conventional laboratory equipment for studying boiling heat transfer was modified so that it could be operated in a stable manner with subcooled liquids in the regions of nucleate, partial film, and complete film boiling. The apparatus employed a secondary stabilizing fluid which flowed through the inside of an electrically-heated stainless-steel tube while the test fluid was flowing through an annulus formed by the tube and a Pyrex jacket. The stabilizing fluid absorbed the excess heat which could not be transferred to the test fluid. This arrangement allowed the apparatus to operate safely in all three boiling regions since the total heat transferred to the stabilizing fluid and the test fluid was a monotonically increasing function of wall temperature up to the melting point of the wall.

The equipment retained the simplicity of electrical heating and was used to study boiling in distilled water which was flowing at various velocities, pressures, and temperatures in an annulus. The results of this investigation and a description of the apparatus are presented together with an approximate method for calculating the heat transfer in the complete film boiling region.

High-speed motion pictures that were taken of the degassed water boiling on the electrically-heated tube showed the types of vapor formation in the three boiling regions. The mechanism of transition from nucleate to partial film and finally to complete film boiling as the wall temperature was increased is discussed.

I. INTRODUCTION

The heat transfer from a hot metal wall to a boiling liquid has been the subject of extensive studies which started with the work of Mosciki and Broder (Cf. Ref. 1). Little progress was made until the need for high rates of heat transfer in nuclear reactors and rocket motors added to the desirability of obtaining a fuller understanding of the boiling heat transfer mechanics. These recent incentives have resulted in contributions to the field of nucleate boiling by many investigators including: McAdams (Cf. Ref. 2), Tramontini (Cf. Ref. 3), and Gunther (Cf. Ref. 4).

It was not possible for these investigators to make a detailed study of the boiling mechanism in all regions because of the inability of existing equipment to maintain stable operation near the peak heat flux and partial film boiling regions. The following discussion of the three boiling regions brings out this inherent difficulty.

Figure 1 shows a typical heat transfer curve in which, for simplicity of the discussion, heat flux is plotted against wall temperature instead of the customary parameter of temperature difference between the hot wall and the fluid. The shape of the curve is unaffected by this substitution for constant fluid temperature, pressure, and velocity.

The region A to B in Figure 1 represents the nonboiling line for either forced or free convection. When the wall temperature increases above the liquid saturation temperature, such as at point B, the liquid against the hot wall boils at small nuclei. If the bulk

of the liquid is below saturation temperature, the bubbles grow to a maximum radius and then collapse. Since the boiling occurs from small active nuclei at the surface of the hot wall in the region from B to C, this type of boiling is called surface or nucleate boiling. High-speed motion pictures of nucleate boiling were taken with the fields of view shown in Figure 2. Several frames of nucleate boiling are shown in Figure 3.

As the wall temperature is increased to point C in Figure 1, the population of nucleate bubbles increases until they become so crowded that several of the individual bubbles coalesce to form a local blanket of vapor. These vapor blankets cover localized areas of the hot wall for periods of about ten to twenty times the lifetime of a nucleate boiling bubble before condensing in the main stream.

As the wall temperature is increased still further, such as from C to D of Figure 1, the wall area covered by the local film blankets increases and causes the over-all heat flux to decrease. The region between C and D is called Partial film boiling, because of the intermittent coverage of the wall by the vapor film. Figure 4 shows one cycle of partial film boiling.

At point D of Figure 1 the local vapor blankets coalesce to form a continuous vapor film. This is the complete film boiling region. In this region the heat is transferred from the hot wall to the liquid principally by conduction across the laminar vapor film. A further increase of wall temperature causes a small increase in vapor film thickness. The thickness, however, increases at a lower rate than

the temperature difference ΔT_{sat}, so that the heat flux increases. At higher wall temperatures the film gets so thick that it is no longer laminar. The roughness of the film, coupled with radiation, makes the heat transfer increase more rapidly with an increase in wall temperature. This increase results in the concave upward curve E to F in Figure 1. The rough film is shown in view a of Figure 5. (This rough film would occur either at high wall temperature or on a very long heating section.) The vapor film is also visible in view b of Figure 5 which shows the film as it is being detached from the heating tube by the sharp corner of the copper bus bar.

In addition to the three regions of boiling heat transfer, the boiling process may be divided into two general categories: one, where the bulk temperature of the liquid is below its saturation temperature (heat transfer to subcooled liquids), and the other, where the liquid bulk temperature is at its saturation temperature (bulk boiling). The fluids used in the regenerative cooling of a rocket motor are an example of boiling in a subcooled liquid, whereas the generation of steam in a boiler is an example of bulk boiling.

It is now possible to discuss the difficulty of measuring the heat flux in the three boiling regions. The conventional laboratory apparatus employed for the study of heat transfer has a high resistance wall (usually a thin metal strip or tube) which is heated electrically. Reference to the solid curve in Figure 6 which represents heat transfer to a subcooled liquid, shows that up to point A any increase in electrical power supplied to the metal wall may be absorbed by the liquid. Thus

the convection and nucleate boiling regions may be studied without difficulty. However, if the power is increased above point A, the wall temperature must jump to point B before the additional power may be transferred to the liquid. At point B, the heat transfer surface temperature required for most liquids is above the melting point of the metallic wall, and failure occurs.

It has been possible to study the nucleate-boiling and complete-film-boiling regions for a bulk boiling liquid as is represented by the dashed line of Figure 6. The peak heat flux shown at point A, is considerably lower than for the same liquid when subcooled. It is seen to be possible also to transfer the peak quantity of heat in the complete-film-boiling region without exceeding the melting point of the wall.

Figure 7 shows Nukiyama's curve (Cf. Ref. 5) of the heat transferred to water from a 0.0055-inch platinum wire in pool bulk boiling. The peak heat transfer shown at point A, is sufficiently low to allow the wall temperature to remain below the melting point in the film-boiling region and still transfer more heat than at the peak point. It is thus possible to study the nucleate-boiling and complete-film-boiling regions for a stagnant pool if the water is at the saturation temperature. Nukiyama's apparatus could not be used to investigate the partial-film-boiling region.

For the case where the water is not at the saturation temperature, there are four possible solutions that would still allow the study to be extended into the complete-film-boiling region. One method would

be to control the wall temperature rather than the power supplied to the wall. In this case, instead of using electrical heating, control could be accomplished by using condensing vapors or fast-flowing hot liquids that would supply the heat to the wall. This arrangement is not desirable since it has many serious difficulties in control, installation, and measurement of the amount of heat supplied to the wall. A second method for eliminating burnout but which still retains the desirable electrical heating would be to make the wall of a high melting point material. However, for any electrical conductor, this method would prevent burnout only over a narrow range of liquid properties. A third method of preventing burnout would be to decrease the electrical power supplied to the wall immediately after it is raised above point A of Figure 6. If the power were carefully controlled, it would be possible to jump from point A to some other point in the film boiling region that required a wall temperature lower than point B. This method requires elaborate electronic equipment that also would not be satisfactory except for limited ranges of liquid properties. Of these three methods, only the first one could operate in the partial-film-boiling region.

A fourth method will be considered which makes it possible to retain the convenience of electrical heating and still maintain stable operation in all three boiling regions for a wide range of liquid variables. As has been seen, the difficulty with the conventional equipment which uses electrical heating is that a small increase in power above the peak point causes the wall temperature to rise above

the melting point. If the heat transfer could be made a monotonically increasing function of the wall temperature, stable operation would be obtained at any heat flux that requires a surface temperature below the melting point of the wall. This condition (Cf. Curve C of Fig. 8) could be realized if some of the electrical power supplied to the wall were dissipated in a manner described by Curve A and the remainder of the heat were transferred to the test fluid illustrated by Curve B. If the following relation is valid for the partial-film-boiling region of the test fluid,

$$\left[\frac{\Delta \frac{q}{a}}{\Delta T_w}\right]_A > \left[\frac{\Delta \frac{q}{a}}{\Delta T_w}\right]_B \qquad (1)$$

the addition of the two heat fluxes would result in a curve such as C; thus the wall temperature would rise only very little for a small increase of electrical power over the peak point.

The simplest method for dissipating the excess heat as required by Curve A of Figure 8 and in addition for supplying the remaining heat to a test fluid is shown in Figure 9. The type of heat transfer shown in Curve A of Figure 8 is obtained by flowing a high-saturation-temperature liquid up through a tube. The high-saturation-temperature allows the tube wall temperature to reach a high value before the liquid boils. Thus Curve A would be a forced-convection line for this liquid. Because of its function, this liquid is denoted as the stabilizing fluid. The fluid under study (test fluid) flows through the annulus formed by the tube and outer jacket. The electrical power supplied to the tube is dissipated outward to the test fluid and inward

to the stabilizing fluid. By controlling the pressure of the stabilizing fluid, it is possible to study the partial-film and complete-film boiling regions for the test fluid over a wide range of variables.

It was thus possible with the use of this apparatus to study the three boiling regions in detail up to the melting point or yield point of the metal wall without danger of tube failure. This equipment was constructed and studies with distilled water have been completed at several different conditions of bulk temperature, pressure, and velocity. These studies were made in order to broaden the basic understanding of the boiling phenomena as well as to obtain design data.

II. APPARATUS

A. Hydraulic Equipment

A schematic diagram of the recirculating system is shown in Figure 10. An Ingersoll Rand, 150-foot head, 15-gal/min pump, powered by a Louis Allis Co. 3-phase, 60-cyc/sec, 5-horsepower motor, was used to circulate the water. After leaving the accumulator which damped the pump pressure oscillations, the water passed through a 6-foot-long, 1-inch-diameter pipe that was electrically heated. This preheater was electrically insulated from the main pipe system with asbestos gaskets. The power was supplied to this heater by a 100-kva, 440-v stepdown transformer whose secondary voltage could be varied from 20 to 40 v in fifty-six steps by means of knife switches tapped from the primary winding (Cf. Fig. 11).

From the preheater the water flowed into the test section and then to a heat exchanger where it was cooled to a temperature suitable for re-entry into the pump. The cooling tap water flowed through an annulus formed by the 18-foot-long, 3/4-inch-diameter test fluid pipe and a 1-1/2-inch-diameter jacket.

The flow rate of the distilled water test fluid was determined by using a double orifice type of flowmeter and a 200-inch Barton differential pressure recorder.

A degassing tank was installed to lower the quantity of gas in the water since it was known from Reference 2 that large amounts of air would influence the boiling. The dashed arrows in Figure 10 show the path for recirculating the water during degassing. The aspirator decreased the pressure to 3 inches Hg while the storage tank heater

was maintaining the water at saturation temperature. After 1/2 hour of recirculating, the gas content of the water was decreased to a value below 0.3 cc/liter as determined by the chemistry section at the Jet Propulsion Laboratory using the Winkler technique.

B. Test Section

These studies were made with distilled degassed water flowing upward in a vertical annulus formed by a 1/4-inch-diameter, stainless-steel heating tube and a 2-1/2-inch-diameter Pyrex jacket (Cf. Fig. 12). Several tests were also made using a 0.61-inch-diameter Pyrex jacket (Cf. Fig. 13).

A 1-foot-length of type 347 stainless-steel tubing with a 0.006-inch-thick wall separated the test fluid from the stabilizing fluid. Two cylindrical copper bus bars were slipped over the tubing and silver soldered 3 inches apart. This spacing provided the 3-inch heated length of the test section. The test section heating tube and assembly details are shown in Figure 14. The stabilizing fluid was sealed at the entrance and exit to the tube with rubber O-rings. This arrangement was adequate to prevent the high pressure stabilizing fluid from leaking and permitted the tube to slide in the O-rings to provide for thermal expansion.

The low value of the ratio of tube heated length to diameter was necessary because of the electrical power limitations and also the desire to prevent large changes in liquid bulk temperature between the inlet and outlet of the test section. Calibration tests indicated no appreciable change in the heat transfer coefficient along the heating tube (Cf. Section IVA.).

C. Electrical Power Supply

It was found that a 60-cyc/sec ac power supply would cause a 120-cyc/sec growth and collapse of the bubbles. Consequently the power supply chosen for this study was obtained from two dc welding generators (manufactured by the Hobart Co.) which generated dc power with the amplitude of the voltage ripple less than one per cent from no load to rated capacity. Regulation of the field current with a rheostat provided smooth control from no load to rated capacity of 24 kw for each generator.

D. Thermocouples

The temperature rise of both the test fluid and the stabilizing fluid was determined from two six-junction copper constantan difference thermocouples. These thermocouples were insulated and then inserted into 1/8-inch stainless steel tubes. The tubes were placed along the center line of the entrance and exit pipes with a 3-inch length immersed in an isothermal region. A mixing chamber was used downstream from the test section so that the thermocouples read a true mixed mean temperature (Cf. Fig. 15).

In addition to the two difference thermocouples, two copper constantan thermocouples were used to measure the inlet temperature of the stabilizing and test fluids. All thermocouples were calibrated at the ice point and boiling point of water. While immersed in well-stirred baths the difference thermocouples were checked over a range of temperatures against standard thermometers.

An ice bath was used as a cold-junction reference, and all thermocouples were read on a manually balanced Rubicon potentiometer.

E. Photographic Technique

Motion pictures of the three types of boiling were taken through the Pyrex jacket at 3000 frames/sec using a 16-mm Fastax camera. The bubbles were illuminated by a General Electric B-H6 mercury vapor lamp (Cf. Fig 16). A concave mirror placed behind the lamp focused the light falling on the tube into a strip 1/4 inch wide and 2 inches long. This arrangement provided sufficient light intensity to give proper exposure on Eastman Kodak Super XX safety film with the camera lens stop set below f/11.

III. TEST PROCEDURE

A. Wall-Temperature Measurement

The wall temperature had to be determined without disturbing either the test fluid or the stabilizing fluid. A calibration was obtained by flowing the stabilizing fluid through the vertical tube without the surrounding test fluid. Three copper constantan thermocouples, electrically insulated from the dc voltage gradient in the tube by using a 0.0005-inch-thick mica sheet, were wrapped around the outside of the tube and spaced one inch apart. Natural Sil-O-Cel insulation was placed over the thermocouples, and the entire assembly was clamped to the tube (Cf. Fig. 17). This arrangement measured wall temperatures within 4 per cent. To check the conduction errors of the readings, hot water was passed through the tube with the electrical power off. The wall thermocouples agreed within 2 per cent with thermocouples immersed in the water which was as hot as 400°F. When a check of the electrical insulating property of the construction was made by reversing the power leads, no shift was noted in the thermocouple readings.

A series of tests was performed to determine the forced convection line for the stabilizing fluid. The data obtained agreed within 10 per cent with the predicted values using the Sieder-Tate equation.

After the forced convection curve was obtained for the stabilizing fluid, the three wall thermocouples were removed. It was then possible to determine the wall temperature without these thermocouples by entering the forced-convection curve with the known heat flux as

determined by the temperature rise indicated by the stabilizing-fluid difference thermocouples. To obtain the temperature of the wall exposed to the test fluid, it was necessary to correct for the temperature change through the wall. The position of zero temperature gradient was obtained by assuming constant electrical resistance through the wall. Then by Figure 18

$$x_1 = \frac{\left(\frac{g}{a}\right)_S}{\left(\frac{g}{a}\right)_A + \left(\frac{g}{a}\right)_S} t = \frac{\left(\frac{g}{a}\right)_S}{EIJ} t \qquad (2)$$

Assuming constant electrical and thermal resistance, the temperature drop from x_1 to the test fluid interface is given by McAdams (Cf. Ref. 2):

$$T_o - T_{W_S} = \left(\frac{g}{a}\right)_S \frac{x_1}{k}\left[\frac{1}{2} + \frac{x_1}{12(r_i + x_1)}\right] \qquad (3)$$

$$T_o - T_{W_A} = \left(\frac{g}{a}\right)_A \frac{x_2}{k}\left[\frac{1}{2} + \frac{x_2}{12(r_i + x_1)}\right] \qquad (4)$$

Then

$$T_{W_A} - T_{W_S} \simeq \left(\frac{g}{a}\right)_A^2 \frac{t}{kEIJ}\left\{\frac{1}{2}\left[\left(\frac{g_S}{g_A}\right)^2 - 1\right] + \frac{\left(\frac{g}{a}\right)_A}{EI}\frac{t}{6D}\left[\left(\frac{g_S}{g_A}\right)^3 - 1\right]\right\} \qquad (5)$$

The temperature variation in the wall as calculated by relation (3) or (4) was always less than 45°F, thus the assumption of constant electrical and thermal resistance was reasonable.

B. Stabilizing Fluids

Distilled water at a pressure of 460 psia and flowing at 40 ft/sec was used as the stabilizing fluid for wall temperatures up to 500°F. This upper limit resulted when the water began to boil and thus maintained the wall temperature substantially constant regardless of any additional electrical power input. Since the wall temperature remained a fixed amount above the boiling point of the stabilizing fluid, higher wall temperatures could have been reached by increasing the pressure of the stabilizing water. However, the small change in saturation temperature with pressure made this solution impractical. As an alternative, another higher-boiling-point liquid or a high-pressure gas could be used instead of the water as the stabilizing fluid. Dry nitrogen gas proved to be a satisfactory stabilizing fluid.

Ten 1.5-cu ft tanks, initially filled with 2200-psia dry nitrogen gas, were connected to the system. A pressure regulator delivered 500-psia nitrogen to the heater tube. After passing through the test section, the nitrogen was discharged at sonic velocity to the atmosphere.

A potential difficulty with the use of nitrogen gas as the stabilizer fluid was the isenthalpic change in temperature with pressure. It was possible, however to employ the nitrogen gas since the stagnation temperature of the gas entering the test section varied less than 35°C during the test. Reference to Figure 19 indicates that, by regulating the nitrogen pressure at 500 psia, the discharge temperature would be expected to remain between + 2°C and - 32°C as the storage tank pressure decreased from 2200 psia to 1000 psia.

The forced convection curve for the nitrogen gas was determined in the same manner as for the water stabilizing fluid. For a constant power input to the tube, the measured wall temperature decreased less than 10 per cent as the storage tank pressure decreased from 2000 psia to 1000 psia. As a consequence, the heat transfer was assumed independent of storage tank pressure when the pressure in the tank was above 1000 psia.

The forced convection curve was slightly concave downward because of the higher exit temperature of the nitrogen from the test section at higher heat flux. The higher exit temperature resulted in a lower density ($\rho \sim \frac{1}{T}$). The exit velocity remained sonic but the velocity of sound increased with temperature ($c \sim \sqrt{T}$). The net effect was a lower mass flow rate ($G \sim \frac{1}{\sqrt{T}}$). The lower mass flow caused a decrease in the gas film coefficient and resulted in a concave downward forced convection curve.

A power balance was obtained by measuring the temperature rise through the test section of the test fluid and the water stabilizing fluid. The heat transfer calculated from these two values agreed with power measurements within five per cent. Because of the difficulty in measuring the temperature rise of the nitrogen, no attempt was made to obtain a power balance when the nitrogen gas was used. The heat transferred to the nitrogen was obtained by subtracting from the total power input the heat absorbed by the test water. The power balance for the previous tests with water as the test and stabilizing fluid indicated that this procedure should give heat flux values accurate to five per cent.

C. Power Measurements

The power delivered to the test section was measured with an ammeter and voltmeter, each accurate to one per cent of full scale reading. For convenience, the voltage measurement was taken across the outer ends of the copper bus bars instead of across the heated length of the tube. This arrangement resulted in less than a one-per cent error. The total estimated error in power measurement was less than 3 per cent. The heat flux was calculated from the measured power value and tube-area measurements. The heat flux was known within an uncertainty of 4 per cent. This method was checked against values obtained by measuring current flow and calculating power input from the product I^2R. Because of a 3-per cent variation in tube wall thickness between various tubes, the second method was discarded in favor of measuring both current and voltage.

IV. DISCUSSION OF RESULTS

A. The Mechanism of Transition Between the Three Boiling Regions

In an effort to understand the mechanism by which heat is transferred from a hot metal wall to a subcooled boiling liquid,* high speed motion pictures were taken of the three boiling regions. Emphasis was placed on the partial and complete film boiling mechanisms; the second part of this report on boiling heat transfer will deal with the complex nucleate boiling process.

A brief discussion of the boiling mechanism is given in the introduction of this paper, but the details of the mechanism by which the boiling process changes from nucleate to partial film and finally to complete film boiling are now discussed.

The first problem to be encountered in understanding the boiling mechanism is the process by which a bubble is generated. Since this problem is beyond the scope of the present study, the commonly accepted conditions are assumed to the effect that the bubbles may form only at nuclei of sufficient size to overcome the initial surface tension force of the liquid and that these nuclei are made up of air or vapor or a combination of both. The size of nuclei

---

* The term subcooled boiling liquid is commonly used for simplicity despite the obvious ambiguity. The term replaces the longer statement "the liquid whose bulk temperature is below saturation temperature but whose boundary layer is superheated so that bubbles may form next to the heat transfer surface".

which is required to initiate boiling in any liquid under given conditions decreases with increasing liquid temperature. Thus for any size distribution of nuclei in a liquid, there is a greater number of active nuclei at higher liquid temperatures and consequently a greater number of bubbles. The following discussion is based on the premise that the population of bubbles increases with the temperature of the liquid. A more detailed discussion of the generation of bubbles is given in Part II, Section IV.

For simplicity in discussing the boiling process, it is considered that a vertical metal wall is immersed in a stagnant pool of degassed subcooled water at 1-atmosphere pressure. Since not all of the dissolved gas has been removed from the water, small bubbles grow near the hot wall from the nuclei that are sufficiently large to overcome the liquid surface tension. The first noticeable effect of bubbles on heat transfer appears in average degassed water (0.3 cc of air per liter of water) when the wall temperature exceeds the liquid saturation temperature by about 30°F. These nucleate boiling bubbles grow and collapse, thereby creating turbulence in the liquid near the wall. The hot liquid near the wall is forced away by this turbulence and replaced by the cooler bulk liquid. The temperature of the local eddies of water may then alternate from superheated to below saturation. Since the wall temperature is only slightly above the saturation temperature, a small number of widely spaced bubbles may maintain the liquid near the wall between the bubbles at a temperature close to saturation. Whenever the liquid temperature increases to the value

needed to evaporate into a nucleus which is present, a new bubble forms.

As the wall temperature is increased, the bubble population also increases since more nuclei are of the size required to initiate a bubble. The population of bubbles increases to the number that is needed to create sufficient turbulence to cool the remaining liquid next to the wall below its nucleation temperature. When the wall is about 100°F above the water saturation temperature, the population has increased so that at maximum size the bubbles cover 100 per cent of localized areas of the hot wall. These localized areas are entirely covered by about a dozen bubbles which coalesce to form a local vapor blanket. At any instant these local areas that are entirely covered with bubbles may occupy only 30 per cent of the total area. At the peak heat flux point, about 50 per cent of the total wall area is occupied by vapor in the form of blankets and individual bubbles (Cf. Fig. 21).

Figure 22 illustrates the vertical wall with a local film blanket for the condition at the transition from nucleate to partial film boiling. The buoyant force on this large vapor blanket exceeds the adhesion force and tends to slide the blanket upward along the vertical wall. However, since the stagnant liquid near the wall above the blanket resists motion more strongly than the liquid far from the wall, the vapor will float out into the liquid as shown. When the vapor detaches from the wall, cool liquid is drawn in as replacement.

These thick local blankets of vapor alternately form from coalescing nucleate bubbles and float out into the main body of the liquid to

condense. The partial film boiling continues until the wall temperature reaches about 1000°F above the saturation temperature. At this high temperature, the bubble population has increased to the point where the bubbles contact one another when only partially grown. For this condition the many local film blankets now occupy 100 per cent of the entire wall and coalesce to form a complete film (Cf. Fig. 21). Since the entire wall is covered, the vapor is forced upward by the buoyant forces rather than floating away from the wall (Cf. Fig. 23). The film thickness is now adjusted so that the vapor flowing upward is just replaced by the evaporation into the film.

It is seen that the individual nucleate-boiling type of bubble plays a prominent role in all three boiling regions. The only difference between the various boiling regions is the population of nucleate bubbles a few milliseconds after the wall is wetted.

A discussion of the reverse process of starting with a hot wall, which is cooled down to the nonboiling temperature, may aid in understanding the mechanism. This process would be the case of quenching a hot metal body in a subcooled liquid.

At the instant when the hot body (at least 1000°F above the liquid saturation temperature) is immersed in the subcooled liquid, nucleate-boiling bubbles form. After a cycle or two of growth and collapse, the bubble population is so great (Cf. Fig. 24) that several bubbles coalesce into local blankets of vapor which in turn coalesce into a complete vapor film. The liquid evaporates into the film, and the vapor flows upward by buoyant forces. The film thickness adjusts so that the evaporation into the film just equals

the mass of vapor flow out of the film. Heat is conducted and radiated from the wall through the vapor film to the liquid. As the wall is cooled, the vapor-film thickness must decrease to maintain the balance between evaporation into the film and mass flow out of the film. The heat transfer by conduction through the film decreases since the temperature difference $T_W - T_{sat}$ decreases faster than the film thickness (Cf. Eq. A-10). In addition, the heat transfer by radiation decreases. The total heat transfer must consequently decrease as the temperature of the wall is lowered.

The film boiling in the pool has caused turbulence in the water. These water currents may at times penetrate the vapor film and wet the wall. If the wall is sufficiently hot, nucleate bubbles form over 100 per cent of the wetted area, and the complete film is again established (Cf. Fig. 24). However, if the film is penetrated by liquid when the wall is no longer hot enough to produce 100 per cent coverage of nucleate bubbles over the entire wetted area, the resulting partial film boiling creates additional turbulence which breaks up more of the film. The film may be broken at any place during the transition from complete to partial film boiling although the liquid is more likely to wet at the bottom of the wall where the film is thinnest. The liquid at this point then boils and creates turbulence which forces the cool liquid against the remaining film. This action causes more of the wall to be wetted and more nucleate bubbles to form. These nucleate bubbles have a population that allows local blankets of vapor to be formed thus creating more turbulence. In this manner the complete film is removed from the wall and replaced

with local blankets in the partial-film-boiling region. Heat continues to flow from the wall into the subcooled liquid by the mechanism of induced turbulence and latent heat transport as the blankets float away from the wall.

The wall continues to be cooled, and the population of local vapor blankets decreases, thus allowing more time for the intermediate nucleate bubbles. This decrease in the population of vapor blankets results in a higher heat transfer. When the wall is cooled to the point where the bubble population is too small to allow coalescence, heat is transferred entirely by the nucleate-boiling mechanism. As the wall temperature is decreased further, the nucleate-bubble population decreases, and the heat transfer consequently decreases. Finally the wall temperature falls below the liquid saturation temperature, and the body is cooled to the liquid temperature by free convection.

In addition to these conclusions regarding the mechanism of boiling, the following experimental results have been obtained.

B. Forced Convection

The heat-transfer curves obtained for the forced-convection nonboiling region (Cf. Figs. 25 through 28) agreed within 10 per cent with values calculated from the Sieder-Tate equation.

$$\frac{q}{a} = C \frac{k}{D} Re^{0.8} Pr^{1/3} \left(\frac{\mu}{\mu_w}\right)^{0.14} (T_w - T_L) \qquad (6)$$

where the best value of C was 0.025 (Cf. Fig. 29).

C. Nucleate Boiling

The nucleate-boiling data correlated in Figure 30 were within 5 per cent of the values given by McAdams (Cf. Ref. 2).

The heat flux in the nucleate-boiling region varied from incipient boiling to the peak heat flux with substantially a constant wall temperature. Because of the small variation of wall temperature with heat flux in this region, only two design facts must be known about the nucleate-boiling process: (1) the maximum heat flux that may be transferred at a reasonably low wall temperature (usually the heat flux at the transition from nucleate to partial film boiling) and (2) the wall temperature required to cause incipient boiling in the boundary layer of the coolant liquid.

The present study has furnished information on the mechanism of nucleate boiling, partial film boiling, and complete film boiling. In order to obtain additional information on the factors controlling the maximum heat flux, more detailed pool-boiling studies of nucleate boiling were made for water, water-Aerosol solution, and carbon tetrachloride containing various amounts of gas. The combined program has resulted in a better understanding of the boiling mechanism which has allowed the formulation of a semi-empirical theory that successfully predicts the peak heat transfer rates (Cf. Part II Sect. V). The calculation of peak heat flux by this method still requires an experimental determination of bubble growth rates.

The second important fact, that of knowing the wall temperature at which the liquid will nucleate boil, is equally difficult to study.

To date, no theory is available which can predict successfully the wall temperature required to initiate boiling. Several unknown facts, such as the average size and distribution of gas nuclei or other foreign nucleation particles, prohibit an analytical solution of the problem at this time. However, a rough estimate of wall temperature may be made since experimental results have indicated that all moderately degassed liquids tested boil when the wall temperature exceeds the liquid bubble-point temperature by less than 100°F.

D. Partial Film Boiling

Reference to the Figures 25, 26, and 27 shows that the wall temperature in the partial-film-boiling region is affected by pressure and subcooling in about the same manner as in nucleate boiling. The wall temperature increases with pressure so that the difference between wall temperature and saturation temperature remains approximately constant at any given heat flux. This correlation is shown in Figure 31, where heat flux is plotted against the difference between wall temperature and liquid saturation temperature.

The high-speed motion pictures of this type of boiling indicate that the cycle consists of the following events: (1) nucleate bubbles form; (2) the population of the bubbles increases until several coalesce into local blankets of vapor; (3) these blankets grow out into the cooler liquid away from the hot wall and are then condensed while still attached to the wall or float away by buoyant force and condense in the main stream (Cf. Fig. 22).

E. Film Boiling

Film boiling may occur in several different types of equipment such

as: nuclear reactors, condensers, binary mercury-water boilers, and quenching apparatus.

The heat transfer in film boiling was found to be independent of the water pressure, velocity, or subcooling over the range investigated (Cf. Figs. 25 through 28).

The water flow at 5 ft/sec was reversed in one test so as to flow from top to bottom. The vapor film continued to flow upward. This result indicated that, for a vertical heat transfer surface and the range of velocities investigated, the main driving force for the vapor film was buoyance, not pressure drop due to friction or shear stress of the water flow. A correlation for the complete-film-boiling heat transfer from a vertical wall is presented in Figure 32a.

Measurements of the photographs indicated that the vapor velocity was about 25 ft/sec regardless of the varied conditions. This value agrees with the calculated estimates given in the Appendix.

In the investigation of film boiling, the electrical power supplied to the heating tube was increased until the tube failed. Failure was not caused by melting of the entire tube but usually resulted from the decrease in allowable stress at high wall temperature. The lower yield point could not support the internal pressure, and the tube bulged as shown in Figure 33a. Another less frequent cause of failure was a local burnout of about 1/32-inch diameter caused by an imperfection in the tube wall. In such a case the stabilizing fluid flowed out of the pinhole and prevented the burnout from spreading (Cf. Fig. 33a).

F. Accuracy of Data

The data which were obtained from this study were probably within 10 per cent of the true heat flux values in the forced-convection, nucleate-boiling, and complete-film-boiling region. The accuracy decreased to about 15 per cent in the partial-film-boiling region because of the difficulty of maintaining a constant-mass-flow rate with the violent growth and collapse of the large vapor masses.

V. CONCLUSIONS

The major aim of this part of the investigation was to study the three boiling regions in order to understand better the mechanism of boiling heat transfer. This program has yielded sufficient information to indicate how the boiling process changes from nucleate into partial film boiling and finally into complete film boiling as the temperature of the heat-transfer surface is raised. The peak heat flux values were seen to occur approximately at the transition from nucleate boiling to partial film boiling.

The equipment that was developed for this program proved satisfactory for studying the "unstable" partial-film-boiling region as well as the complete-film-boiling region. With slight modification to allow for the use of a higher-pressure stabilizing gas, the apparatus may be used to study the boiling regions of water flowing at higher velocities than were employed in this program (e.g., the use of 1000-psia nitrogen gas would stabilize water flowing at any velocity up to 25 ft/sec). Other liquids that have lower peak heat-flux values than water may be stabilized with nitrogen gas at much lower pressures.

PART II

A DETAILED PHOTOGRAPHIC STUDY OF NUCLEATE POOL BOILING

SUMMARY

The second phase of the investigation consisted of a study of pool boiling using distilled water and commercially pure carbon tetrachloride. The experimental program was aimed at obtaining fundamental information on the behavior of nucleate bubbles forming on a stainless-steel heating strip and the role they play in boiling heat transfer. High-speed motion pictures were taken of the nucleate bubbles at a liquid pressure of one atmosphere, liquid temperature range from 170°F below saturation to saturation temperature, and heat fluxes from incipient boiling to the transition from nucleate to partial film boiling. In addition, the effects of dissolved gas and surface tension on bubble dynamics were studied.

As a result of this program it has been possible to propose a mechanism of the growth and collapse of nucleate bubbles. An empirical expression has been obtained that relates the measured bubble velocity and size to the heat flux at the transition from nucleate to partial film boiling. This relation is

$$\frac{hr}{k} = 0.053 \left(\frac{\rho \dot{r} r}{\mu} \right)^{0.8} \left(\frac{c\mu}{k} \right)$$

The velocity and effective radius appearing in this equation still have to be determined experimentally; all other factors are liquid properties. The values of the peak heat transfer calculated from this relation agree within 15 per cent with the experimental data.

I. INTRODUCTION

A. Nucleate-Boiling Applications

The high combustion gas temperatures and gas film heat transfer coefficients in rocket motors result in heat transfer rates far in excess of the values encountered in the conventional industrial heat transfer equipment. Heat fluxes of the order of 10 Btu/sq in.-sec are not uncommon in the modern rocket motors. To cool these motors by regenerative forced convection would require excessively high velocities with a resulting high pressure drop. In addition the coolant passages would in many cases be so small that maintaining the required tolerances would cause undesirable manufacturing difficulties. It is possible, however, to transfer these high heat fluxes by nucleate boiling at much lower velocities. Reference to Figure 26 shows that for the given conditions ten times as much heat may be transferred by nucleate boiling than could be transferred by the nonboiling forced convection at the same free stream velocity. The wall temperature increased only 40°F to result in this tenfold increase in heat flux. Since this small temperature increase could not change the physical properties of the rocket-motor wall to any extent, the only important design data needed are the wall temperature required to initiate nucleate boiling and the peak heat flux which may be transferred. Although the variation of heat flux with wall temperature in the nucleate boiling region is of little importance for design purposes, it is of interest in understanding the process of boiling heat transfer as will

be seen in the discussion of bubble dynamics.

In addition to the application of nucleate boiling to the cooling of rocket motors, the process is of importance in the design of nuclear reactors and the proper quenching of metals. Although the conventional heat exchangers and condensers usually are not limited in size and weight to the same extent as flight equipment, it would be advisable economically to design this equipment to operate in the nucleate-boiling region also whenever possible.

B. Literature Review

The more significant advances in the field of pool-boiling heat transfer up to the present will be discussed briefly in this section of the introduction.

Mosciki and Broder (Cf. Ref. 1) were the first to investigate the variation of heat flux with wall temperature in the free convection and nucleate boiling region by employing an electrically heated wire in a pool of water. Nikiyama (Cf. Ref. 5) extended the study for bulk-boiling water to include the complete film boiling region.

Drew and Mueller (Cf. Ref. 8) postulated that in the region of rapid increases in heat flux for small increases in wall temperature the liquid boiled on the heating surface at active nuclei. This proposal resulted in terming the boiling region nucleate boiling.

McAdams, et al, (Cf. Ref. 9) found that the heat transfer in nucleate boiling was independent of wire diameter from 0.016 to 0.024 inch. For wire diameters of 0.004 to 0.008, McAdams stated that at any given heat flux the temperature difference between the wall and the water increased for larger wire size. (It should be

noted that these conclusions do not include the peak heat flux values.)

Jakob (Cf. Ref. 7) proposed that the increase in heat transfer in the nucleate boiling region for bulk boiling was due to the agitation of the liquid near the wall caused by the detaching bubbles. This conclusion was reached after showing that the latent heat transport mechanism alone was insufficient to account for the high heat flux obtained by nucleate boiling.

King (Cf. Ref. 10) found that the wall temperature exceeded the liquid saturation temperature by an amount which decreased with the addition of dissolved gases to the liquid, the presence of solid impurities in the liquid, or by increasing the pressure of the liquid.

Sauer (Cf. Ref. 11), Akin and McAdams (Cf. Ref. 12), and Farber and Scorah (Cf. Ref. 13) showed that different metal heating surfaces produced appreciable variations in the nucleate-boiling heat transfer for any given temperature difference between the wall and liquid. According to Kanlakis and Sherman (Cf. Ref. 14) the surface roughness of the heating surface did not influence the value of the peak heat flux.

Gunther (Cf. Ref 15) employed a high speed camera to study nucleate boiling and speculated that the high rates of heat transfer were due to induced liquid turbulence.

In addition to the interest in bubble dynamics as affecting boiling heat transfer, considerable effort has been expended in the study of cavitating flow. Unlike the preceding studies of boiling heat transfer, the hydraulic cavitating flow has been studied in de-

tail, both analytically and experimentally, by many investigators, including Knapp and Hollander (Cf. Ref. 16); Harvey, et al (Cf. Ref. 17); Plesset (Cf. Ref. 18); Ellis (Cf. Ref. 19); Dergarabedian (Cf. Ref. 20); and Gilmore (Cf. Ref. 21).

C. Purpose of Present Study

The study of nucleate boiling heat transfer may be divided into three phases:

1. Bubble generation
2. Bubble growth and collapse
3. Influence of bubble dynamics on heat transfer

The subject may be subdivided further into the categories of boiling in a pool and boiling with forced convection.

The phases chosen for this experimental investigation were bubble growth and collapse as well as the influence of bubble dynamics on heat transfer in pool boiling. Two liquids with large differences in physical properties were chosen for this investigation: water and carbon tetrachloride. In addition, since preliminary investigations had indicated that the surface tension and gas content of the liquid played an important role in the nucleate boiling process, a water-Aerosol solution and water containing different amounts of air were investigated.

II. DETERMINATION OF PEAK HEAT FLUX

A. Description of Equipment

1. Purpose

The discussion contained in the introduction to this phase of the report explained the desirability of knowing the maximum heat flux that could be transferred to any liquid by the process of nucleate boiling. This point, which occurs where the heat transfer mechanism changes from nucleate to partial film boiling, was determined by increasing the power supplied to the heat transfer strip until the surface melted. The factors responsible for this failure of the heat transfer surface have been discussed in detail in Part I.

The present study was made in an attempt to obtain a basic understanding of the mechanism of the nucleate-boiling process that would aid in obtaining a correlation that could predict the peak heat-transfer rates. To simplify the problem, it was decided to confine this phase of the study to pool boiling. This condition eliminated the complications which would result with forced convection where the nucleate bubbles move downstream at about 8/10 of the free stream velocity (Cf. Ref. 4).

2. Distilled Water

The tests with distilled water were carried out using a 1/8-inch wide, 1/2-inch long and 0.0043-inch thick, type 304 stainless-steel heating strip immersed in distilled water. The test tank was made of a Pyrex glass 2 1/2-inch diameter cylinder, 2 inches long, with flat

ends (Cf. Fig. 32b). The distilled water was boiled in a 2-liter flask until one half of the water was evaporated. This procedure lowered the dissolved gas content to less than 0.2 cc of air per liter of water as determined by the chemistry section of the Jet Propulsion Laboratory using the Winkler technique. After degassing, the water was drawn by means of an aspirator into the test section where the bubbles could be photographed through the flat ends of the tank. A thermometer was placed 1/2 inch above the heating strip to measure a reference bulk liquid temperature.

The power supply for electrically heating the stainless-steel strip was obtained from a dc welding generator manufactured by the Hobart Co. Regulation of the field current by the use of a rheostat provided smooth control from no load to the rated capacity of 24 kw with the amplitude of the voltage ripple less than one per cent.

The heating strip was cut from a roll of type 304 stainless steel with precision shears. The strips chosen for these tests varied less than 0.001 inch in the 0.125-inch width and less than 0.0001 inch in the 0.0043-inch thickness. To determine the electrical resistance of the heating strip, five, 1 1/2-volt, dry cell batteries arranged in parallel were connected in series with a 3-ohm resistor, a 0.5 per cent ammeter, and the stainless-steel strip. The voltage drop across a 1-inch length of the strip was determined by the use of a hand-balanced precision potentiometer. The average resistivity measured in this manner was 0.0263 ohm per inch of length. Figure 33b shows the curve of heat flux vs

current that was obtained and then used for the present program. The variation of the resistivity of the strip with temperature was negligibly small over the range of interest. The heat flux determined in this manner was estimated to be within 1 per cent of the true value.

3. Carbon Tetrachloride

Considerable difficulty was encountered in an effort to remove the dissolved gas from the carbon tetrachloride. When this liquid was subjected to the same degassing technique as had proved satisfactory for the water, large quantities of noncondensable gas bubbles were produced during a boiling test. As a result, another method was developed to remove the gas from the liquid. It was found that the carbon tetrachloride could be degassed satisfactorily by evaporating the liquid and then recondensing the vapor while drawing a high vacuum to remove the noncondensable gases. This tedious process was carried out using the system shown in Figure 34. All containers and lines were fabricated of Pyrex glass. The procedure for degassing was as follows:

> The carbon tetrachloride was poured into container A, and container B was surrounded by a liquid nitrogen bath. Heat was supplied to container A to cause the liquid to evaporate. The vapor flowed over to container B where it condensed and solidified. The vacuum pump maintained the system at about 2 inches Hg abs and drew off the gas that would not condense. After all of the liquid was evaporated from container A, the

liquid nitrogen bath was removed from B and placed under A. The liquid was then evaporated from B back into A after suitably adjusting the control valves. The procedure had to be repeated about four times before the desired amount of gas was removed from the liquid. Container B was then filled with the degassed liquid and valves 1 and 2 closed and valves 3 and 4 opened. Container B was heated to increase the pressure and the liquid was then drawn into the test section. Figure 34 shows the liquid level when the system is ready for the start of the test. Valve 4 was closed, and the liquid in container B was heated to give the desired pressure while the liquid in the test section was cooled. In this manner, it was not necessary to expose the degassed liquid to the atmosphere or other contaminating gas in order to obtain the required 1 atm abs pressure.

The test section was similar to the water test tank with the exception that the entrance and exit lines were both glass welded to the top of the cylinder body (Cf. Fig. 35).

To maintain the carbon tetrachloride at a constant temperature during the high-subcooling tests, it was necessary to surround the tank with a coolant. Figure 36 is a schematic drawing of the test tank surrounded by ethyl alcohol that was used as the cooling

liquid. A clear frost-free view of the boiling was possible with the use of purging tubes bled with dry nitrogen gas.

4. Wall-Temperature Measurement

It was desirable to measure the wall temperature required to initiate boiling in the carbon tetrachloride; the excess wall temperature required for water was known (Cf. e.g. Ref. 15). The high dc voltage gradient in the heating strip added to the usual difficulty of obtaining accurate measurement of wall temperature by the direct attachment of a thermocouple to the wall. The most satisfactory arrangement that was obtained for determining the wall temperature is shown in Figure 37. The heating strip was sealed into the Plexiglass holder with acetone. The thermocouple assembly was screwed into the holder until electrical contact was obtained between the strip and the thermocouple. The screw was then rotated so that the thermocouple was withdrawn about 0.0005 inch from the heating strip. The Plexiglass holder was used only during the tests conducted to measure the wall temperatures.

B. Experimental Data

1. Degassed Water

It was found that the peak heat flux data for degassed distilled water containing less than 0.2 cc air per liter of water were reproducible within about ±10 per cent. In view of the inherent statistical nature of the burn-out point, it is not surprising that the data were not reproducible within closer limits (Cf.p.19 Part I). The values of peak heat flux plotted in Figure 38

varied from 5.8 Btu/sq in.-sec at 80°F to 0.3 Btu/sq in.-sec at the saturation temperature.

Employing the values of wall temperature plotted in Figure 39, the heat transfer coefficient was determined. It is seen from Figure 40 that the heat transfer coefficient decreased with an increase in liquid temperature although at a slower rate than the peak heat flux.

It should be recalled that the liquid temperature was measured at a position about 1/2 inch directly above the heating strip.

A second thermometer located below and to the side of the strip measured temperatures about 25°F lower at a heat flux of 5 Btu/sq in.-sec and 10°F at a heat flux of 1 Btu/sq in.-sec. The thermometer located 1/2 inch above the strip has been used as the reference since its reading probably was more representative as an effective liquid temperature.

2. Aerated Water

Aerating the water so that it contained more than 30cc air per liter of water resulted in the formation of bubbles which contained appreciable quantities of noncondensable gases. The effect of the gas was to lower the values of the peak heat flux about 25 per cent below the degassed water data (Cf. Fig. 38). At liquid temperatures exceeding 110°F, a large stagnant gas bubble having a diameter about 10 times as large as the normal nucleate bubble would form on the heater strip. This large gas

bubble limited the transfer of heat from the strip into the water and resulted in causing the wall to melt at lower values of heat flux. The peak heat flux values that were obtained with large gas bubbles on the heat transfer surface also are shown in Figure 38. The large gas bubble could be obtained occasionally at liquid temperatures below 110°F.

3. Aerosol-Water Solution

It was desired to investigate the effect of a change in surface tension on the value of peak heat flux without any appreciable change in the other physical properties of the water. A 1 per cent solution of Aerosol (dihexyl sodium sulfosuccinate) and water was used since its surface tension was only 34 dynes/cm compared to 72 dynes/cm for distilled water. The interesting result was that the peak heat flux decreased to about half the value for degassed distilled water at 80°F (Cf. Fig. 38).

The wall temperature for the Aerosol-water solution was about 15°F lower than the values obtained in distilled water. (Cf. Fig. 39).

After degassing the solution in the same manner as the distilled water, the gas content was about 0.7 cc air per liter of liquid.

It is interesting to notice that the degassed water, aerated water, and Aerosol-water solution curves all approach a common value of 0.3 Btu/sq in.-sec at the saturation temperature (Cf. Fig. 38).

4. Degassed Carbon Tetrachloride

The peak heat flux data for the degassed carbon tetra-

chloride also decreased with an increase in liquid temperature as shown in Figure 41. The data easily were reproducible within ±5 per cent.

Measurements of the wall temperature indicated that the excess in wall temperature over the saturation temperature at the peak heat flux was about 15°F less than for degassed water (Cf. Fig. 39).

5. Aerated Carbon Tetrachloride

Aeration of the carbon tetrachloride resulted in larger bubbles which contained appreciable quantities of a noncondensable gas. The value of peak heat flux was about half as large as the degassed carbon tetrachloride at 20°F (Cf. Fig. 41). Unlike the aerated water only one size of gas bubble could be observed at any given liquid temperature.

It is noted from Figure 41 that the degassed and aerated carbon tetrachloride curves approach a common value of 0.13 Btu/sq in.-sec at the saturation temperature.

A qualitative explanation of the relative positions of the five peak heat flux curves will be given in Section V after discussing the proposed mechanism of boiling heat transfer.

III. MEASUREMENT OF BUBBLE GROWTH AND COLLAPSE RATES

A. Description of Equipment

1. Water Tests

Tests with water were carried out using the Pyrex glass container and heating strip described in the preceding section on peak heat flux measurements. A General Radio, 35-mm, shutterless camera was used with a Kerr-cell, electro-optical shutter (Cf. Ref. 22). The Kerr-cell was operated from a 14,000-volt power supply for a maximum period of 0.05 sec. The exposure time on each frame was about 2 microseconds. A relay system allowed the camera to accelerate to the required 15,000 frames/sec in about 1.2 sec before actuating the Kerr-cell and firing the flash bulb. With this arrangement about 5 feet of the 100 feet of film were exposed.

The moderate resolution of the high-speed camera prevented inspection of distances smaller than 0.001 inch.

2. Carbon Tetrachloride Tests

The much lower growth and collapse rates of the carbon tetrachloride bubbles were determined by photographing the bubble at 3000 frames/sec on 16-mm Eastman Kodak Super XX motion-picture film using a Fastax camera.

The same degassing technique and equipment were used during this phase of the study as were described in the preceding section on peak heat flux.

B. Photographic Results

1. Degassed Water

It may be concluded from Figure 42 that the nucleate bubble formed somewhere in the liquid within 0.001 inch of the heating strip. The bubble grew to a maximum size and, for liquid temperatures below 170°F, collapsed while remaining within 0.001 inch of the wall. When the water temperature was between approximately 170°F and saturation, the bubbles detached from both the upper and lower surfaces of the heating strip and floated into the bulk of the liquid before collapsing (Cf. Fig. 43). For simplicity of reference, these bubbles which condense (within the visible 0.001 in.) will be denoted as vapor bubbles.

It was observed at all liquid temperatures (Cf. Fig. 44) that the base of some of the vapor bubbles separated from the heat transfer surface just prior to the collapse phase of the bubble lifetime cycle. Since this type of bubble could be seen on the lower as well as the top surface of the heating strip, the motion of the bubble away from the strip could not be attributed to the buoyance force.

The effect of heat flux on the bubble size and population can be seen from Figure 45, which shows several frames from each of the four motion pictures taken of the boiling at 31, 34, 63, and 74 per cent of the peak heat flux. Five bubbles were measured from each of these films and the data plotted in Figures 46 through 49. The average values of maximum radius and lifetime are plotted in Figure 50. The average of the bubble growth and collapse rates, hereafter termed bubble velocity, was obtained by dividing the maximum bubble radius by half the lifetime. It is seen that the three factors are

relatively insensitive to the magnitude of the heat flux.

In the next series of tests the heat flux was set at 50 per cent of the peak heat flux for six different bulk temperatures (62, 78, 112, 132, 177°F), and motion pictures were taken of the bubbles. Several frames from three of these films are reproduced in Figure 51. The data taken from five bubbles at each liquid temperature are plotted in Figures 52 through 57. The average values of bubble maximum radius, lifetime, and bubble velocity are plotted in Figure 58. The maximum bubble radius increased from .0135 inch at 62°F to .022 inch at 177°F. The lifetime increased faster than the radius and resulted in a decrease in bubble velocity from 4.1 ft/sec at 62°F to 3.3 ft/sec at 177°F.

The large deviation from the average values of maximum radius and lifetime for the bubbles should be noted in Figures 46 through 49 and Figures 52 through 57. As a result of these large variations, the average values plotted in Figures 50 and 58 should not be expected to be closer than about 25 per cent from the true values.

A qualitative discussion of the effect of liquid temperature and heat flux on the bubble dynamics will be given in Section IV.

2. Aerated Distilled Water

The motion pictures of the nucleate boiling of aerated water indicated that the bubbles did not condense while remaining against the wall as was usually the case for the vapor bubbles at liquid temperatures below 170°F.

Two types of gas-vapor bubbles were observed in the aerated

water. One type grew to about the same size as the pure vapor bubble and then collapsed leaving a small residual gas bubble; the other type of gas-vapor bubble grew to about ten times the maximum size of the vapor bubble and remained substantially stagnant on the heat transfer surface. The latter, stagnant gas-vapor bubble, occurred most frequently in water which was super-saturated with gas and at temperatures above 110°F. The collapsing small gas-vapor bubble occured most frequently in cooler water that was under-saturated with gas.

The stagnant gas-vapor bubble grew to about the same size as the vapor bubble at approximately the same rate. After this radius was reached, the bubble continued to grow at a much lower rate to sizes up to ten times the vapor bubble maximum radius (Cf. Fig. 59). At low heat flux several of these large bubbles could be seen on the strip. As the heat flux and consequently the bubble population was increased, the interference of neighboring bubbles occasionally would cause these gas-vapor bubbles to detach from the strip after reaching about the same size as the vapor bubble. However, usually the stagnant gas-vapor bubbles would cause burnout of the heater strip before sufficient turbulence could be created in the liquid boundary to detach the bubble.

The large gas-vapor bubble would decrease less than ten per cent in radius when the electrical power was no longer supplied to the heating strip. This large residual volume of gas indicated that the bubble must have been filled mainly with a noncondensable gas

rather than water vapor. The rate at which the gas in these stagnant bubbles rediffused back into the liquid after the electric power was shut off was measured to be less than 10^{-5} times the rate at which the bubble formed.

The influence of the liquid temperature and heat flux on the dynamics of the short life gas-vapor bubble was similar to the effects on the vapor bubble. However, the large stagnant bubble was relatively unaffected by liquid temperature.

The maximum bubble radius and bubble velocity could not be measured for heat fluxes exceeding approximately 25 per cent of the peak heat flux. At high values of heat flux the stagnant bubbles remaining on the heating strip and the noncondensing gas bubbles that detached from the strip obscured the field of view. The meager data that were obtained indicated that the bubbles grew in the aerated water at about the same rate as in the degassed water.

Two additional phenomena were noticed in the motion pictures of the aerated water. The first was that occasionally the small gas-vapor bubbles were forced an appreciable distance away from the heating surface. When these bubbles were ejected from the lower surface of the strip, they traveled about 1 1/2 inches before changing direction to float upward with the buoyant force (Cf. Fig. 60). The second fact that could be seen in the motion pictures was a stream of warm liquid flowing downward against buoyant force from the pole of the large gas bubbles on the underside of the strip. This warm stream changed direction about 1 inch below the strip and,

as would be expected, floated upward. Graphite powder was placed on the surface of these streaming bubbles to trace the liquid currents. A close photographic inspection indicated that the liquid film forming the bubble boundary was rotating as indicated in Figure 61.

These detaching and streaming bubbles will be discussed further in Section IV.

3. Aerosol-Water Solution

The nucleate bubbles that were formed in the degassed solution of 1 per cent Aerosol and water were generated within 0.001 inch of the strip and grew to about the same size as the vapor bubble. This type of bubble differed from the vapor bubble in three main factors: (1) the bubble usually detached from the strip before collapsing completely (Cf. Fig. 62); (2) the rate of growth was considerably lower than for the vapor bubble (Cf. Fig. 63); (3) for low population, about 50 per cent of the bubbles grew to the maximum radius and then remained stagnant on the strip.

The bubble maximum radius and lifetime increased with an increase in liquid temperature in a similar manner to the degassed water. The bubble velocity decreased slightly with an increase in liquid temperature as seen in Figure 64. The effect of increasing the heat flux on the bubble dynamics was to dislodge the stagnant bubbles from the wall and thus increase the average bubble velocity (Cf. Fig. 65).

4. Degassed Carbon Tetrachloride

The nucleate bubbles formed in the degassed carbon tetrachloride were very similar to the Aerosol-water bubble. The bubbles formed on, or very near, the strip, grew considerably slower than the water-vapor bubble, and detached from the wall before condensing. No residual gas bubbles could be seen. Occasionally a bubble was forced away from the bottom of the strip. At low heat flux about 50 per cent of the bubbles grew to a maximum size and then remained stagnant on the heating strip as was observed also for the water-Aerosol solution.

Another effect could be seen in the shadowgraph series of motion pictures. Figure 66 shows that, as the carbon tetrachloride bubble grew, a thermal layer was stretched over the bubble surface and slowly approached the wall.

The influence of liquid temperature on bubble dynamics can be seen in Figure 67. The data taken from this series are plotted in Figures 68 through 71. The bubble maximum radius, lifetime, and velocity are plotted in Figure 72. It is noted that the bubble radius and lifetime increases while the bubble velocity decreases for higher liquid temperatures. This effect is similar to the water-vapor bubble.

Figure 73 summarizes the effect of heat flux on bubble dynamics. The large change in bubble velocity between 25 and 50 per cent of peak heat flux was not observed for the nucleate bubbles in water but was similar to the bubbles forming in the Aerosol-water solution. The photographs in Figures 67 and 75 show the effects of

liquid temperature and heat flux on the size and population of the bubbles.

5. Aerated Carbon Tetrachloride

The nucleate bubbles that formed in aerated carbon tetrachloride were similar to the stagnant gas-vapor water bubbles. The bubbles did not collapse unless detached from the strip by neighboring bubbles. In this case a small residual gas bubble could be seen for several seconds after the bubble detached from the heat-transfer surface.

The same difficulty was encountered in measuring the maximum bubble radius and bubble velocity as for the aerated water. The small quantity of data which could be obtained indicated the bubble grew slightly slower in the aerated carbon tetrachloride than in the degassed carbon tetrachloride.

IV. PROPOSED MECHANISM OF NUCLEATE-BUBBLE GROWTH AND COLLAPSE

A. Introduction

The photographic study of water and carbon tetrachloride has resulted in supplying sufficient information to suggest a mechanism of the dynamics of nucleate bubbles that is presented in this section. Some of the mechanics of the bubble formation, growth, and collapse are conclusively shown in the motion pictures; other factors are deducible from the photographs; and some of the remaining details have not been clarified by this study. It will be seen that it is possible to separate the bubble life cycle into several individual processes.

There are four basically different types of nucleate-boiling bubbles which will be discussed. These types occur respectively in

(1) Degassed-subcooled water

(2) Degassed bulk-boiling liquid

(3) Aerated liquid

(4) Degassed-subcooled carbon tetrachloride

B. Bubble Formation

The first problem encountered in understanding the basic mechanism of bubble dynamics is the initiation of a bubble. The study of surface phenomena to determine the role of nuclei in the formation of bubbles is beyond the scope of the present investigation. However, some of the observations on nucleation which were obtained

incidental to this investigation together with some of the well-known facts regarding the conditions necessary to rupture a liquid will be discussed briefly in this Section.

It is believed that a nucleus which contains gas or vapor, or a combination of both must be present in the liquid in order to initiate the bubble, and that the nucleus is held in a stable equilibrium position by a solid particle. To support this conclusion two conditions may be investigated: (1) the formation of cavities in a liquid by the random motion of the molecules without the aid of solid particles and (2) stable gas-vapor nuclei.

The size of a spherical cavity that is needed to form a bubble may be estimated by the well-known relation

$$p_i - p_o = \frac{2\sigma}{r} \tag{7}$$

where $(p_i - p_o)$ is the pressure difference within the cavity that is needed to overcome the surface tension for a nucleus radius of r. For the case of cavities forming within a liquid, by the random molecular motion, the nuclei would contain only vapor. Equation (7) then becomes

$$p_v - p_o = \frac{2\sigma}{r} \tag{8}$$

Equation (8) is plotted in Figure 76. This curve represents the radius of the nucleus that is required in order to have the surface tension force of the liquid film surrounding a nucleus in equilibrium with the excess pressure. For a given excess pressure,

if the nucleus radius is lower than the equilibrium radius, the capillary pressure will exceed the excess pressure, and the nucleus will collapse completely. If the nucleus radius is larger than the equilibrium radius, the excess pressure will exceed the capillary pressure and the nucleus will grow into an infinite radius bubble. Thus for a given liquid temperature and pressure (i.e., a given $p_v - p_o$) only one size of vapor nucleus may be in equilibrium, and this equilibrium would be unstable.

With the aid of the thermodynamic relation of Clapeyron-Clausius, neglecting the specific volume of the liquid

$$\frac{dp}{dT} \simeq \frac{\lambda}{T}\rho_v$$

Equation (8) then becomes for a perfect gas, approximately

$$T_v - T_{sat} = \frac{RT_{sat}T_v}{\lambda} \ln\left(1 + \frac{2\sigma}{pr}\right)$$

where T_v is the saturation temperature of the vapor within the nucleus at pressure p_v and T_{sat} is the saturation temperature at pressure p_o. It is known from experiments that a heat-transfer surface temperature of 30^{o}F above the saturation temperature of the liquid will cause bubble formation in water. Substitution of this excess temperature into Equation (9) results in a required nucleus radius of approximately 10^{-4} inch in order to have the pressure and surface tension forces in equilibrium. This value is about 10^{4} times larger than the maximum cavity size that would be expected to occur by molecular fluctuations with any reasonable frequency (Cf. Ref. 23). As a consequence, any cavity

that does form in the liquid would be smaller than the equilibrium radius, and thus would be collapsed by the surface tension force. The number of nuclei having a diameter exceeding 10^{-4} in. which arise from random molecular fluctuations can be estimated according to Volmer (Cf. Ref. 27) to be much less than one per cubic inch per hour.

From the above discussion, it is reasonable to eliminate free vapor nuclei which arise from molecular fluctuations as likely nucleation cavities. We now may consider the possibility of a gas nucleus acting as a bubble generation cavity.

Some brief mention of the way in which a gas may be held in a liquid will be of interest. A stagnant liquid exposed to a gas will absorb the gas in the form of single molecules dispersed through the liquid. Henry's Law states that for a gas mixture such as air, the number of single molecules of any of the component gases in solution with the water will vary as the solubility and partial pressure of the component gas. When the liquid is agitated, for example, by pouring from one container into another, submicroscopic bubbles of the surrounding gas may be trapped in the liquid to form a colloidal solution. If the liquid is not completely saturated (i. e. filled with the maximum number of single gas molecules), these gas nuclei will eventually dissolve into the liquid to approach a saturation condition. This rate of saturating has been estimated by Epstein and Plesset (Cf. Ref. 24) to be of the order of several seconds in water which is undersaturated with the gas. However, the gas nuclei may be stabilized on nonwettable

solid particles, and exist indefinitely in the liquid. In addition to the gas, these nuclei would contain vapor at the saturation pressure corresponding to the liquid temperature. The gas-vapor cavities would be surrounded by the surface of the solid and a convex surface of the liquid. For this condition, the total pressure within the cavity would be less than the liquid pressure. The partial pressure of the gas would be reduced below the pressure corresponding to a saturation condition of the liquid, and as a result the gas would no longer continue to diffuse into the liquid.

To see how these gas-vapor nuclei that are stabilized on solid particles may act as generation points for the bubbles, consider the effect of increasing the temperature of the liquid in contact with the nuclei. The temperature of the liquid may increase until the partial pressure of the vapor within the nuclei increases to the value required to make the total pressure sufficiently great to force some of the gas-vapor mixture out of the solid. Assuming the gas-vapor nuclei are spherical when forced out of the solid, we may rewrite Equation (7) as

$$p_v + p_g - p_o = \frac{2\sigma}{r}$$

where: the sum of the partial pressure of the vapor and the gas $(p_v + p_g)$ is the total pressure within the cavity. For a perfect gas the relation may be written

$$p_v - p_o = \frac{2\sigma}{r} - \frac{w_g R_g T_v}{\frac{4}{3}\pi r^3} \qquad (10)$$

It is seen that the gas decreases the effect of surface tension and thus decreases the critical excess pressure.

Equation (10) may be rewritten (with the same approximations as before) in terms of the excess temperature as

$$T_v - T_{sat} = \frac{R T_{sat} T_v}{\lambda} \ln\left(1 + \frac{2\sigma_{eff}}{pr}\right) \tag{11}$$

or for small temperature differences

$$T_v - T_{sat} = \frac{2\sigma_{eff} R T_{sat}^2}{p\lambda r}$$

where: $$\sigma_{eff} = \sigma - \frac{3 w_g R_g T_v}{8\pi r^2}$$

The critical radius (i.e. maximum radius for which a nucleus containing a given quantity of gas will be in stable equilibrium) becomes

$$r_c = 3\sqrt{\frac{w_g R_g T_v}{8\pi\sigma}} \tag{12}$$

and the excess pressure that would be required to cause the nucleus to form a growing bubble would be

$$(p_v - p_o)_c = \frac{4}{9}\sigma\sqrt{\frac{8\pi\sigma}{w_g R_g T_v}} \tag{13}$$

The term bubble will be used to define a cavity having a radius greater than the critical radius; the term nucleus will be used to define a cavity having a radius smaller than the critical radius.

Equation (10) is plotted in Figure 77. It is seen that unlike the pure-vapor nuclei, a nucleus smaller than the equilibrium size (and below the critical radius) will grow to the equilibrium radius while a gas-vapor nucleus exceeding the equilibrium size (but below the critical radius) will decrease to the equilibrium radius. It

also may be noted from Figure 77, that decreasing the mass of gas within the nucleus increases the value of the excess pressure at the critical radius.

After several bubbles have been formed from a nucleus which is stabilized on a solid particle, most of the gas would be purged out of the cavity. In this case the generating nucleus would contain vapor only. When this condition is reached the vapor nuclei which have radii exceeding the critical value when forced out of the solid will form bubbles; the nuclei which have radii smaller than the critical will collapse after leaving the solid. Another possible means by which pure-vapor nuclei may form is by the random fluctuations of the liquid molecules as discussed above. The vapor nuclei formed in this manner and not stabilized on solid particles were shown to be too small to form a bubble at any reasonable liquid temperature. However, if the vapor nuclei are stabilized on solid particles, it theoretically would be possible for these nuclei also to act as bubble generation points. The formation of bubbles from these vapor nuclei is unlikely since it requires the improbable condition of having the stabilizing particle at the point of cavity formation.

It is concluded that for a given value of liquid superheat the gas-vapor nuclei which exceed r_c after being forced out of the solid will form bubbles. As the heat-transfer surface temperature increases, the vapor pressure increases and consequently there will be more active or bubble forming nuclei (Cf. Fig. 77). The nuclei which contain the smallest amount of gas will have the greatest excess pressure and temperature.

In addition to the nuclei that are held in the bulk of the

liquid by submicroscopic foreign particles, there would be some gas trapped within the heat transfer surface. The capacity of the foreign particles on the heat transfer surface to act as nucleation points is determined mainly by the cavity sizes and nonwetting character.

The bubbles may form more readily against the heat-transfer surface than in the bulk of the liquid if the surface free energy of the liquid in contact with vapor is greater than the energy of the liquid in contact with the wall. An additional factor favoring rupture of the liquid at the wall rather than in the bulk of the liquid is the higher temperature at the wall. It is evident that the surface condition of the heating strip should affect the conditions necessary for nucleation.

Assuming the existence of gas-vapor nuclei stabilized on solid particles, it is possible to explain the high superheat that is obtainable in a liquid that has been subjected to a high pressure. We may investigate the result of increasing the liquid pressure to several hundred atmospheres and then carefully decreasing the pressure to the original one atmosphere. From Henry's Law it is known that the solubility of the gas in the liquid would increase for higher pressures. Thus, some of the gas within the cavity would diffuse into the liquid. When the liquid pressure is decreased to the original one atmosphere, the liquid may still hold the gas in a supersaturated condition. In this case, the amount of gas in the nucleus would be less than the original value. Thus when the gas-vapor mixture is forced out of the solid to form a nucleus, the partial pressure of the

gas would be lower. As a result the vapor pressure (superheat) that is required to form a bubble would be greater than the value before the liquid was subjected to the high pressure. This high superheat has been noted by several investigators (Cf. e.g. Ref. 17).

Assumptions that will be necessary for discussing the generation of bubbles have been presented briefly in this discussion; they may be summarized as follows:

1. Gas-vapor nuclei stabilized on solid particles are present even though the liquid is not saturated with the gas.

2. The excess pressure necessary to form a bubble from a nucleus which has been forced out of the stabilizing particle varies with the surface tension, the partial pressure of the gas within the nucleus and the nucleus size (Cf. Eq. (7)).

3. The liquid may rupture near the heat transfer surface more easily than in the bulk of the liquid.

C. The Dynamics of Bubbles in Degassed Subcooled Water

1. Bubble Growth and Collapse Mechanism

The dynamics of nucleate bubbles forming in degassed distilled water will be the first type discussed because these bubbles have the simplest life cycle.

Several frames from a motion picture of the growth and collapse of a typical water vapor bubble are shown in Figure 42. The following enumerations refer to the sketches in Figure 78.

The horizontal heat transfer surface is immersed in degassed distilled water.

(a) The wall temperature and the adjacent liquid film are above the liquid saturation temperature.

(b) A gas-vapor nucleus has been forced out of a solid particle. If the excess temperature of the liquid surrounding the nuclei is greater than the value given in Equation (13), the equilibrium pressure force would exceed the surface tension force and the nucleus will become a bubble.

The motion pictures of the bubble formation indicated that the nucleus was within 0.001 in. of the wall. For atmospheric pool boiling, assuming the bubble forms on the wall which has a temperature of 250^{o}F (Cf. Fig. 39), the excess pressure would be 15 psi. Thus from Figure 77, it is seen that any nucleus having a radius greater than 3×10^{-5} in. will grow to form a bubble. This estimate is in agreement with Parkin's prediction (Cf. Ref. 25) that nuclei having a radius of the order of 10^{-5} in. would initiate cavitating bubbles. Every bubble that forms at a wall temperature of 250^{o}F would grow from nuclei containing more than 2.3×10^{-18} lbs of gas. For a constant bubble-liquid-film temperature, the rate of growth of the bubbles will depend on the difference between the excess pressure existing at the critical radius and the equilibrium excess pressure (Cf. Fig. 77). However, since the liquid film surrounding the bubble will be cooled by the latent heat removed in forming the vapor and the heat transferred to the bulk of the liquid, the growth rate will be

lower than the isothermal rate (Cf. Fig. 77).

(c) The resistance of the wall to the spherical growth of the bubble results in approximately a hemispherical shape (Cf. Fig. 42). It is probable that the bottom of the bubble is separated from the wall by a thin layer of liquid since the viscous and adhesion forces in the liquid prevent the bubble from wiping the wall clear of water and the evaporation rate may not be sufficiently large to evaporate any appreciable thickness of liquid at the bubble base. However, it seems likely that the bubble could be "dry" at one point on the base. The bubble is forced against the thin layer of water next to the wall during the growth portion of the lifetime by the inertia force of the pool of water. It was not possible to verify the existence of this thin film because of the limited resolution power of the camera lens system. However, the proposed mechanism of growth or collapse of the bubble will be the same regardless of the existence or nonexistence of this film.

The layer of superheated water that was above the nucleation volume is pushed away from the wall by the bubble (Cf. shadowgraph Fig. 66). This water film is stretched over the top of the bubble with the result that the temperature gradient within the film is increased. Heat is removed from the displaced film by conduction and convection to the cooler surrounding liquid (dotted arrows) and by evaporation of liquid

into the bubble (solid arrows). The probable shape of the temperature profile in the liquid at the top of the bubble is shown in Figure 79. It is seen that the heat would be removed from the film and transferred to the bulk of the liquid as well as into the bubble.

The liquid surrounding the bubble has been set in motion by the motion of the bubble during growth (large solid arrows).

(d) At the instance shown in this sketch the liquid film at the top of the bubble has been cooled to the vapor saturation temperature, and evaporation ceases from this region. The bubble continues to grow although slower than previously because of the lower rate of evaporation per unit bubble volume. The liquid film surrounding the bubble still loses heat by evaporation from the lower portion of the bubble and conduction from the entire bubble surface to the cooler bulk liquid.

The excess pressure within a spherical bubble during growth may be estimated by the Bernoulli relation which for an inviscid-incompressible-infinite liquid with zero surface tension becomes

$$\frac{p_v - p_\infty}{\rho_L} = \frac{3}{2}\dot{r}^2 + r\ddot{r} \qquad (14)$$

The capillary pressure may be neglected for a bubble having a radius of 0.005 inch ($p_i - p_o = \frac{2\sigma}{r} \leq 0.2$ psi). Using a

typical growth rate of 10 ft/sec (Cf. e.g. Fig. 49) for the bubble radius from .001 inch to .010 inch and neglecting the acceleration term, Equation (14) may be used to obtain an average value for the excess pressure, as follows:

$$p_v - p_o = \frac{3}{2}(10)^2 \frac{62.4}{144(32.2)} = 2.0 \text{ psi}$$

The corresponding excess of the temperature of the vapor within the bubble is 6°F.

These values indicate the order of magnitude of the excess pressure and temperature that would be expected to exist within the bubble. An exact solution would require corrections for the influence of the wall and mass addition. For the present discussion it is sufficient to note that the 15 psi excess pressure within the initial cavity to balance the surface tension force has been dissipated to 2.0 psi average pressure by the time the bubble has reached .005-inch diameter. This excess pressure of 2 psi is the average unbalanced force which caused the bubble to grow. The excess temperature of the vapor also has decreased markedly from 40 to 6°F. As suggested on page 58 insufficient heat was conducted to the bubble liquid surface to maintain an isothermal condition.

It is possible to investigate the plausibility of the proposed mechanism further by considering the maximum evaporation rate that may be expected under these conditions and comparing this value with the observed bubble growth rate. Using an analy-

sis similar to that given in Reference 18, the heat that was removed from the liquid to form a spherical bubble of 0.005-inch radius would be

$$Q = \frac{4}{3}\pi r^3 \lambda \rho_v$$
$$= \frac{4}{3}\pi \frac{(0.005)^3}{1728} 1000\,(0.0385) = 7.0 \times 10^{-9}\ \text{Btu}$$

The thickness of the liquid film from which this heat may be removed was

$$\delta \simeq \sqrt{Dt} = \sqrt{2.5\times10^{-4}(50\times10^{-4})} \simeq 1.1\times10^{-4}\ \text{in.}$$

Removing 7.0×10^{-9} Btu from a liquid film 1.1×10^{-4} inches thick would lower the film temperature approximately

$$\Delta T \simeq \frac{Q}{4\pi r^2 \rho_L c \delta} = 6\ ^\circ F$$

Assuming no other loss of heat and a straight line temperature gradient, the bubble liquid surface temperature would be $[250 - 2\,(6)] = 238^\circ F$.

The evaporation into the bubble may be calculated from the Knutsen equation corrected with the accommodation coefficient ϵ.

$$\Delta \dot{m}\, 4\pi r^2 \rho_v = \epsilon\left[\rho_L\sqrt{\frac{T_L R g}{2\pi}} - \rho_v\sqrt{\frac{T_v R g}{2\pi}}\right] 4\pi r^2 = \frac{d}{dt}\left(\frac{4}{3}\pi r^3 \rho_v\right)$$

or

$$\dot{r} \simeq \epsilon\sqrt{\frac{Rg}{2\pi}}\left[\frac{\rho_L}{\rho_v}\sqrt{T_L} - \sqrt{T_v}\right] \qquad (15)$$

$$= .04\sqrt{\frac{85.6(32.2)}{2\pi}}\left[\frac{.059}{.042}\sqrt{698} - \sqrt{678}\right] \simeq 9.3\ \text{ft/sec}$$

In this calculation, a value of .04 was used for the accommodation coefficient as suggested in Reference 26.

In view of the assumptions employed in this estimate, the close agreement between the measured value of 10 ft/sec and the estimated value of 9.3 ft/sec is fortuitous. For higher wall temperatures, which may be obtained by increasing the heat flux, the agreement is not as good. Nevertheless, the agreement of the rough calculation with experimental data even at higher wall temperatures is sufficiently close to support the proposed mechanism. For an accurate analysis corrections would have to be made for the non-spherical bubble shape, the heat transfer to the subcooled bulk liquid, mass addition, latent heat transport, and for an initial bubble film temperature lower than the wall temperature. With these modifications the agreement between the estimated bubble growth rate and the measured growth rate is expected to be close for all wall temperatures.

(e) In Sketch e the water surrounding the top region of the bubble is now well below the saturation temperature and some of the vapor within the bubble condenses at the pole. The base of the bubble is still surrounded by superheated liquid. As a result, there is a flow of vapor from the hot base of the bubble to the cool pole. The transport of heat by the flowing vapor has been calculated by Plesset (Cf. Ref. 27) for a one dimensional flow to be of a lower order of magnitude than the

total heat flux in nucleate boiling. In addition this condition of vapor streaming through the bubble occurs for only a fraction of the total time that heat is removed from the heating strip. Consequently, the flow of vapor through the bubble may be eliminated as a prime source of heat transfer.

The bubble shown in Sketch e is drawn for the condition where the evaporation rate is equal to the condensation rate. Under this condition there would be no net flow of vapor into the bubble. The liquid surrounding the bubble still has an appreciable outward velocity. It is this momentum that was stored in the liquid during the growth of the bubble that tends to carry the bubble away from the heat transfer surface and into the bulk of the liquid after the bubble has reached a maximum radius. The photograph in Figure 44 clearly shows the bubble deformation that results from resisting the drag of the surrounding liquid. Since this bubble was on the bottom surface of the heating strip, buoyancy cannot account for the deformation.

(f) In this figure the inertia force of the water has been dissipated and the excess pressure within the bubble changed from positive to negative. The bubble has been deformed and the volume increased by the outward flow of the surrounding liquid. The deformation also results in moving the bubble base out into the cooler liquid. The evaporation from the base of the bubble decreases and the condensation from the pole increases . In this figure the net condensation results in a negative excess pressure

within the bubble allows the water to collapse the bubble back to the same size as in Sketch e.

(g) However, now the rates of evaporation and condensation are not equal as they were for this radius during the growth period. More heat has been removed from the superheated film and transferred to the bulk of the liquid. As a consequence, condensation will occur over a larger area and the bubble will continue to collapse (Cf. Fig. 42).

(h) The regions of evaporation and condensation are separated by the saturation temperature isothermal indicated in Sketch h. The liquid surrounding the top of the bubble continues to lose heat to the cooler surrounding liquid, and the saturation temperature isotherm approaches the wall. The cooler surrounding liquid now has an appreciable inward radial velocity.

(i) If the bubble collapses faster than the isotherm can approach the wall, once again, as in the growth portion of the life cycle, the rate of evaporation could equal the rate of condensation. Even under this extreme condition the bubble usually will not stop the collapse since the displaced superheated liquid film continues to transfer heat into the subcooled bulk liquid. This transfer of heat lowers the saturation isotherm and again causes the condensation to exceed the evaporation. The inrushing water also acts as an additional collapsing force by compressing the vapor within the bubble, thus increasing the va-

por saturation temperature and resulting in increased condensation. This increase in saturation temperature would not be expected to occur until the collapse velocity of the bubble exceeds the condensation rate near the end of the collapse portion of the bubble lifetime.

There is one possibility for the bubble to stop the collapse and remain stagnant. This condition may be reached for a suitable combination of liquid subcooling, conductivity, latent heat and condensation rate. In this case, the heat supplied by condensation would balance the heat lost to the bulk liquid. This stagnant bubble was never observed in degassed-subcooled water.

(j) The inrushing cool water has lowered the saturation temperature area below the free convection position, and the bubble has collapsed back to the critical size.

(k) The hot wall is splashed with the cool liquid and the local wall temperature decreases.

(l) The liquid near the wall has been once again superheated, and the bubble cycle may repeat.

2. Bubble Lifetime cycle on Excess Pressure Curve

It is interesting to trace the bubble growth and collapse cycle as described above on a graph of excess pressure vs. bubble radius. Figure 77 shows the equilibrium positions for a typical nucleus. Point A on the graph is the assumed starting equil-

ibrium position. As the heat transfer surface temperature is increased, the temperature of the liquid film surrounding the nucleus also increases. The resulting higher vapor pressure causes the nucleus radius to increase so that the growth of the nucleus follows the line A-B. When the critical liquid film temperature is exceeded, the nucleus grows to form a bubble. Since heat is removed from the liquid film surrounding the bubble, the vapor pressure falls below the isothermal line. The bubble grows following a line such as B-C. At Point C, sufficient heat has been removed from the liquid film to lower the bubble path line to the equilibrium position. The bubble would remain stagnant at this point were it not for the transfer of heat from the liquid film into the cooler bulk liquid. An additional factor which decreases the vapor pressure in the bubble is the decreased evaporation as a result of the movement of the bubble base away from the hot wall. As a result of decreasing the average liquid film temperature, the vapor pressure within the bubble falls below the surrounding liquid pressure. The bubble then collapsed back to radius A along a path such as C-D.

As soon as the liquid film has received sufficient heat from the wall, the cycle may repeat.

3. Influence of Liquid Conditions on Bubble Dynamics

In order to substantiate further the proposed mechanism of bubble dynamics in degassed water, an attempt will be

made to predict the effects of liquid temperature, wall temperature, heat flux and liquid pressure on the bubble size and velocity. These predictions will then be compared with the experimental data.

(a) Effect of Liquid Temperature

In the proposed mechanism of bubble growth it was indicated that the degree of superheat in the liquid film controlled the growth rate, Equation (15). Since the initial superheat is determined by the quantity of gas within the nuclei and the magnitude of the liquid surface tension, Equation (11), it would be expected that the initial growth rate would remain substantially independent of liquid temperature. The average growth rate however, would be lowered slightly for a lower liquid temperature because of a more rapid decrease of the temperature of the liquid film surrounding the bubble. The collapse rate should be more strongly influenced by the liquid temperature. The bubble collapse rate would increase with decreasing liquid temperature because of the lower bubble film temperature and consequently greater condensation rate. These effects are seen in the experimental results shown in Figures 52 through 58. In these Figures the life cycles of five different bubbles are shown for liquid temperatures from $62^{o}F$ to $177^{o}F$. The pressure was 1 atm for all of these cases and the heat flux was at 50 per cent of the peak value. Under these conditions the average bubble growth-rate was

within 8 per cent of 3.8 ft/sec for the six different temperatures whereas the collapse rates were 5.6, 4.0, 3.9, 3.5 and 3.1 ft/sec at 62, 78, 125, 135, 177°F, respectively.

For a constant pressure, the bubble should reach a smaller maximum radius as the liquid bulk temperature is decreased. This prediction follows directly from the fact that the growth rate would be constant or slightly decreased and the knowledge that a lower bulk temperature will decrease the growth time by removing the superheat from the liquid film surrounding the bubble more rapidly. Consequently, the bubble radius at which condensation and evaporation are equal should decrease for a lower liquid bulk temperature. Reference to Figure 58 shows that the typical maximum radii decreased from .022 in. to .0135 in. as the bulk temperature was decreased from 177°F to 62°F. The trend of the experimental data agrees with the prediction.

Since (1) the growth rate is substantially independent of liquid temperature, (2) the collapse rate increases for lower liquid temperature, and (3) the maximum bubble radius decreased for decreased liquid temperature, it is obvious that the total lifetime should also decrease. Referring again to the results shown in Figure 58, the average lifetimes of the bubbles decreased from 1100 microsec at 177°F to 500 microsec at 62°F.

As seen from the foregoing comparison, the growth rate, maximum radius and lifetime as determined from the motion pictures actually are influenced by the bulk temperature of the liquid as predicted from the proposed mechanism.

(b) Effect of Wall Temperature

The temperature of the heat transfer surface may be increased by supplying more power to the heating strip. As a result the adjoining liquid film temperature will increase and result in activating a greater number of nuclei. The bubbles will create turbulence in the liquid close to the wall and thus cool the liquid film surrounding the neighboring bubbles. This increased cooling rate over the value obtained at a lower bubble population decreases the time needed to lower the liquid film temperature to the value needed to balance the evaporation and condensation rates. Because of the increased cooling, the collapse rate of the bubble should increase. Thus, an increase in the heat flux (i.e. wall temperature) should result in lower maximum bubble radius and shorter lifetime.

Figures 46 through 49 show bubble cycles at 1 atm. pressure and at heat fluxes of 31, 34, 63 and 74 per cent of the peak heat flux. The corresponding maximum radii are 0.0195 in., 0.0195 in., 0.0185 in., and 0.0175 in.; the lifetimes are 900 microsec, 900 microsec, 850 microsec, and 800 microsec. respectively. The decrease in size and lifetime that was pre-

dicted is evidenced by these experimental data.

It should be realized that the possible increase in wall temperature by increasing the heat flux is limited by the rapid increase in bubble population with wall temperature which soon results in burnout of the heating strip. The effects discussed above were correspondingly small. The effect of increasing wall temperature while maintaining the bubble population constant (e.g. by increasing the liquid pressure) will be discussed in the next section.

(c) Effect of Pressure

It has been proposed in the preceding pages that a bubble was generated when the vapor pressure was sufficiently great to overcome the surface tension force. The temperature of the liquid film surrounding the bubble corresponded to the saturation temperature at the required vapor pressure. The growth rate was controlled by the rate of evaporation into the bubble, and the evaporation rate was controlled by the liquid film temperature. As a consequence of the bubble generation being controlled by the vapor pressure, a large change of saturation temperature with pressure would result in a high bubble growth rate. With this fact in mind, we may discuss the influence of pressure on the bubble dynamics.

The effect of increased liquid pressure would be to tend to drive the gas in the nuclei into solution with the liq-

uid. However, the solubility may not increase since the liquid film temperature would increase with higher pressures and thus tend to decrease the solubility. Assuming as a first approximation that the mass of gas contained within any nucleus does not decrease at higher pressures, the critical excess pressure at a liquid pressure of 2000 psi as calculated by Equation (13) would be 5 psi. The corresponding excess temperature is less than 1°F. The excess pressure at the high liquid pressure was about 1/3 the value at 1 atm because the higher wall temperature resulted in a lower surface tension. The excess wall temperature was 1/60 of the value at 1 atm because of the small change of saturation temperature with pressure at a liquid pressure of 2000 psi.

From Figure 81 taken from Reference 3, it can be seen that the measured excess temperature for degassed water decreases from 60°F at 1 atm to 5°F at 2000 psi. The lack of solubility data for water at high pressures and temperatures prevents a rigorous calculation from being made to predict the excess temperature variation with pressure. The assumption of no increase in solubility at the higher liquid pressures results in an estimated excess temperature curve having the same trend but considerably below the experimental data (Cf. Fig. 81). If the solubility of air in water does increase at higher pressures, the two curves would be in better agreement.

Having estimated that the excess temperature would decrease with an increase in liquid pressure, we may predict the influence of pressure on the behavior of the nucleate bubbles.

The lower excess temperature at higher pressures would decrease the evaporation rate and consequently decrease the bubble growth rate. This prediction is compatible with the small amount of data available on the growth rate of bubbles at high liquid-pressures.

The alternate case of boiling in a liquid having a very low pressure now may be considered. The large change of saturation temperature with pressure would result in high evaporation rates. The bubble would be expected to grow more rapidly in the liquid having a low pressure. As an example, bubbles forming in water subjected to an absolute pressure of 0.1 psi would be expected to have a liquid film excess temperature of 150°F as calculated from Equation (11). The high evaporation rate for this excess temperature would maintain a high excess pressure while the bubble grew to a much larger size than bubbles forming in a liquid having a higher pressure and equal subcooling. The extremely high superheat should cause the bubbles to form in an explosive manner. The well-known high bubble-growth rates obtained in vacuum distillation apparatus substantiates this prediction.

The collapse rate of the bubble depends on the liquid subcooling and the condensation rate. For constant subcooling, the bubble collapse rate should be lower at the higher pressures.

The change in latent heat of evaporation has to be considered at the very high pressures. If the latent heat decreases, the heat which has to be taken from the liquid surrounding the bubble to fill the cavity with vapor is decreased also. The lower latent heat will tend to keep the temperature of the film surrounding the growing bubble at a value closer to the initial film temperature and thus tend to increase the evaporation rate. The initial difference between the film temperature and the saturation temperature, however, is so strongly affected by pressure, as mentioned above, that the effect of the latent heat should be almost negligible in comparison.

D. The Mechanics of Bubble Growth and Collapse in a Degassed-Bulk Boiling Liquid

The formation and growth of a bubble in a degassed-bulk boiling liquid should be the same as in the degassed-subcooled liquid. The only difference is that the maximum bubble size is larger for the bulk boiling as would be expected from the discussion in Section IV-C-3. Since no net condensation can occur, the bubble will grow until the buoyant force or sur-

rounding liquid current carries it off of the heat transfer surface. At high bubble population the neighboring bubbles may create sufficient turbulence in the liquid to wipe the bubble off of the wall. Several frames of bulk boiling water shown in Figure 82 support these conclusions. It should be noted that bubbles forming in a liquid having a small subcooling would also exhibit this life cycle. In this case, the condensation rate is small so that the bubble may travel an appreciable distance away from the wall before condensing (Cf. Fig. 83).

The bubbles forming in a bulk boiling liquid would be expected to have a smaller growth rate at higher liquid pressures for the same reasons as presented in the preceding section.

E. The Mechanism of the Dynamics of Bubbles in an Aerated Liquid

The life cycle of a bubble growing in a liquid which contains a high concentration of gas is considerably different from the vapor bubble described in Section IVC. This gas-vapor type of bubble occurred in tests of water having more than 18 cc air/liter water (water at 212°F and 1 atm. is saturated when 13 cc air is dissolved in one liter of water).

As before, the growth and collapse process will be discussed in steps. The Sketches of Figure 84 correspond to the

enumerations of the following paragraphs.

a) The liquid next to the wall is superheated.

b) A nucleus of sufficient size is present so that the bubble may form. Because of the high concentration of gas in the liquid, the nuclei would contain a greater gas pressure. As a result the wall temperature required to initiate boiling would be expected to be less than for the degassed liquid (Cf. Fig. 77).

c) Since the solubility of most gases decreases with temperature, the liquid film surrounding the nucleus may be supersaturated with the dissolved gas even though the bulk of the liquid is undersaturated with gas. The bubble to be described in the first part of this section is growing in a liquid which has been saturated with gas. As a consequence, the superheated boundary layer would be supersaturated with gas. (A bubble growing in a liquid which is undersaturated with gas is discussed on Page 79). The liquid also contains an appreciable quantity of gas in the form of sub-microscopic gas-vapor nuclei. It would be expected that the number of these nuclei would be greater than in the degassed liquid and that there consequently would be a greater number of large nuclei that would form bubbles at a relatively low excess pressure. Thus the average bubble growth rate should be somewhat less than for the vapor bubble for the reasons given in Section IV-B. As the bubble grows, the gas contained in the liquid film surrounding the bubble would diffuse into the bubble.

d) Let us now consider the instant at which the evaporation and condensation rates are equal. This instant is illustrated in Sketch d of Figure 84. Unlike the pure vapor bubble, there still will be a net mass addition into the gas-vapor bubble because of the diffusion of gas. If the rate at which the gas enters the bubble is sufficiently great, the bubble will maintain its shape.

e) The partial pressure of the vapor in the bubble decreases since the film has lost heat to the cooler bulk liquid. The condensation rate now exceeds the evaporation rate. Since the bubble base was not dragged away from the heat transfer surface by the surrounding low-velocity liquid, the net condensation will be small. If we assume a diffusion rate that is higher than the net condensation rate, the bubble will continue to grow slowly. This would be the case for a high concentration of gas in the liquid.

f) In the next step the saturation temperature isotherm has reached an equilibrium position where the heat lost by the combined processes of conduction to the cooler liquid and evaporation is balanced by the heat supplied by the processes of conduction from the wall and condensation. The bubble continues to grow although at an extremely low rate since gas continues to diffuse into the bubble. The bubble contains an appreciable amount of gas as has been verified experimentally. When the electrical power was shut off, the bubble decreased less than

10 per cent in radius and thus it was indicated that the majority of the bubble was filled with a non-condensable gas. At first, it is difficult to explain the large diffusion rate because the normal rate of diffusion of air in water is less than 10^{-5} times the rate at which this bubble formed. One has to realize, however, that the liquid film is super-saturated with gas, and that an additional increase in rate over the diffusion rate in still water is possible since the liquid film surrounding the bubble was supplied continuously with non-degassed liquid due to the induced currents. These currents were examined experimentally. Close photographic examination of the bubble indicated that the liquid film was rotating at a maximum velocity of approximately 3 in./sec. Figure 61 is a series of pictures taken of graphite traces on the bubble surface. It is concluded that the gas-vapor bubbles forming in a liquid containing a high concentration of dissolved gases will grow to a maximum size and remain substantially stagnant on the heat transfer surface. Although the initial growth rate of these bubbles is close to the growth rate for the vapor bubbles, the gas-vapor bubble will not collapse when the net evaporation into the bubble ceases. The bubble continues to grow because of diffusion of gas into the cavity. A series of photographs showing a bubble growing in water saturated with air is given in Figure 85.

Bubbles forming in water which is undersaturated with gas

would be expected to exhibit a behavior similar to both the degassed liquid and gas-saturated liquid. The pressure of the gas within the nuclei for this case should be lower than in the liquid that is saturated with gas. As a result the wall temperature required to initiate boiling would be slightly higher than for the saturated liquid. One would expect the diffusion of gas into the bubble to be lower for the under-saturated liquid. In such a case the condensation rate may exceed the gas diffusion rate and the bubble would tend to collapse. A small residual gas bubble would remain after the vapor has been condensed. If the gas bubble is not stabilized on a nonwettable solid, the gas would diffuse into the liquid for the reasons presented in Section IV-B.

Bubbles have been observed in water containing less than 12 cc air/liter of water. In this intermediate aerated liquid, the bubbles grew to approximately the same size as the vapor bubble and collapsed, leaving a small residual gas bubble as predicted (Cf. Fig. 60).

F. The Mechanism of Bubble Growth and Collapse in Degassed-Subcooled Carbon Tetrachloride

Figure 86a shows a typical photographic sequence of a bubble forming in degassed-subcooled carbon tetrachloride. In addition a series of Sketches is given in Figure 86b to illustrate the steps in the following discussion.

a) In Sketch a of Figure 86 the temperature of the heat transfer surface is above the liquid saturation temperature.

b) Assuming the same size of nuclei as was required to form a bubble in water, it is seen from Figure 87 that the excess pressure would be about 5 psi. The corresponding excess temperature is about 20^{o}F. This value agrees with the experimental data presented in Figure 39. It is interesting to note that an assumed nucleus radius of 3×10^{-5} in. results in a correct estimate of wall temperature for both the carbon tetrachloride and the water.

As a result of the lower excess pressure, the initial growth rate of the carbon tetrachloride bubble would be about half of the water bubble growth rate. The measured growth velocities for carbon tetrachloride bubbles at atmospheric pressure are shown in Figures 68 through 71. The average bubble velocities for various liquid temperatures are shown in Figure 72. It is seen by comparing Figures 58 and 72 that the carbon tetrachloride-vapor bubble velocity is about 1/4 as great as for the water-vapor bubble at the same condition.

As a result of the slower bubble growth in carbon tetrachloride, the surrounding liquid would be forced away from the wall at a lower velocity.

c) The bubble continues to grow thereby stretching the superheated film of liquid. Heat is transferred from the film

to the subcooled bulk of the liquid.

d) The film surrounding the pole of the bubble has been cooled to the saturation temperature and evaporation ceases from this area.

e) The saturation temperature isotherm which separates the evaporation and condensation areas has approached the wall so that the condensation area has increased.

f) All of the liquid that is now evaporated from the lower area of the bubble is condensed on the upper area of the bubble. Since there is no net flow of vapor into the bubble, there is no further growth (except for the small change in the volume of the bubble that is necessary to decrease the excess pressure to a zero value). The low growth rate of the bubble coupled with the lower thermal conductivity has resulted in a maximum bubble size approximately one half that for the water vapor bubble (compare Fig. 58 and 72).

g) In Section IV-B, it was seen that the initial rate of growth of any bubble in a given liquid depended on the pressure of the gas within the nucleus. The low thermal conductivity of the carbon tetrachloride is insufficient to transfer enough heat from the liquid film surrounding the bubble to cause a net condensation, unless the base of the bubble is moved away from the heat transfer surface. As a result of these two factors, it may be concluded that the bubbles orig-

inating from some nuclei may collapse while the bubbles originating from other nuclei will grow to a maximum size and remain stagnant.

Figure 86 shows a bubble that has originated from a nucleus having a suitable geometry and containing a small quantity of gas so as to result in a high evaporation rate and thus a relatively high growth rate. The surrounding carbon tetrachloride has been forced away from the wall by the growing bubble with sufficient velocity to drag the bubble away from the wall when the net evaporation ceases.

It will be recalled that the water-vapor bubble that was discussed in Section IV-C had a similar tendency to detach from the heating strip. However, the higher thermal conductivity in the water resulted in greater rate of heat transfer so that the water vapor was condensed and thus the bubble collapsed before it could be carried away from the wall. At very low subcooling, the heat transfer from the water film into the bulk of the liquid was lower and the bubble was carried an appreciable distance away from the heat-transfer surface before collapsing.

Figure 88 shows a bubble that has originated in carbon tetrachloride from a nucleus with conditions which result in a low evaporation rate and thus relatively low growth velocity. The surrounding liquid has insufficient velocity to drag the

bubble away from the hot wall. In this case the heat transferred from the liquid film to the cooler bulk liquid is balanced by the heat supplied by condensation and conduction from the hot wall. As a result the bubble remains stagnant on the heating strip.

The addition of Aerosol to water decreased the surface tension of the solution to approximately the same value as for the carbon tetrachloride. As would be expected from the above discussion, bubbles forming in Aerosol-water solution resembled the carbon tetrachloride bubble by growing slowly and aften remaining stagnant on the strip (Cf. Fig. 62). It may be concluded that the thermal conductivity of the water is also insufficiently great to result in conducting more heat away from the bubble pole than is transferred to the pole. As a result the bubble will not collapse unless the base is removed from the hot liquid adjacent to the heat transfer surface.

The remainder of this discussion will describe the collapse phase of the life cycle for the bubbles which are dragged away from the wall.

h) The bubble which detaches from the heat transfer surface floats into the subcooled bulk of the liquid and is replaced at the wall by cool liquid.

i) The vapor within the bubble condenses on the subcooled film. The latent heat from the condensation is transferred to

the surrounding subcooled liquid. The rate of condensation is lower than for the water-vapor bubble because of the smaller subcooling in the bubble film as a result of the low thermal conductivity. The latent heat per unit volume of vapor also is a factor controlling the bubble film temperature. However, this quantity is about equal for water and carbon tetrachloride under the existing conditions.

j) The velocity of the liquid near the wall has decreased and the boundary layer has been heated.

k) The boundary layer has been superheated so that the bubble cycle may repeat.

The carbon tetrachloride vapor bubbles can be seen several maximum bubble diameters away from the heat transfer surface, while the water vapor bubbles usually collapsed entirely while remaining within 0.001 in. of the wall. The major cause for this different behavior is the lower thermal conductivity of the carbon tetrachloride and the resultant longer collapse time.

The bubbles forming in degassed-subcooled carbon tetrachloride would be affected by changes in the bulk temperature, wall temperature, and liquid pressure in a similar manner to the bubbles forming in degassed-subcooled water for the same reasons as given in Section IV-C.

V. PROPOSED MECHANISM OF NUCLEATE-BOILING HEAT TRANSFER

A. Introduction

The bubble growth and collapse cycle discussed in the preceding Sections may be used to predict the variation of boiling heat transfer for various liquid conditions.

It was discussed in Section IV-C-1 that the rate of transport of latent heat through the bubble was insignificant compared to the measured total heat transfer. Jakob (Cf. Ref. 7) calculated the heat required to fill nucleate bubbles with vapor and concluded that this mechanism also could not account for the high rates of boiling heat transfer. As a result, Jakob proposed that the high rates of heat transfer that were observed in pool bulk boiling were the result of the agitation of the liquid near the hot wall by the action of the nucleate bubbles. Gunther (Cf. Ref. 15) performed similar calculations and suggested that this same mechanism of induced liquid turbulence may account for the high heat transfer rates in subcooled liquids.

B. Bubble Induced Liquid Turbulence

It was noted in the discussion of bubble dynamics that the liquid surrounding the bubble was forced away from the heat-transfer surface during the growth period of the bubble. For vapor bubbles forming in subcooled water, the liquid was drawn back toward the wall during the collapse period of the bubble

cycle. The resulting liquid flow pattern is shown in Figure 89 (a). The same liquid flow pattern would not be formed by the gas-vapor bubbles or carbon tetrachloride bubbles. Since the latter two types of bubbles detached from the heat transfer surface before collapsing, the induced liquid flow would be as shown in Figure 89 (b). It is believed, however, that the liquid velocity induced by either the non-detaching bubbles or the detaching bubbles may be related to the bubble growth and collapse velocities. In attempting a correlation, it seems reasonable to select the average bubble velocity (i.e. $\frac{\text{max. bubble diameter}}{\text{bubble lifetime}}$) as the typical velocity for both the degassed-water bubble and the carbon tetrachloride vapor bubble. The local induced liquid velocity may be related to this typical velocity.

In addition to depending on the bubble velocity, the average liquid velocity over the entire heat-transfer surface also would depend on the distribution of the bubbles causing the liquid velocity. In order to include the effect of the distribution of bubbles on the induced liquid velocity, a bubble population parameter, ξ, will be introduced, so that

$$v_L \sim \varphi_1(\xi)\,\varphi_2(\dot{r})$$

where: v_L = effective velocity of the liquid to cool the wall

ξ = bubble population parameter

$\dot{r}$ = bubble velocity

To relate the effective liquid velocity to the heat flux, we may try the usual dimensionless parameters that have correlated successfully forced-convection heat transfer. The Nusselt number is related to the Reynolds and Prandtl number as follows:

$$Nu = C Re^{\alpha} Pr^{\beta}$$

Substituting the effective velocity and bubble radius into this relation results in the following expression for nucleate boiling heat transfer:

$$\frac{q}{a} = C_1 \frac{k}{r_{max}} \left(\frac{\rho \xi \dot{r} r_{max}}{\mu} \right)^{\alpha} \left(\frac{c\mu}{k} \right)^{\beta} \left(T_W - T_L \right) \qquad (16)$$

where: $(\xi \dot{r})$ has replaced the free-stream velocity and the maximum bubble radius has replaced the hydraulic diameter.

It was shown in the introduction that the principal information needed for the design of heat-transfer apparatus operating in the nucleate-boiling region are the peak-heat-flux values for a range of liquid conditions. As a result, it would be important to rewrite Equation (16) to apply at the peak-heat-flux point. The Equation may be rewritten after recalling some of the experimentally determined facts about nucleate boiling.

It was seen in Section V-C of Part I, that the heat

flux in the nucleate-boiling region could be increased appreciably with little change in the wall temperature or bubble velocity. Thus, if Equation (16) represents the heat transfer properly, the heat transferred by nucleate boiling may be increased from incipient boiling to the peak heat flux with the major change being the population of the nucleate bubbles. The population parameter ξ which relates bubble velocity to induced liquid velocity should be a function of (1) the ratio of average distance between bubbles to the average bubble radius and (2) the Reynolds number based on bubble velocity. As the bubble population increases, a point would be reached at which the average induced liquid velocity would be a maximum. This point of maximum liquid velocity should correspond to the point of peak heat flux. As a first approximation, it seems permissible to replace the population parameter by the product of the Reynolds number to some power and a factor which is relatively insensitive to the liquid properties and conditions at the peak heat flux point. The validity of this assumption may be verified by rewriting Equation (16) and comparing the predicted values of peak heat flux with the experimental data. At the point of maximum liquid velocity, it seems permissible to replace the population parameter, ξ , with a factor that should be approximately constant regardless of liquid properties or conditions. Therefore, we may write the peak heat flux as

$$\left(\frac{q_b}{a}\right)_p = C_2 \frac{k}{r_{max}} \left(\frac{\rho \dot{r} r_{max}}{\mu}\right)^{\alpha} \left(\frac{c\mu}{k}\right)^{\beta} (T_w - T_L) \qquad (17)$$

where: C_2 has replaced the product $C_1 (\xi)^{\alpha}$ of Equation (16).

The three constants appearing in Equation (17) may be evaluated by choosing the values which best fit the experimental data for distilled water, water-Aerosol solution and carbon tetrachloride. The values were: $C_2 = 0.053$, $\alpha = 0.8$, $\beta = 1.0$.

The calculated peak-heat-flux values for distilled water and water-Aerosol solution are shown in Figure 90. It is seen that the experimental peak-heat-flux points are within 15 per cent of the estimated curve. The calculated peak-heat-flux values for degassed carbon tetrachloride are plotted in Figure 91. The experimental data again are seen to be within 15 per cent of the estimated curve.

It will be of interest to consider the factors responsible for the trend and the relative positions of the peak-heat-flux curves plotted in Figures 38 and 41 for the degassed water, Aerosol-water solution, aerated water, degassed carbon tetrachloride and aerated carbon tetrachloride. The trend and relative positions of the curves are discussed in the following Section.

C. Effect of Liquid Conditions on Peak Heat Flux

1. Shape of Peak-Heat-Flux Curves

As the bulk-liquid temperature was decreased, the bubble collapse velocity increased slightly (Cf. Sect. IV-C-3), and the physical properties of the liquids also changed slightly. For all liquids studied, the changes of bubble velocity and physical properties with liquid temperature were small compared to the change in the factor $(T_W - T_L)$. As a result, the peak heat flux decreased with an increase of liquid temperature.

2. Relative Positions of Peak-Heat-Flux Curves

To investigate the effect of surface tension on the

boiling process, one per cent of Aerosol was added to the water. The photographic study showed that the bubble velocity decreased to about 1/2 the value for the bubbles growing in distilled water. The lower bubble velocity resulted from the decrease in surface tension for the reasons discussed in Section IV-F. From Equation (17) it can be predicted that the lower bubble velocity should produce a lower peak heat flux. It is seen in Figure 38 that the burnout values for the Aerosol-water solution are considerably lower than for the distilled water.

The carbon tetrachloride bubble velocity was about 1/4 the distilled water bubble velocity. The lower bubble velocity coupled with lower thermal conductivity resulted in lower peak-heat-flux values for the carbon tetrachloride (Cf. Fig. 41).

It was proposed in Section IV-E that the amount of gas dissolved in a liquid up to the saturation condition corresponding to the wall temperature, would be expected to decrease the bubble velocity a small amount. However, increasing the concentration of gas above the wall temperature saturation condition would be expected to cause a significant decrease in the bubble velocity and result in stagnant bubbles. It was also noted, as predicted, that the difference between the wall temperature and the saturation temperature was slightly decreased (Cf. Fig. 39). From Equation (17), it is predicted

that the lower wall temperature and smaller bubble velocity would result in a lower peak heat flux. It is seen in Figures 38 and 41 that both aerated water and aerated carbon tetrachloride had lower peak-heat-flux values than the corresponding degassed liquids.

3. Liquid Pressure and Free-Stream Velocity

The present investigation of the mechanism of nucleate boiling heat transfer was confined to a study of atmospheric pool boiling. Although no data were taken to study to effects of liquid pressure and free-stream velocity, it will be of interest to consider, briefly, the possible influence of these two factors on the boiling process.

It was seen in Section IV-C-3 that the bubble velocity would be expected to decrease for an increase of liquid pressure. As a result, the heat-transfer coefficient would tend to be lower at high pressures. This decrease, however, may be overcome by the higher wall temperature and resulting lower liquid film viscosity. Since no data are available for the bubble velocity at high pressures, it is not possible to check the validity of the proposed correlation in Equation for a range of pressures.

The effect of forced convection on boiling heat transfer also has not been studied in detail. It is known that the nucleate bubbles slide downstream at about 8/10 of

the free-stream velocity. The sliding motion may be visualized as coupling with the bubble velocity to produce additional turbulence in the liquid boundary layer. Regardless of the manner in which the free stream velocity and the bubble velocity combine, it would be expected that: (1) an increase in the free stream velocity would increase the peak heat flux values (2) for free stream velocities much lower than the bubble velocity, the peak heat flux should be insensitive to changes in free-stream velocity and (3) for free-stream velocities much greater than the bubble velocity, the peak heat flux should be more sensitive to changes in the free-stream velocity.

These general predictions have been verified experimentally: (1) Figure 92 from Reference 15 shows that the peak heat flux increases with velocity (2) McAdams found for low free-stream velocity that the peak heat flux correlated with the free-stream velocity to the 1/3 power for velocities from 1 to 12 ft/sec and (3) Gunther found for high free-stream velocities that the peak heat flux correlated with free-stream velocity to the 1/2 power for velocities from 5 to 40 ft/sec.

D. Conclusion

The agreement between the calculated peak heat flux and the measured burnout points supports the assumption that the principal mechanism of heat transfer by nucleate boiling is not latent-heat transport but rather convective heat transfer

by the induced liquid velocity. As discussed previously, the bubble velocity data may be in error as much as 20 to 30 per cent. However, the predicted-heat-flux curves would still be in reasonable agreement with the experimental data.

In view of the small heat transfer that may be accounted for by latent heat transport and the agreement between the predicted and experimentally determined values of peak heat flux when using Equation (17), it seems likely that the induced turbulence in the liquid boundary layer is the basic mechanism by which heat is transferred in the nucleate boiling region.

REFERENCES

1. Mosciki, I., and Broder, J., Heat Transfer from a Platinum Wire, Roczniki Chemii, 6:319-354, 1926 (complete English translation on file at Engineering Research Laboratory Experimental Station, E. I. du Pont de Nemours and Company, Wilmington, Del.)

2. McAdams, W. H., Addoms, J. N., and Kennel, W. E., Heat Transfer at High Rates to Water with Surface Boiling, Report No. ANL-4268, Cambridge: Massachusetts Institute of Technology, December 1948.

3. Tramontini, V. N., et al, Studies in Boiling Heat Transfer, Final Report. Los Angeles: University of California, March, 1951.

4. Gunther, F. C., Photographic Study of Surface-Boiling Heat Transfer to Water with Forced Convection, Trans. ASME, Vol. 73 No. 2, Feb. 1951.

5. Nukiyama, S., J. Soc. Mech. Engrs, Japan: 37:367, 1934.

6. Bromley, L., Heat Transfer in Film Boiling from Horizontal Tubes, Report No. MDDC-1628, Oak Ridge, Tenn: Technical Information Division, U. S. Atomic Energy Commission.

7. Jakob, M., Heat Transfer, New York: John Wiley and Sons, 1949.

8. Drew and Mueller, Boiling, Trans. AICE, Vol. 33, 1937, pp. 449-473.

9. McAdams, et. al., Heat Transfer from Single Horizontal Wires to Boiling Water, Chem. Eng. Progress, Vol. 44, 1948, pp. 639-646.

10. King, W. J., The Basic Laws and Data of Heat Transmission, Part VI, Evaporation and Condensation, Mech. Eng., Vol. 54, 1932, pp. 560-565.

11. Sauer, E. T., Heat Transfer to Boiling Liquids, Thesis, Mass. Inst. Tech., 1937.

12. Akin and McAdams, Boiling Heat Transfer in Natural Convection Evaporators, Trans. AICE Vol. 35, 1939, pp. 137-155.

13. Farber and Scorah, Heat Transfer to Water Boiling Under Pressure, Trans. ASME, Vol. 70, 1948, pp. 369-384.

14. Kaulakis and Sherman, Effect of Pressure on Heat Transfer to Boiling Liquids, Thesis, Mass. Inst. Tech., 1938.

15. Gunther and Kreith, Photographic Study of Bubble Formation in Heat Transfer to Subcooled Water, Prog. Rept. No. 4-120, Jet Prop. Lab., Calif. Inst. Tech., March 1950.

16. Knapp and Hollander, Laboratory Investigation of the Mechanism of Cavitation, Trans. ASME, Vol. 70, 1948, p. 419.

17. Harvey, E. N., et. al., On Cavity Formation in Water, J. App. Ph., Vol. 18, 1947, p. 162.

18. Plesset, M. S., The Dynamics of Cavitation Bubbles, J. App. Mech., September 1949.

19. Ellis, Observations on Cavitating Bubble Collapse, Thesis, Calif. Inst. Tech., 1953.

20. Dergarabedian, P., The Rate of Growth of Vapor Bubbles in Superheated Water, Thesis, Calif. Inst. Tech., 1952.

21. Gilmore, F., The Dynamics of Condensation and Vaporization, Thesis, Calif. Inst. Tech., 1951.

22. Bowersox, R. B., Use of Kerr Cells in a High-Speed Camera, Progress Report No. 4-114 JPL Calif. Inst. Tech., Oct. 1949

23. Frenkel, J., Kinetic Theory of Liquids, Oxford at the Clarendon Press, 1946.

24. Epstein and Plesset, On the Stability of Gas Bubbles in Liquid-Gas Solutions, J. Chem. Ph., Vol. 18, No. 11, 1950, pp. 1505-1509.

25. Parkin, B. R., Scale Effects in Cavitating Flow, Rept. No. 21-8, Hydrodynamics Laboratory, Calif. Inst. Tech., July 1952.

26. Penner, S., On the Kinetics of Evaporation, J. Ph. Chem., Vol. 56, 1952, pp. 475-479.

27. Volmer, M., Kinetik Der Phasenbildung, Verlag Von Theodor Steinkopff, 1939.

28. Roebuck, J. and Osterberg, H., The Joule-Thomson Effect in Nitrogen Trans. ASME, Vol. 48, 1935, p. 450.

APPENDIX

ANALYSIS OF FILM BOILING ON A VERTICAL HEATING SURFACE

A rigorous analysis of the film-boiling heat-transfer mechanism is beyond the scope of this experimental investigation. However, a simple analysis may be carried out and the results compared with the experimental data by employing the following assumptions:

1. The vapor flow is steady with physical properties independent of temperature.
2. Vapor body forces are negligible compared with viscous pressure, and inertia forces.
3. The change in vapor velocity along the tube is small compared with the radial-velocity gradient (i.e. $\frac{\partial u}{\partial x} << \frac{\partial u}{\partial y}$). It is also assumed that $u \frac{\partial u}{\partial x} << v \frac{\partial u}{\partial y}$.
4. The evaporation rate is constant along the tube (i.e., $\dot{m} = \rho_v v \neq \dot{m}(x,y)$).
5. The vapor density is independent of the radial (y) position, [i.e., $\rho_v = \rho_v(x) \neq \rho_v(y)$] .
6. The pressure drop along the tube due to liquid flow is much less than the buoyant forces (i.e., $\frac{\partial p}{\partial x} \simeq -\rho_l$).
7. The water velocity at the water vapor interface is small compared with the average velocity of the vapor in the film (i.e., the vapor-film velocity is substantially zero at the tube surface and the water interface).

8. Heat is transferred across the vapor film from the wall to the water by conduction and radiation only.
9. All the heat leaving the tube is used to vaporize the liquid. (This assumption neglects the heat that may be transferred to the bulk of the liquid as well as the heat that may be absorbed by the vapor to increase its temperature above the saturation point.)
10. The vapor film is smooth.
11. The vapor-liquid interface is at the saturation temperature.

The general momentum equation in the x direction may be written as

$$\frac{\rho}{g}\frac{du}{d\theta} = -\frac{\partial p}{\partial x} + \rho_g X + \frac{1}{3}\mu\frac{\partial \Theta}{\partial x} + \mu\nabla^2 u \qquad \text{(A-1)}$$

Using assumption 1 through 5 and neglecting the effect of evaporation on the momentum change, this equation may be simplified for the vapor film as follows:

$$\frac{\partial^2 u}{\partial y^2} - \frac{1}{\mu}\frac{\partial p}{\partial x} = 0 \qquad \text{(A-2)}$$

By assumption 6

$$\frac{d^2 u}{dy^2} + \frac{\rho_l}{\mu} = 0 \qquad \text{(A-3)}$$

Integration of Equation (A-3) gives

$$u = C_1 + C_2 y - \frac{\rho_l}{\mu}\frac{y^2}{2} \qquad \text{(A-4)}$$

The boundary conditions given by assumption 7 are

$$u = 0 \quad \text{at} \quad y = t \quad \text{and} \quad y = 0$$

Then

$$u = \frac{\rho_\ell g}{2\mu}\left[t\frac{y}{2} - \frac{y^2}{2}\right] \tag{A-5}$$

The velocity may be eliminated and an expression obtained for the film thickness t by the continuity requirement

$$\int \dot{m}\,\pi D\,dx = \int \rho_v\,\pi D u\,dy \tag{A-6}$$

where x = o at the start of the heating section.

For $\dot{m}$ and ρ_v independent of x and y, respectively,

$$\frac{\dot{m}x}{\rho_v} = \int_0^t u\,dy \tag{A-7}$$

The velocity may now be eliminated by substituting Equation (A-5) in Equation (A-7) and integrating

$$\frac{\dot{m}x}{\rho_v} = \frac{\rho_\ell t^3}{\mu\ 12} \tag{A-8}$$

For the case where the radiant heat transfer is negligible, assumptions 9, 10 and 11 may be used to eliminate the evaporation rate from Equation (A-8)

$$\frac{q}{a} = k\,\frac{\Delta T_{sat}}{t} = \dot{m}\lambda$$

or

$$\dot{m} = k\,\Delta T_{sat}/t\lambda \tag{A-9}$$

Then Equation (A-9) and (A-8) lead to

$$t^4 = 12 \frac{k \Delta T_{sat}}{\lambda} \frac{\mu x}{\rho_L \rho_v} \tag{A-10}$$

or defining a heat transfer coefficient for the heat conducted across the vapor film at point x

$$h'_{C_x} = \frac{\frac{q}{a}}{\Delta T_{sat}} = \frac{k}{t}$$

Then

$$h'_{C_x} = \left[\frac{\lambda \rho_L \rho_v k^3}{12 \Delta T_{sat} x \mu} \right]^{\frac{1}{4}} \tag{A-11}$$

Equation (A-11) represents the heat-transfer coefficient at the position x. To obtain the average heat transfer coefficient for a heating length L

$$h_C = \int_0^L h'_{C_x} \frac{dx}{L}$$

$$= \int_0^L \left[\frac{\lambda \rho_L \rho_v k^3}{12 \Delta T_{sat} x \mu} \right]^{\frac{1}{4}} \frac{dx}{L}$$

$$= \frac{4}{3} \left[\frac{\lambda \rho_L \rho_v k^3}{12 \Delta T_{sat} L \mu} \right]^{\frac{1}{4}} \tag{A-12}$$

where ΔT_{sat} is the average value between x = o and x = L.

It is not surprising to note that Equation (A-12) with the exception of the factor 12 is the same as the heat-transfer coefficient for film condensation. The constant factor 12 differs because

of the difference in boundary condition at y = t (Cf. Ref. 6 and 7).

The heat transfer by radiation may be expressed by the conventional relation

$$h_R = \frac{\frac{q}{a}}{\Delta T_{sat}} = \frac{\sigma}{\frac{1}{\varepsilon_w} + \frac{1}{\varepsilon_L} - 1}\left[\frac{(T_{w_\Delta} + 460)^4 - (T_{sat} + 460)^4}{\Delta T_{sat}}\right] \qquad \text{(A-13)}$$

This relation is valid if all the heat is absorbed in the water near the vapor-liquid interface.

Since the radiant heat transfer affects the thickness of the vapor film, the conduction and radiation are inextricably related. An appreciable deviation from a rigorous solution is necessary to account for the radiation in a simple manner.

Equation (A-9) becomes

$$\dot{m} = \frac{k \Delta T_{sat}}{t \lambda} \frac{q_C + q_R}{q_C}$$

and Equation (A-10) is modified to

$$t^4 = 12 \frac{k \Delta T_{sat} \mu x}{\rho_w \rho_L \lambda} \frac{q_C + q_R}{q_C}$$

The heat-transfer coefficient at point x is

$$h_{C_x} = \frac{k}{t} = \left(\frac{q_C}{q_C + q_R}\right)^{\frac{1}{4}} \left(\frac{\lambda \rho_w \rho_L k^3}{12 \Delta T_{sat} x \mu}\right)^{\frac{1}{4}}$$

or the average heat-transfer coefficient over a distance L is

$$h_C = \frac{4}{3}\left(\frac{q_C}{q_C + q_R}\right)^{\frac{1}{4}} \left(\frac{\lambda \rho_L \rho_w k^3}{12 \Delta T_{sat} L \mu}\right)^{\frac{1}{4}}$$

For the range of variables encountered in this study, the factors $\left(\frac{q_C}{q_C + q_R} \right)^{\frac{1}{4}}$ varied less than 20 per cent from unity. The error in total heat transfer that would result from neglecting this variation would be less than 10 per cent. The average total heat-transfer coefficient for the length L may be written as

$$h = h_C + h_R$$

$$= \frac{4}{3}\left[\frac{\lambda \rho_L \rho_V k^3}{12 \Delta T_{sat} L \mu}\right]^{\frac{1}{4}} + \frac{\sigma}{\frac{1}{\varepsilon_w} + \frac{1}{\varepsilon_L} - 1}\left[\frac{(T_{w_A} + 460)^4 - (T_{sat} + 460)^4}{\Delta T_{sat}}\right] \qquad \text{(A-14)}$$

A comparison of the experimental data and the heat-transfer coefficient calculated by Equation (A-14) is shown in Figure 32 where the calculated heat flux is slightly lower than the experimental data.

A detailed study of the vapor film was beyond the scope of the present investigation. However, it is interesting to compare the film thickness calculated from Equation (A-10) with the film thickness estimated from the photographs. By projecting the 16-mm picture so that the image was enlarged 100 times, it was possible to estimate the film thickness using the 0.250-inch-diameter heating tube as the base scale.

The vapor-film thickness was calculated from Equation (A-10) and the data for test number 39

$$t = \left[12\ k \frac{\Delta T_{sat}\ x \mu}{\lambda \rho_v \rho_L}\right]^{\frac{1}{4}}$$

$$= \left[12\ \frac{3.16 \times 10^{-3} (1380)\, 3 (1.81 \times 10^{-9})}{1000\ (2.29 \times 10^{-5})(3.62 \times 10^{-2})}\right]^{\frac{1}{4}} = \quad 0.0136 \text{ in.}$$

The vapor film in the photograph for test 39 was approximately 0.020 inch thick. The 32 per cent difference between the calculated and measured values is less than the probable error in estimating the vapor-film thickness shown in the photographs.

An interesting point in the region of film boiling heat transfer is the condition at which the smooth vapor film transposed into a rough film. It is reasonable to suppose that this transition would occur when the vapor in the film changed from laminar to turbulent flow. Using the data from test 23 and an arithmetic mean temperature, the Reynolds number based on equivalent pipe diameter was 220. The vapor film for this test was rough. The critical Reynolds number for turbulent flow in a pipe with forced convection is approximately 3000. In view of this high critical value, the Reynolds number of 220 obtained for this test should have been too small to produce turbulent flow.

The Reynolds number based on distance from the leading edge for flow over a flat plate was approximately 14,000 compared with the conventional critical value of 80,000. Here again the value of Reynolds number is well below the conventional critical value.

Correcting both of these Reynolds-number criteria for non-isothermal flow with mass addition probably would not account for the large discrepancies. It is possible that the rough vapor film resulted from other external factors such as variations in water flow or pressure surges from the pump.

One more rough quantitative comparison may be made between the experimental data and the calculated values. The mean vapor velocity for steady, uniform, viscous flow with accelerating forces neglected may be written as

$$u_m = -\frac{t^2}{12\mu}\frac{dp}{dx} \qquad \text{(A-15)}$$

Substituting the relation for t from Equation (A-10) gives

$$u_m = \sqrt{\frac{k\,\Delta T_{sat}\,x\,\rho_l}{12\,\lambda\,\rho_v\,\mu}}$$

$$= \sqrt{\frac{8.14 \times 10^{-7}(1200)3(.0361)}{12\,(970)(1.21 \times 10^{-5})(3.78 \times 10^{-9})}}$$

$$= 356 \text{ in/sec} = 29.6 \text{ ft/sec}$$

The estimated mean velocity obtained from measuring the photographic data was roughly 25 ft/sec.

It is concluded that, over the range of variables investigated, the derived equation will give satisfactory engineering estimates of the heat transfer in the complete-film-boiling region for a vertical heat-transfer surface. However, a more rigorous analysis should be made and experimentally verified to give better understanding of the process. Further study of the complete-film-boiling region should include measurements of the vapor-film thickness, velocity, and stability characteristics. With slight modifications, the equipment described in this report would be suitable for this detailed study of the complete-film-boiling region.

TABLE I

NOMENCLATURE

a	-	area (sq in.)
c	-	velocity of sound (in./sec)
c	-	specific heat (Btu/lb)
C, C_1, C_2	-	constants (dimensionless)
c_p	-	specific heat at constant pressure (Btu/lb-^oF)
D	-	thermal diffusivity (sq in./sec)
D	-	outside diameter of tube (in.)
D_e	-	equivalent diameter (in.)
E	-	voltage drop across the heating tube (volts)
g	-	acceleration of gravity (in./sec^2)
G	-	mass flow rate per unit area (lb/sq in.-sec)
h	-	total heat transfer coefficient (Btu/sq in.-sec-^oF)
h_C	-	conduction heat transfer coefficient when radiation is negligible (Btu/sq in.-sec)
h_C	-	conduction heat transfer coefficient when radiation is appreciable (Btu/sq in.-sec-^oF)
h_R	-	radiation heat transfer coefficient (Btu/sq in.-sec-^oF)
I	-	current (amps)
J	-	conversion factor ($\frac{\text{Btu/sec}}{\text{watt}}$)
k	-	thermal conductivity (Btu/sq in.-sec-^oF/in.)
L	-	length of heat transfer surface (in.)

$\dot{m}$ - evaporation rate per unit area (lb/sq in.-sec)

Nu - Nusselt number

p - pressure (lb/sq in.)

p_g - pressure of gas (psi)

p_i - pressure inside bubble (psi)

p_o - pressure of liquid (psi)

p_v - pressure of vapor (psi)

Pr - Prandtl number (C_p u/k (dimensionless))

q - heat flux (Btu/sec)

q_C - heat transfer by conduction (Btu/sec)

q_R - heat transfer by radiation (Btu/sec)

$(\frac{q}{a})_A$ - heat flux per unit area transferred to the test fluid (Btu/sq in.-sec)

$(\frac{q}{a})_S$ - heat flux per unit area transferred to the stabilizing fluid (Btu/sq in.-sec)

$(\frac{q}{a})_T$ - total heat flux per unit area, $(\frac{q}{a})_A$ $(\frac{q}{a})_S$ (Btu/sq in.-sec)

Q - heat content (Btu)

r - radius

$\dot{r}$ - bubble velocity (ft/sec)

r_i - inside radius of tube (in.)

R - electrical resistance (ohm)

R - gas constant(ft/^oR)

Re - Reynolds number, $\frac{\rho u D}{\mu}$ (dimensionless)

t - tube or vapor thickness (in.)

T - temperature (^{o}R)

T_f - arithmetic mean temperature of the vapor film (^{o}F)

T_L - liquid temperature (^{o}F)

T_o - maximum temperature inside of tube wall (^{o}F)

T_{sat} - liquid saturation temperature (^{o}F)

T_v - vapor saturation temperature (^{o}F)

T_{W_A} - tube wall temperature next to test fluid (^{o}F)

T_{W_S} - tube wall temperature next to stabilizing fluid (^{o}F)

ΔT_A - temperature rise of test fluid in annulus (^{o}F)

ΔT - $T_{W_A}-T_L$ or $T_{W_S} - T_L$(^{o}F)

ΔT_S - temperature rise of stabilizing fluid (^{o}F)

ΔT_{sat} - $T_{W_A}-T_{sat}$ (^{o}F)

ΔT_{sub} - $T_{sat}-T_L$ (^{o}F)

u - vapor velocity in direction of tube axis (in./sec)

v - vapor velocity in direction of tube radius (in./sec)

v_L - effective liquid velocity (ft/sec)

w_g - mass of gas (lbs)

x - direction parallel to tube axis (in.)

X - vapor film body force per unit mass ($lb/\frac{lb}{in./sec^2}$)

y - direction parallel to tube radius (in.)

y_1 - distance from inside tube wall to point of maximum temperature (in.)

y_2 - distance from outside tube wall to point of maximum temperature (in.)

y - dimensionless distance

ε - accommodation coefficient

ε_W - emissivity of tube wall (dimensionless)

ε_L - emissivity of liquid (dimensionless)

λ - latent heat (Btu/lb)

ρ_L - liquid density (lb/cu in.)

ρ_v - vapor density (lb/cu in.)

σ - Stefan Baltzmann constant (Btu/sq in.-sec-^{o}R)

σ - surface tension

τ_o - shear stress at wall (lb/in.^{2})

θ - time (sec)

Θ - $\frac{\partial u}{\partial x} + \frac{\partial v}{\partial y}$

μ - viscosity (lb-sec/in.^{2})

∇^2 - $\frac{\partial^2}{\partial x^2} + \frac{\partial^2}{\partial y^2}$

ξ - bubble population parameter

TABLE II

EXPERIMENTAL DATA AND CALCULATED VALUES USING WATER STABILIZER

Press = 16 psia

Subcooling = 50° F

Vel. = 1.1 ft/sec

Test No.	I Amps	E Volts	$(\frac{q}{a})_T$ Btu/sq in.-sec	ΔT_A °F	$(\frac{q}{a})_A$ Btu/sq in.-sec	ΔT_S °F	$(\frac{q}{a})_S$ Btu/sq in.-sec	$\frac{(\frac{q}{a})_T}{(\frac{q}{a})_A + (\frac{q}{a})_S}$	T_{W_A} °F
1	204	4.2	0.35	0.9	0.04	1.6	0.30	1.03	196
2	250	5.2	0.52	1.3	0.06	2.4	0.44	1.04	210
3	302	6.3	0.77	1.9	0.09	3.7	0.67	1.01	231
4	328	6.9	0.92	2.5	0.12	4.4	0.80	1.00	246
5	360	7.6	1.11	5.1	0.25	4.7	0.86	1.00	252
6	440	9.3	1.66	11.7	0.57	6.2	1.12	0.98	265
7	510	10.4	2.15	20.4	0.99	6.3	1.14	1.01	285
8	600	13.1	3.13	21.5	1.05	1.2	2.10	1.01	376
9	625	13.7	3.46	20.0	0.95	1.3	2.34	1.05	420

TABLE III

EXPERIMENTAL DATA AND CALCULATED VALUES USING NITROGEN GAS STABILIZER

Press. = 16 psia

Subcooling = 50° F

Vel. = 1.1 ft/sec

Test No.	I Amps	E Volts	$(\frac{q}{a})_T$ Btu/sq in.-sec	ΔT_A °F	$(\frac{q}{a})_A$ Btu/sq in.-sec	$(\frac{q}{a})_S$ Btu/sq in.-sec	T_{W_A} °F
10	150	3.1	0.19	0.9	0.04	0.15	196
11	186	3.8	0.29	1.3	0.06	0.23	210
12	228	4.7	0.44	1.9	0.09	0.35	231
13	245	5.2	0.52	2.5	0.12	0.40	246
14	286	6.1	0.72	5.1	0.25	0.47	252
15	360	7.6	1.11	11.7	0.57	0.54	265
16	436	9.2	1.63	20.2	0.99	0.64	285
17	490	10.8	2.15	21.5	1.05	1.10	376
18	500	11.2	2.27	19.5	0.95	1.32	420
19	540	12.9	2.82	13.5	0.66	2.16	545
20	544	13.1	2.88	8.2	0.40	2.48	615
21	562	14.0	3.19	5.2	0.26	2.93	690
22	640	17.6	4.55	2.2	0.11	3.44	970
23	775	22.7	7.13	2.5	0.12	7.01	1520
24	786	23.0	7.34	2.9	0.14	7.20	1560
25	812	24.5	8.05	3.0	0.15	7.90	1710

Press. = 16 psia

Subcooling = 50° F

Vel. = 5 ft/sec

26	162	3.4	0.22	1.9	0.09	0.13	190
27	272	5.7	0.63	5.6	0.27	0.36	235
28	332	7.0	0.94	9.8	0.48	0.46	265
29	456	9.6	1.77	26.7	1.30	0.47	276
30	530	11.6	2.50	38.9	1.90	0.60	325
31	540	11.9	2.59	40.0	1.95	0.64	345
32	545	13.0	2.87	21.5	1.05	1.82	537
33	550	13.2	2.94	19.4	0.95	1.99	540
34	555	13.9	3.12	12.3	0.60	2.52	630
35	585	14.6	3.46	6.5	0.32	3.14	765
36	600	15.6	3.79	3.1	0.15	3.64	810
37	685	19.8	5.50	2.0	0.10	5.40	1350
38	700	21.0	5.95	2.2	0.11	5.84	1450
39	741	22.2	6.65	2.2	0.11	6.54	1600

TABLE III
(cont.)

EXPERIMENTAL DATA AND CALCULATED VALUES USING NITROGEN GAS STABILIZER

Press. = 16 psia

Subcooling = 100° F

Vel. = 1.1 ft/sec

Test No.	I Amps	E Volts	$(\frac{q}{a})_T$ Btu/sq in.-sec	ΔT_A °F	$(\frac{q}{a})_A$ Btu/sq in.-sec	$(\frac{q}{a})_S$ Btu/sq in.-sec	T_{V_A} °F
40	174	3.5	0.24	0.9	0.04	0.20	150
41	234	4.7	0.44	1.5	0.08	0.36	182
42	291	6.0	0.72	2.6	0.12	0.60	216
43	348	7.3	1.02	5.8	0.28	0.74	250
44	466	10.3	1.94	20.5	1.00	0.94	270
45	571	13.1	3.03	32.9	1.60	1.43	350
46	615	14.7	3.67	20.7	1.01	2.66	600
47	620	15.4	3.86	11.3	0.55	3.31	660
48	625	15.6	3.95	7.8	0.38	3.57	690
49	641	16.7	4.34	5.2	0.26	4.08	860
50	651	17.6	4.65	3.1	0.15	4.50	870
51	852	25.5	8.79	2.9	0.14	8.65	1570

Press. = 60 psia

Subcooling = 50° F

Vel. = 1.1 ft/sec

52	191	4.0	0.31	1.2	0.06	0.25	285
53	219	4.8	0.43	1.7	0.08	0.35	302
54	265	5.8	0.62	3.8	0.15	0.47	324
55	298	6.6	0.79	5.1	0.25	0.54	335
56	356	7.8	1.13	11.3	0.55	0.58	341
57	400	8.8	1.43	17.0	0.83	0.60	343
58	490	11.3	2.25	25.4	1.24	1.01	413
59	517	12.4	2.60	17.4	0.85	1.75	523
60	585	14.6	3.46	7.8	0.38	3.08	740
61	600	15.6	3.78	6.2	0.30	3.48	786
62	684	18.5	4.96	2.6	0.13	4.83	990
63	870	26.1	9.20	2.5	0.12	9.08	1690

TABLE IV

T_w	T_f	h_C	h_R	$(\frac{q}{a})_C$	$(\frac{q}{a})_R$	$(\frac{q}{a})_T$	T_{sat}
	$\frac{T_w + T_{sat}}{2}$	By Eq. (A-12)	By Eq. (A-13)	$h_C \Delta T_{sat}$	$h_R \Delta T_{sat}$	$(\frac{q}{a})_C + (\frac{q}{a})_R$	
^oF	^oF	Btu/sq in.-sec-^oF	Btu/sq in.-sec-^oF	Btu/sq in.-sec	Btu/sq in.-sec	Btu/sq in.-sec	^oF
1000	610	4.57×10^{-5}	1.45×10^{-5}	.0356	.0113	.0469	780
1200	710	4.54×10^{-5}	2.10×10^{-5}	.0444	.0198	.0642	980
1500	810	4.54×10^{-5}	3.06×10^{-5}	.0580	.0391	.0971	1280
1800	1010	5.15×10^{-5}	4.42×10^{-5}	.0815	.0700	.1515	1580
2000	1110	5.12×10^{-5}	5.45×10^{-5}	.0910	.0971	.1881	1780

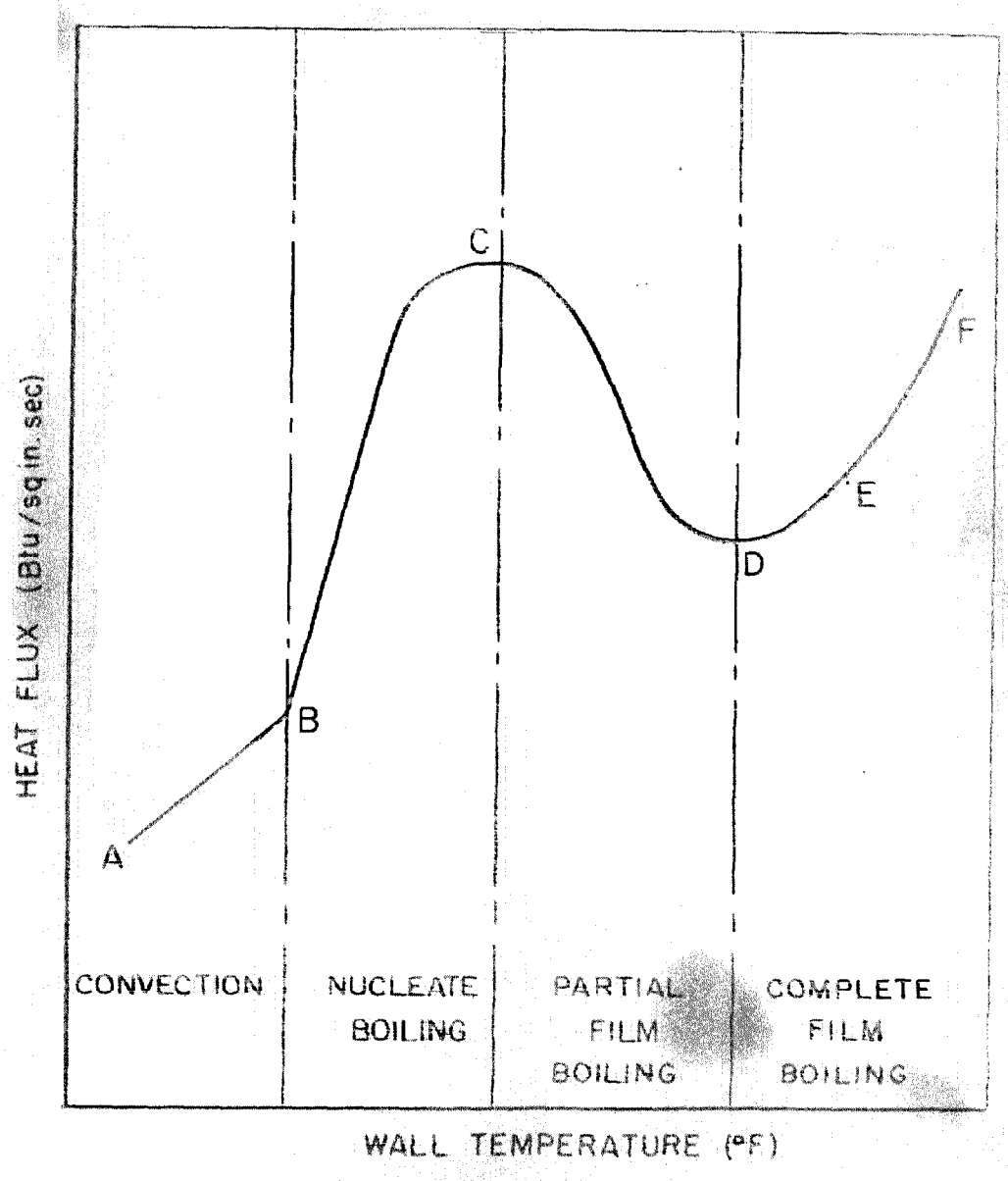

Figure 1. Typical Boiling Curve

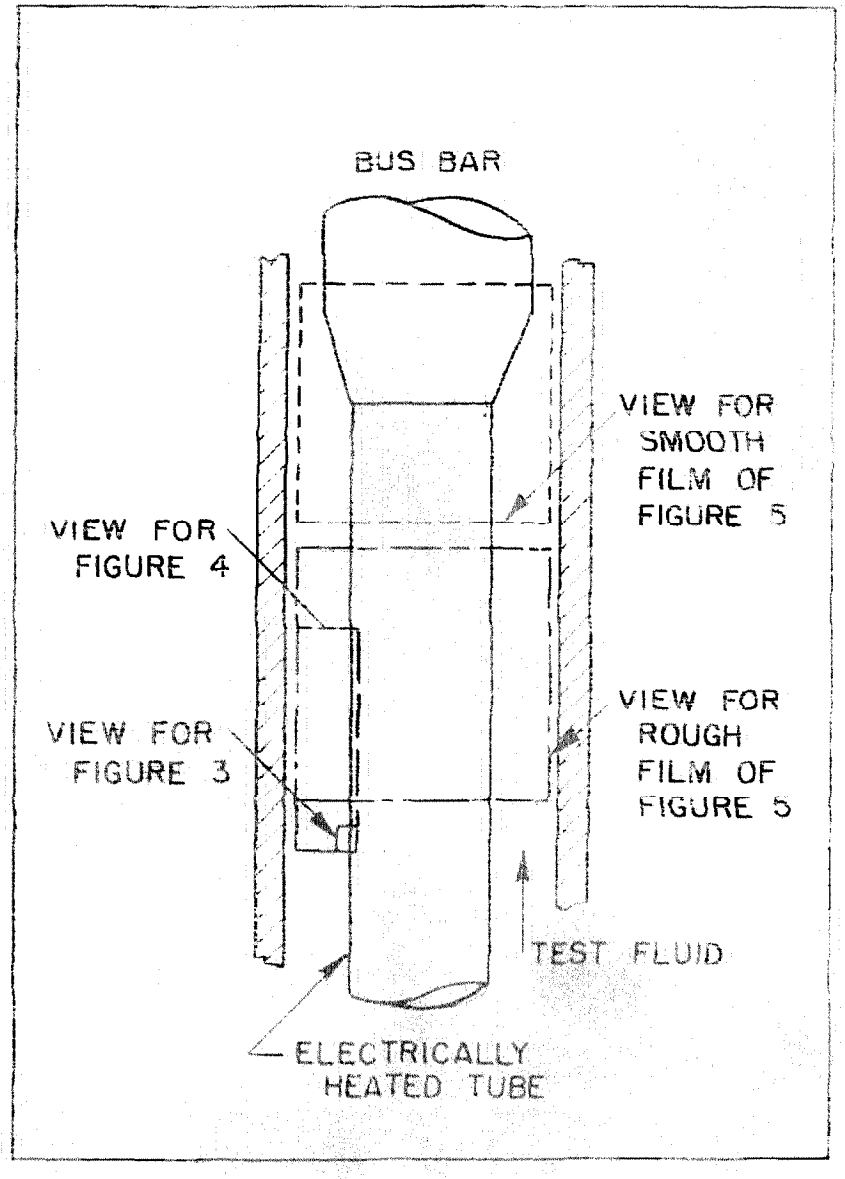

Figure 2. Camera Fields of View

TIME

Figure 3. Photographs of Nucleate Boiling

TIME

Figure 4. Photographs of Partial Film Boiling

a) Rough Film

b) Detecting Film

Figure 5. Complete Film Boiling Photographs

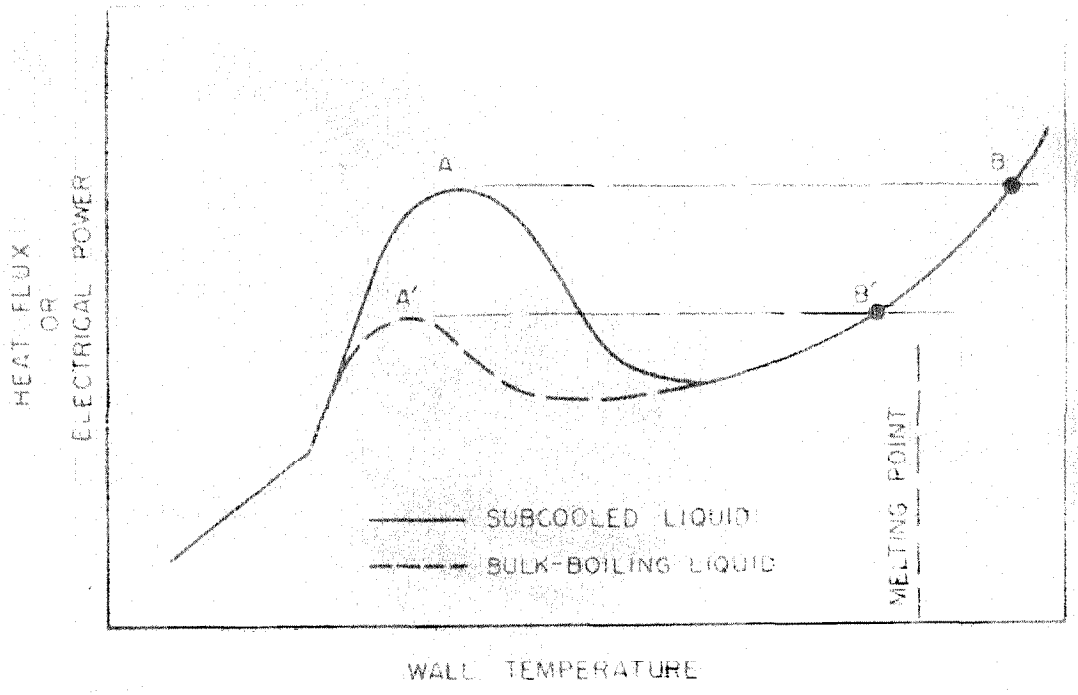

Figure 6. Wall Temperature Rise Causing Burnout

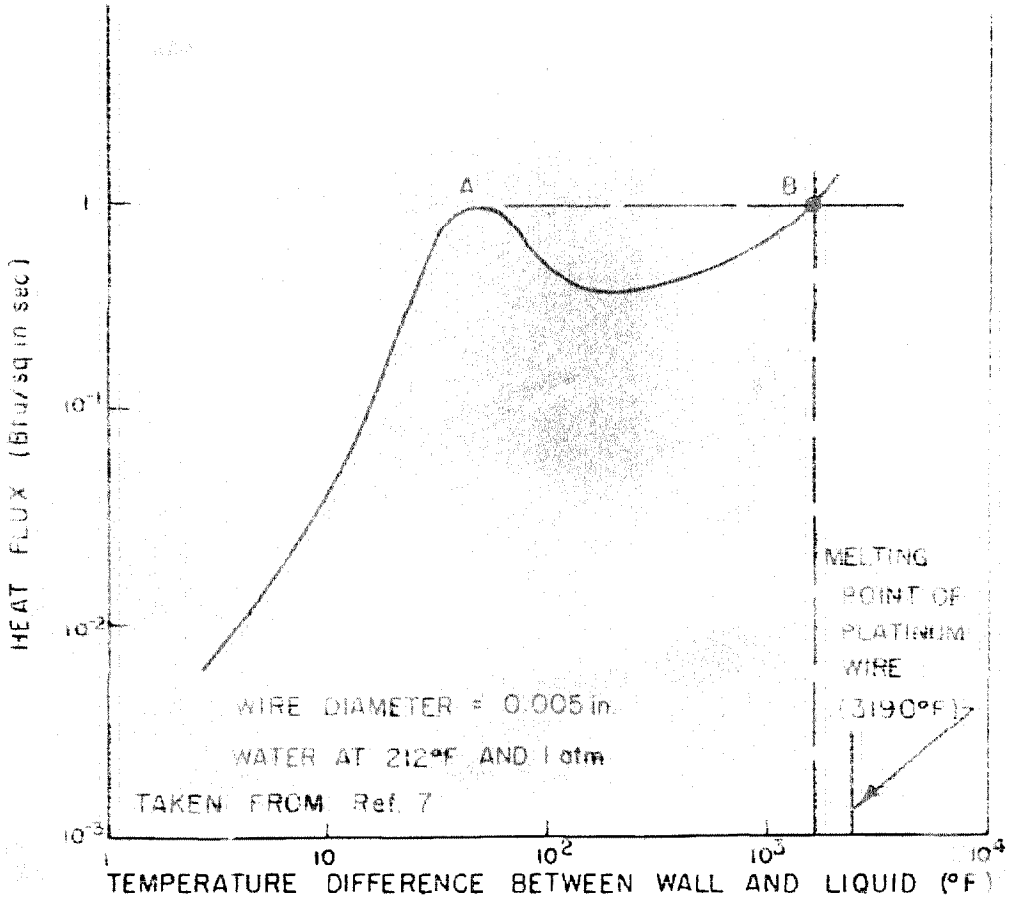

Figure 7. Bulk Boiling in Pool by Nukiyama

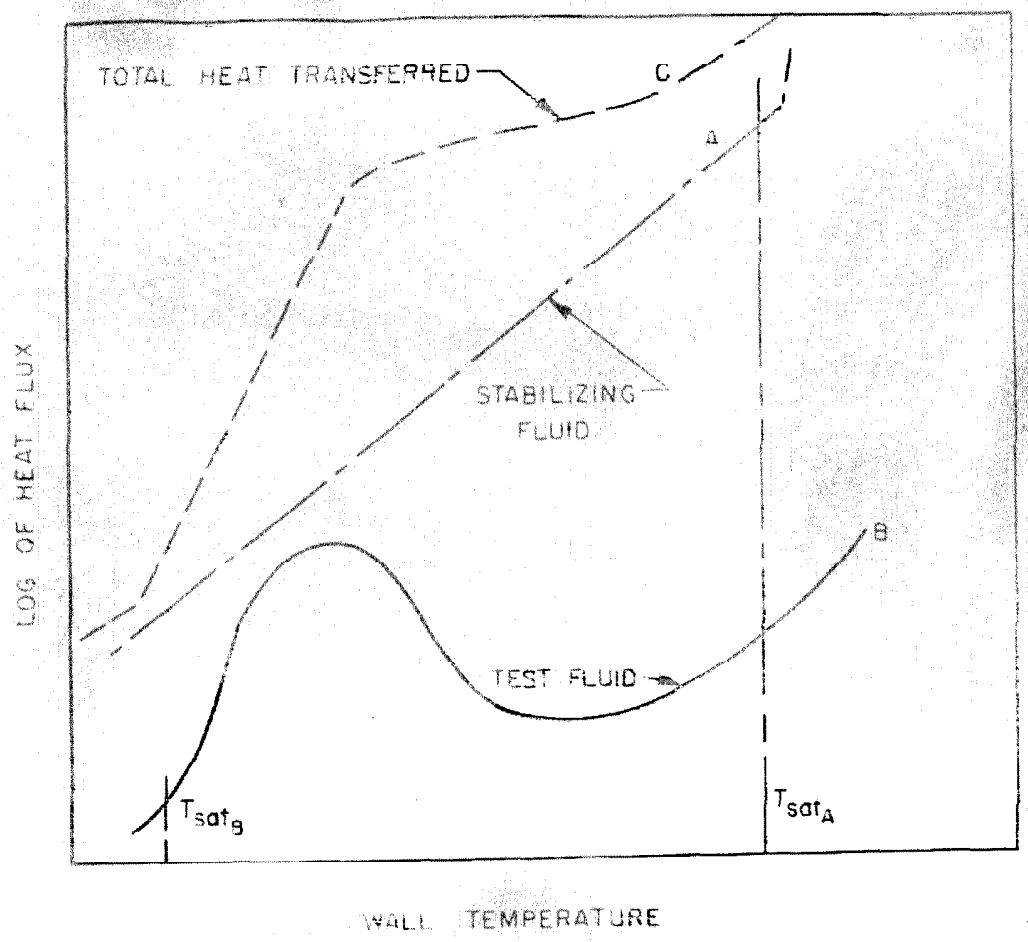

Figure 8. Method to Prevent Burnout

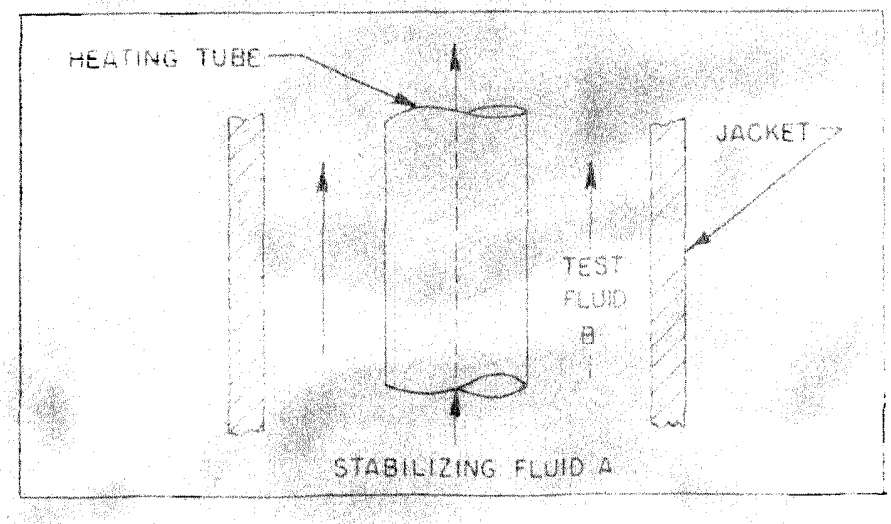

Figure 9. Apparatus to Prevent Burnout

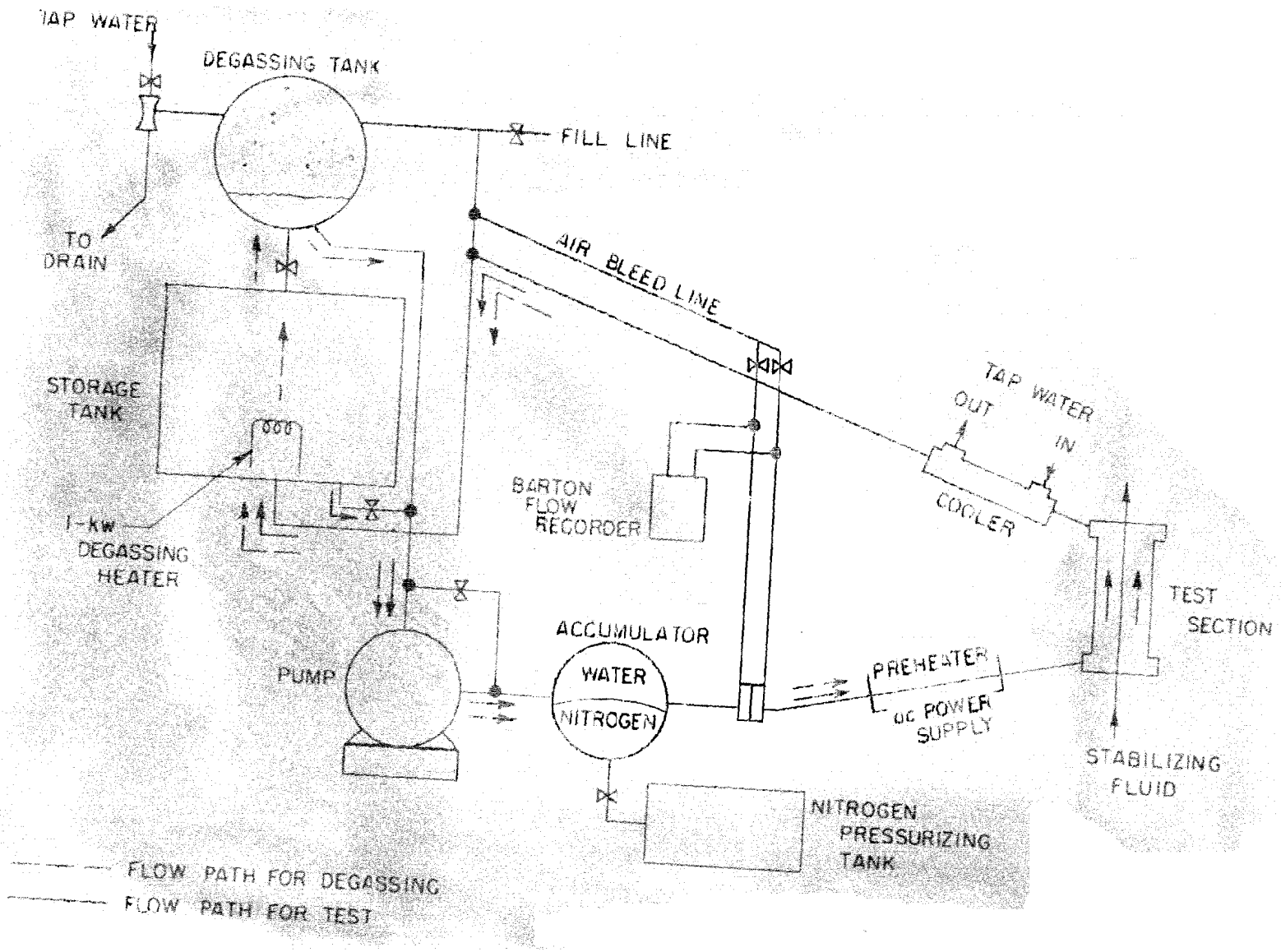

Figure 10. Diagram of Flow System

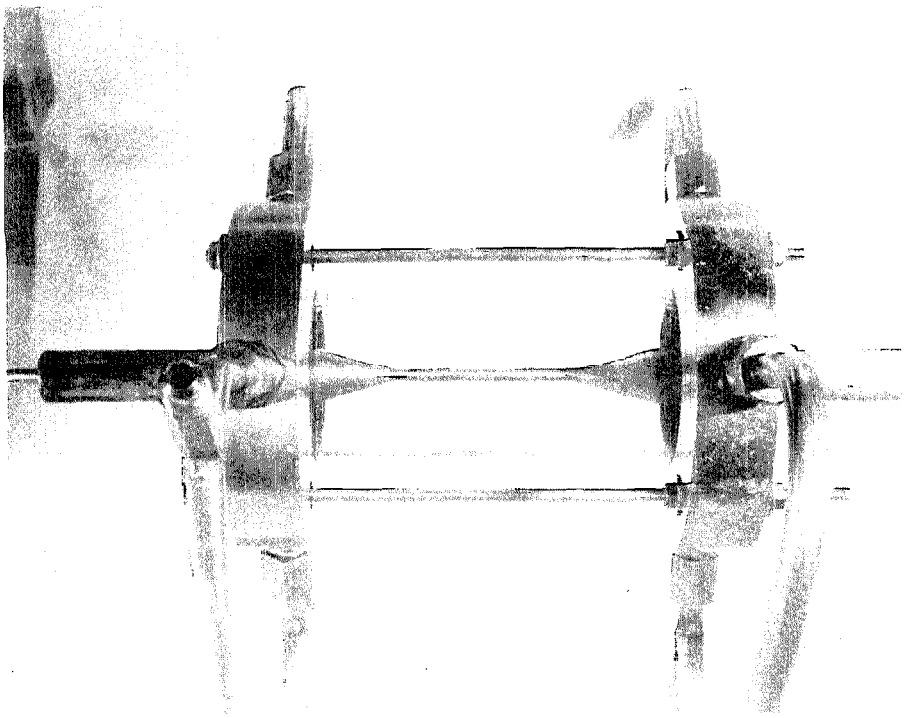

Figure 10. Test Section Assembly Inlet Side, Front

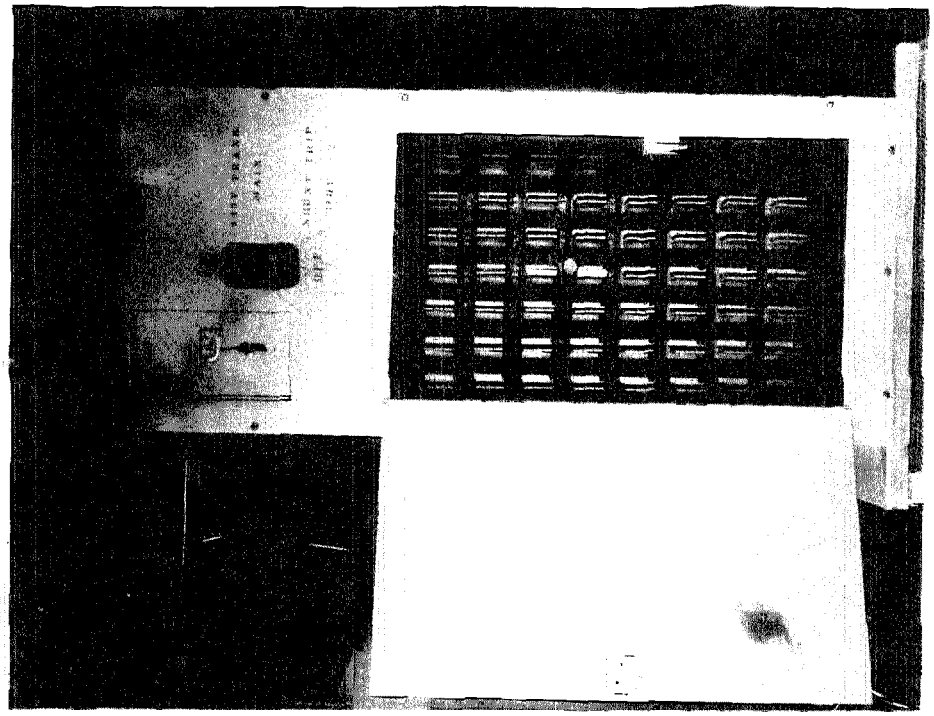

Figure 11. Pressure Control Valve

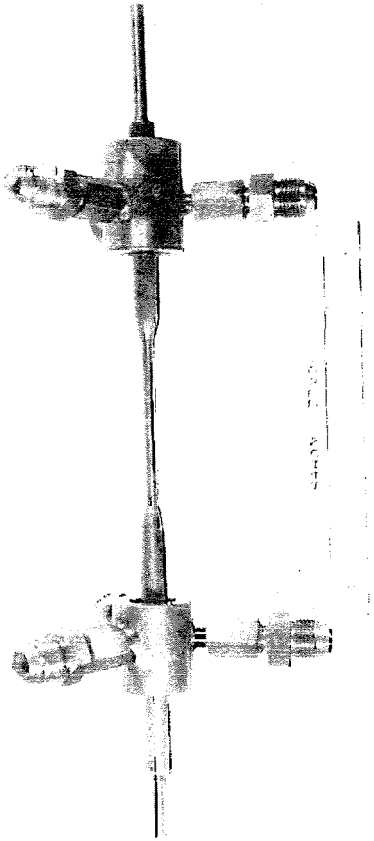

Figure 13. Test Section Assembly Having 0.61-in.-dia. Jacket

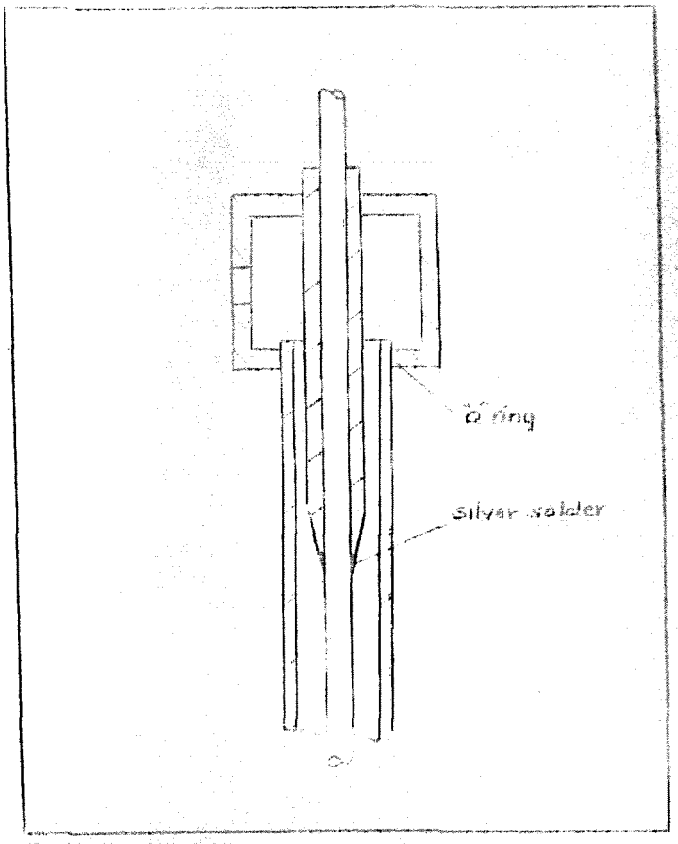

Figure 14. Test Section Details

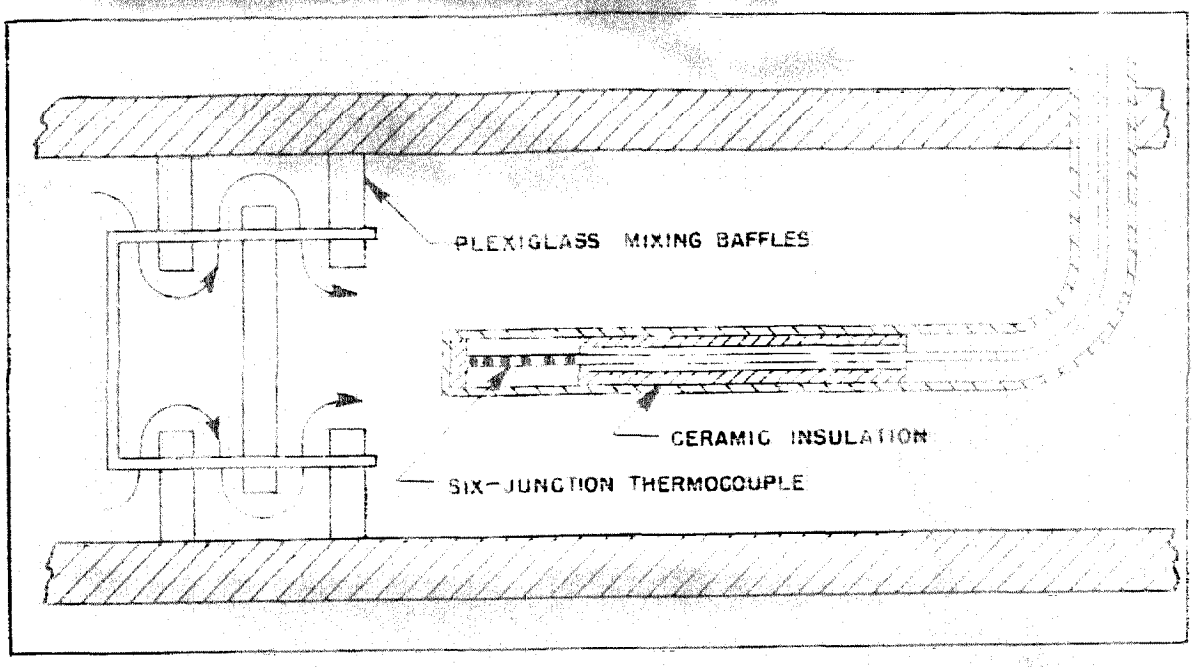

Figure 15. Thermocouple Assembly for Measuring Rise in Bulk Temperature Through Test Section

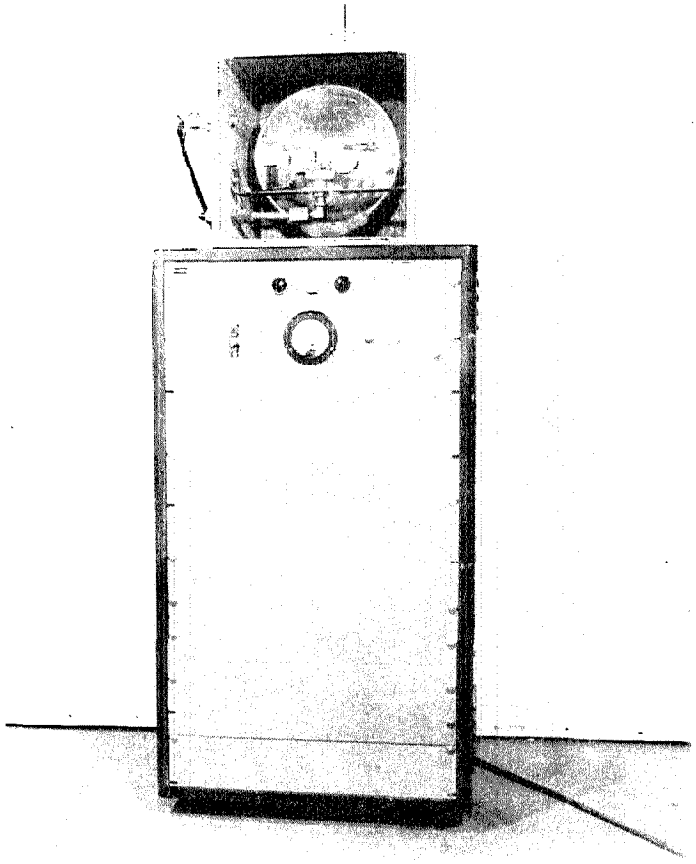

Figure 16. Mercury Vapor Lamp and Power Supply

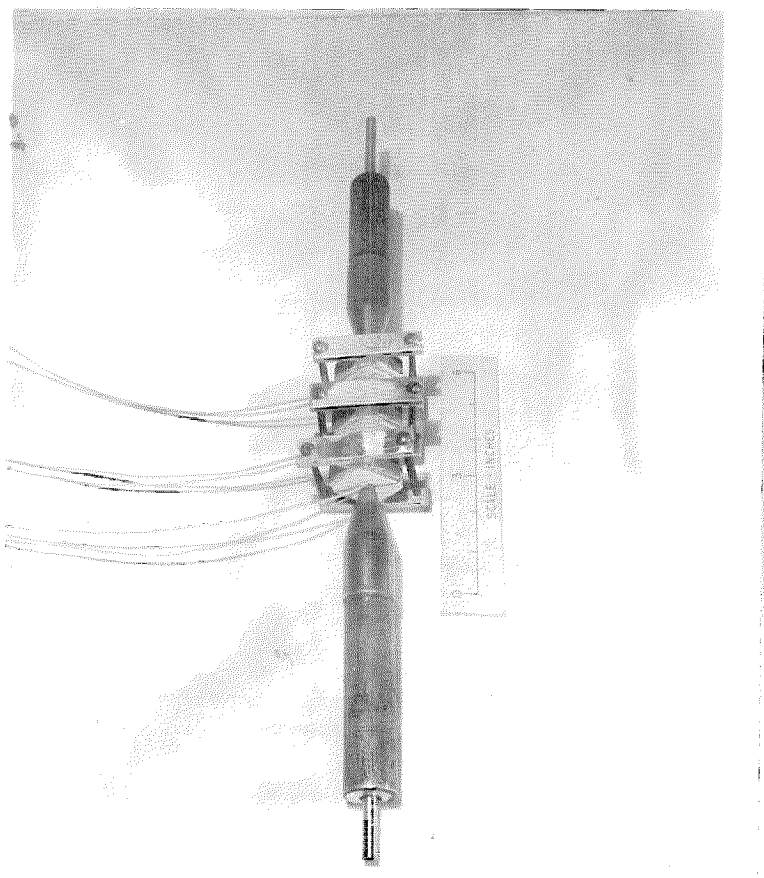

Figure 17. Thermocouple Assembly for Measuring Wall Temperature

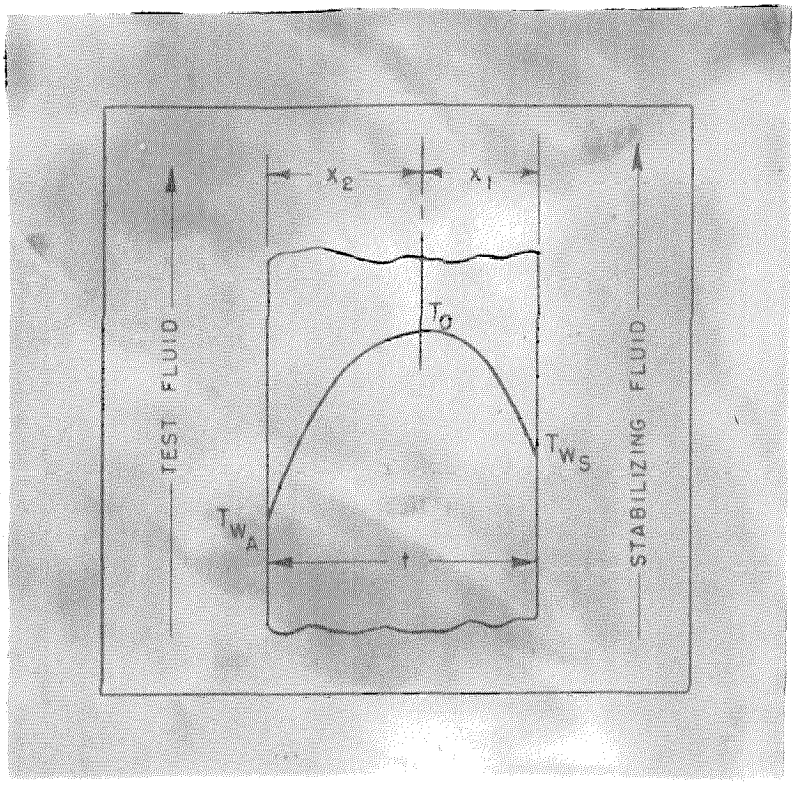

Figure 18. Temperature Distribution Through Heating Tube Wall

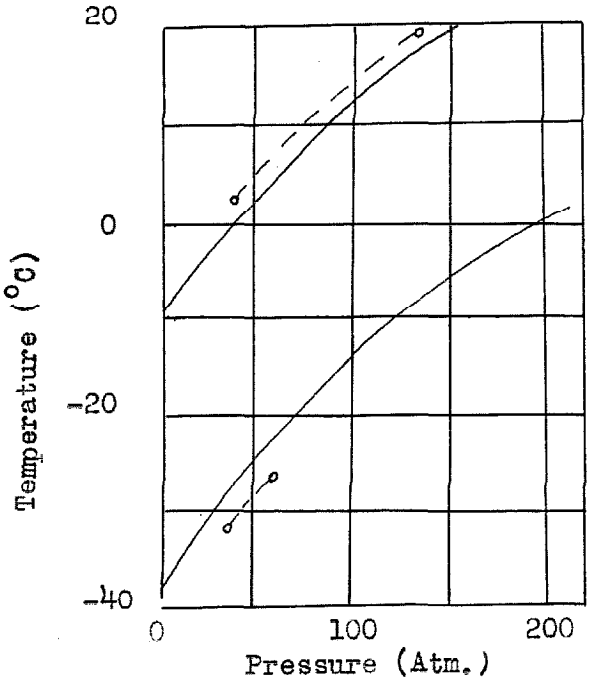

Figure 19. Isenthalpic Curves for Nitrogen Gas
(By Roebuck Ref. 28)

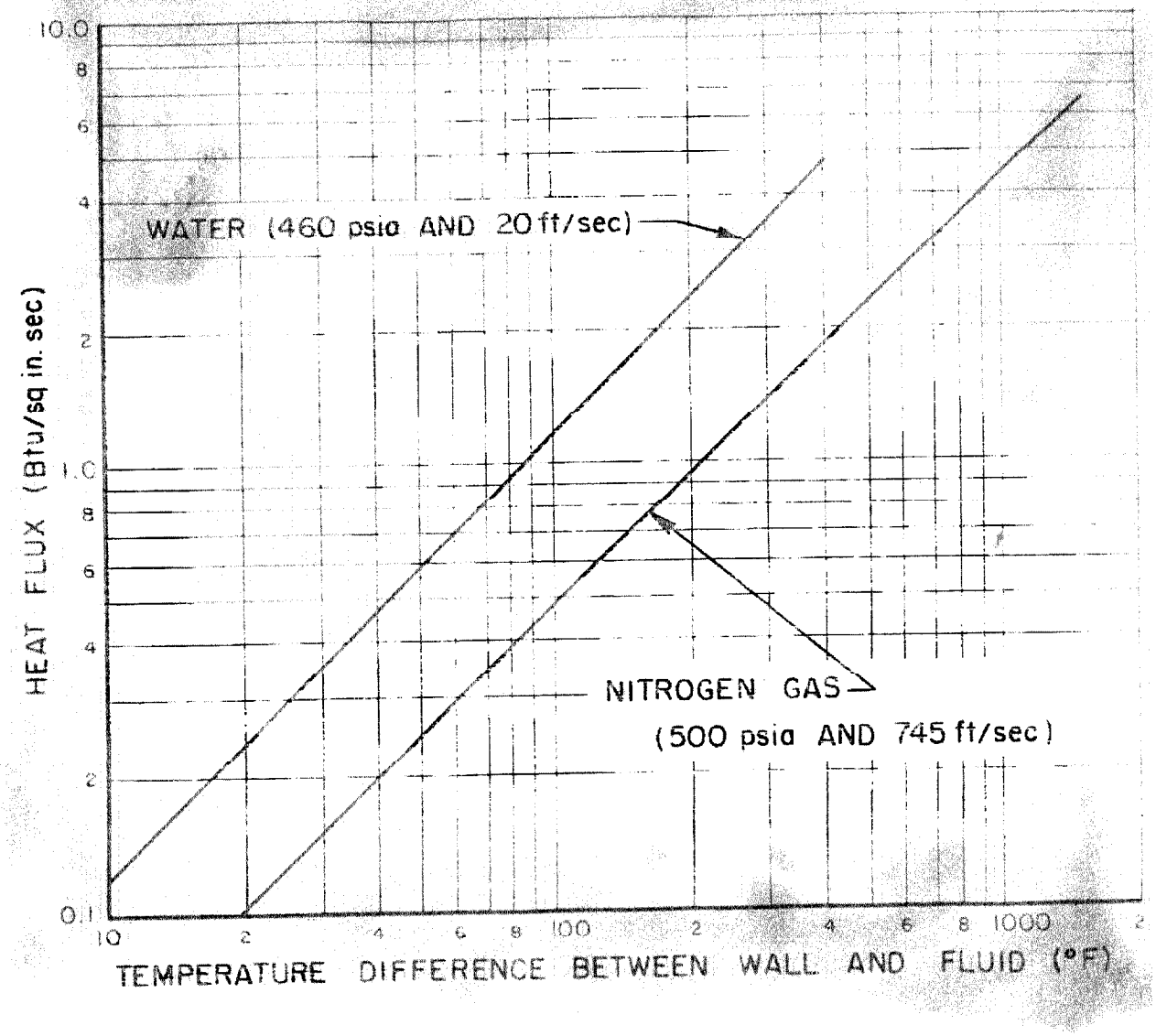

Figure 20. Stabilizer-Fluid Heat Transfer Curves

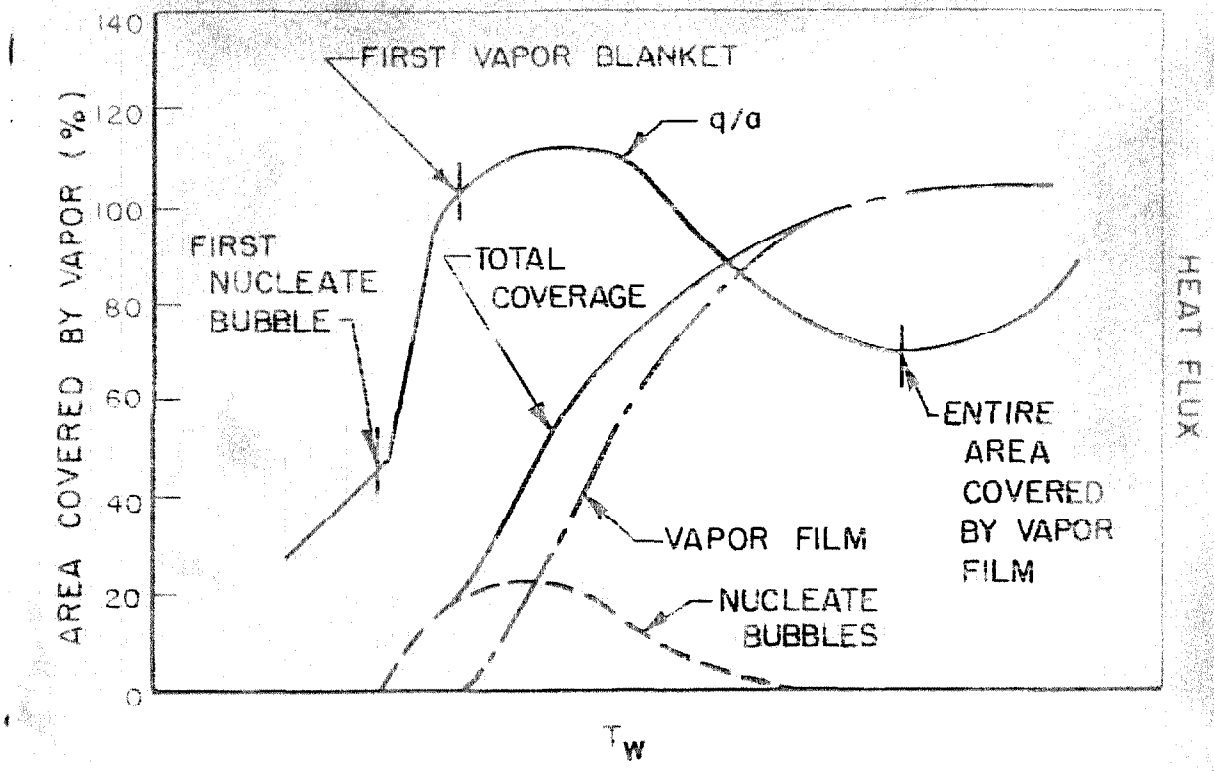

Figure 21. Area of Heat Transfer Surface Covered by Vapor

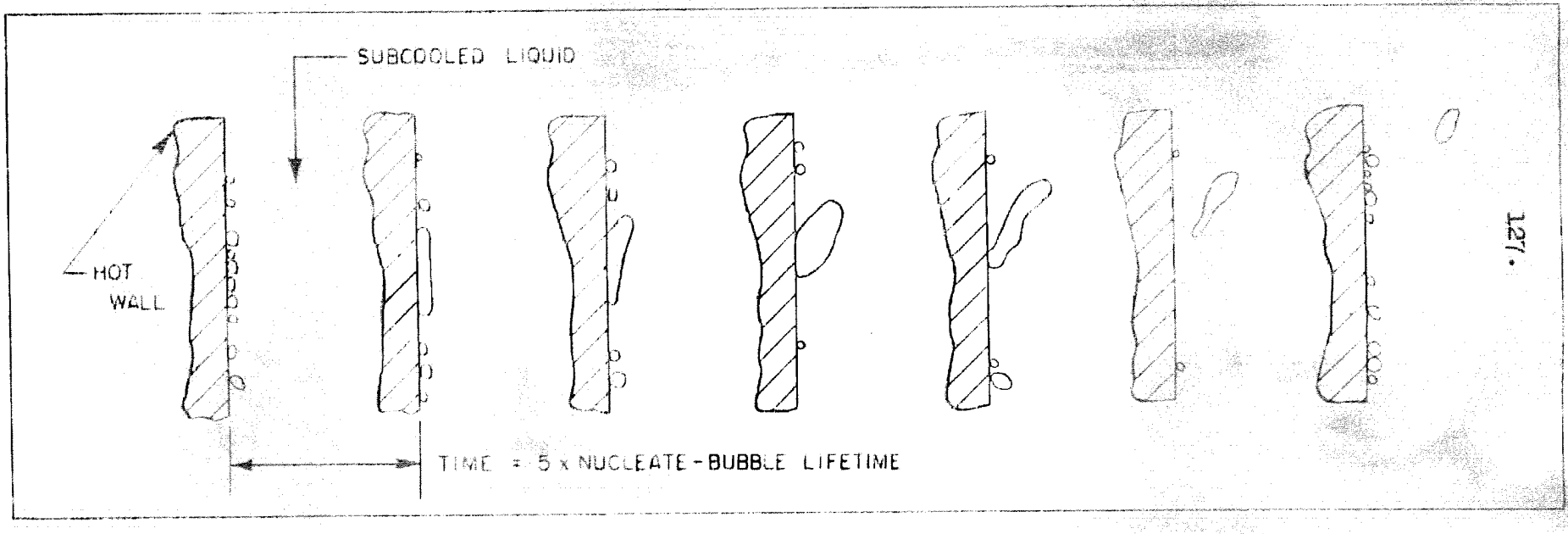

Figure 22. Partial Film Boiling on Vertical Heating Surface

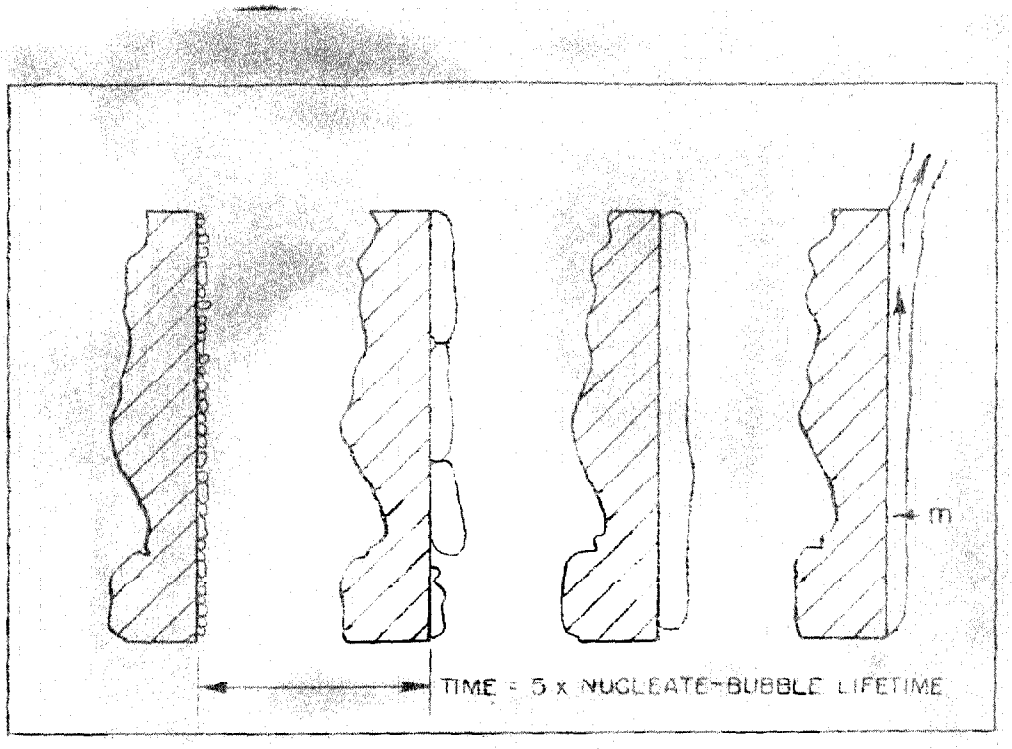

Figure 23. Formation of a Complete Vapor Film on Vertical Heating Surface

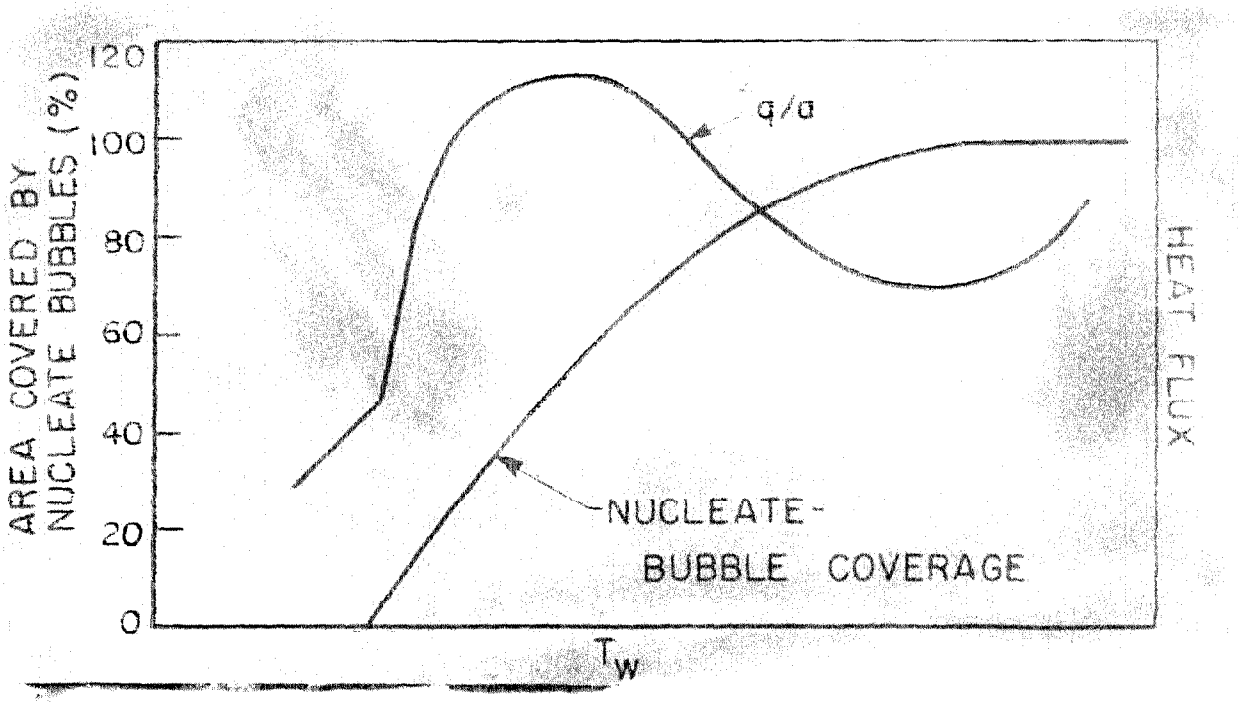

Figure 24. Per cent of Area Covered by Nucleate Bubbles Over Bubble Lifetime After Heat-Transfer Surface is Heated

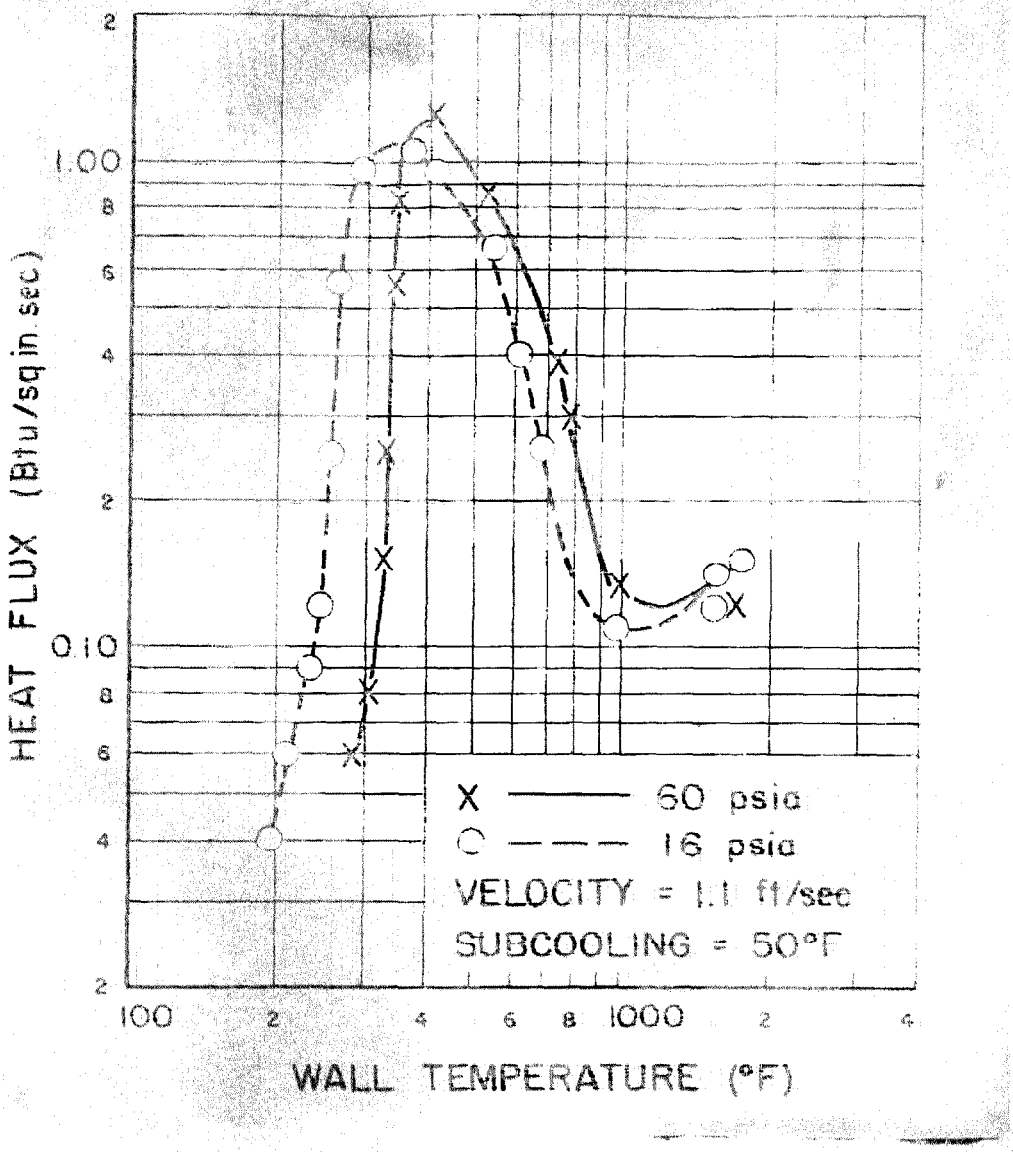

Figure 25. Effect of Pressure on Temperature Difference

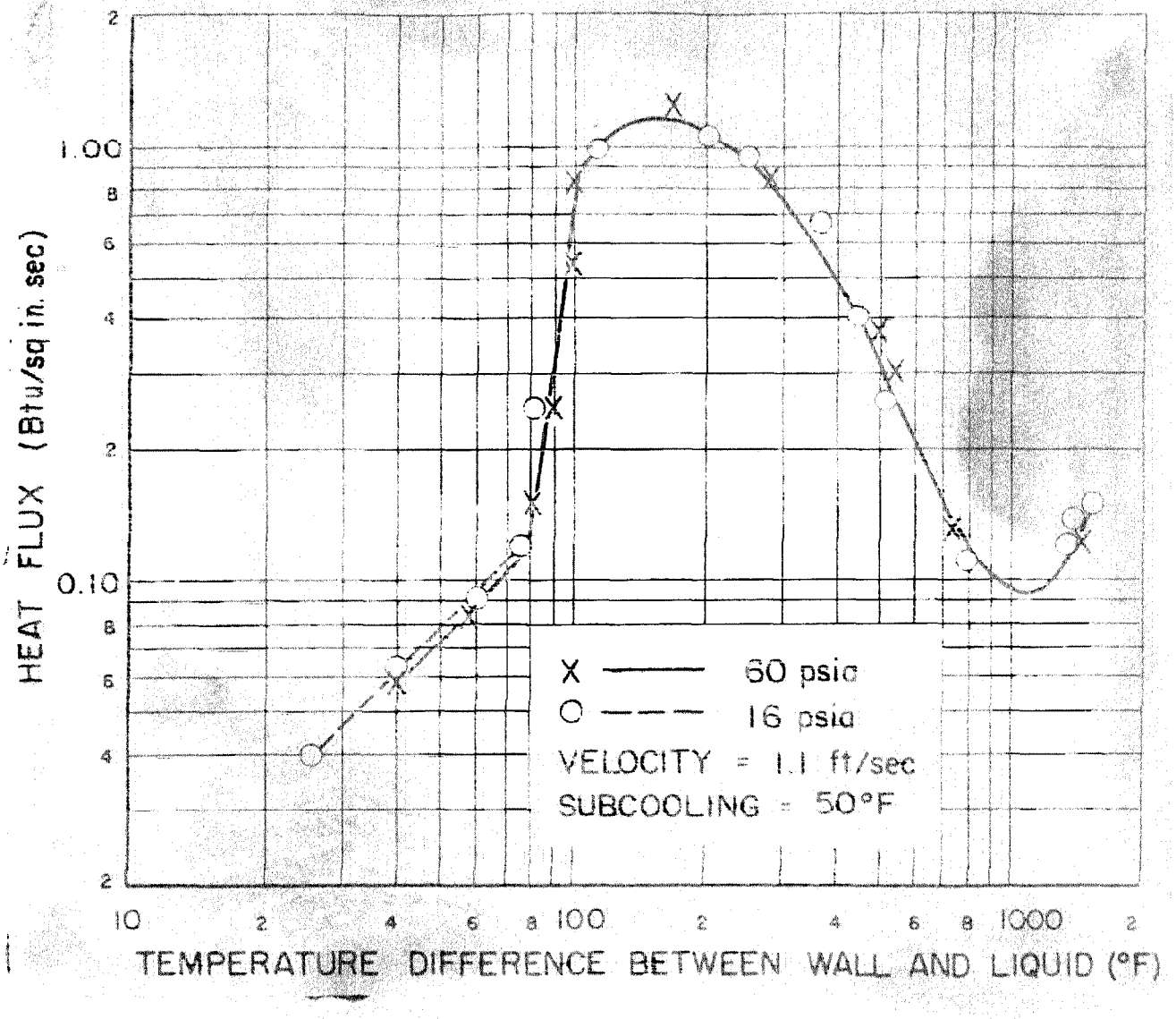

Figure 26. Effect of Pressure on Wall Temperature

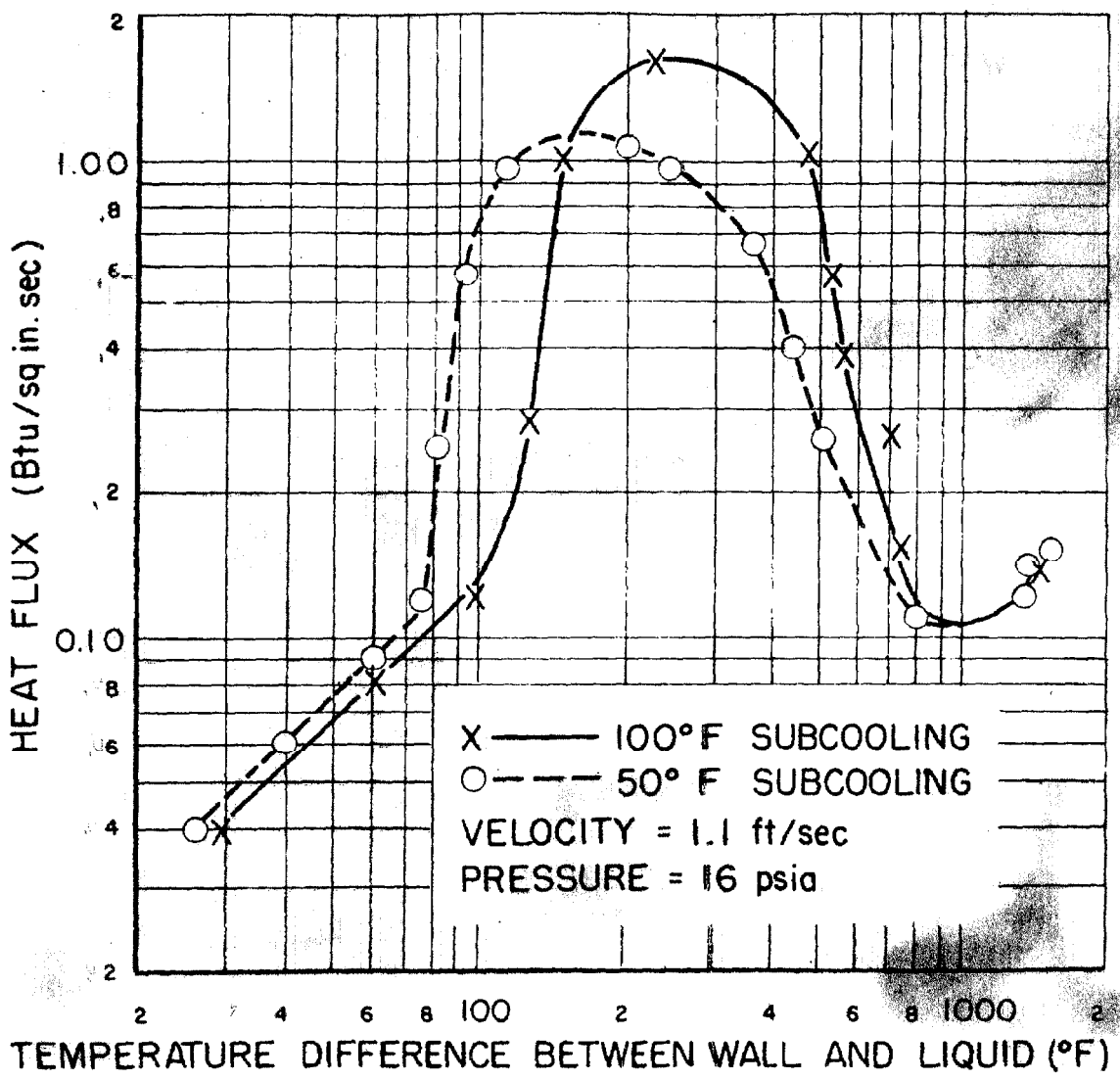

Figure 27. Effect of Subcooling on Temperature Difference

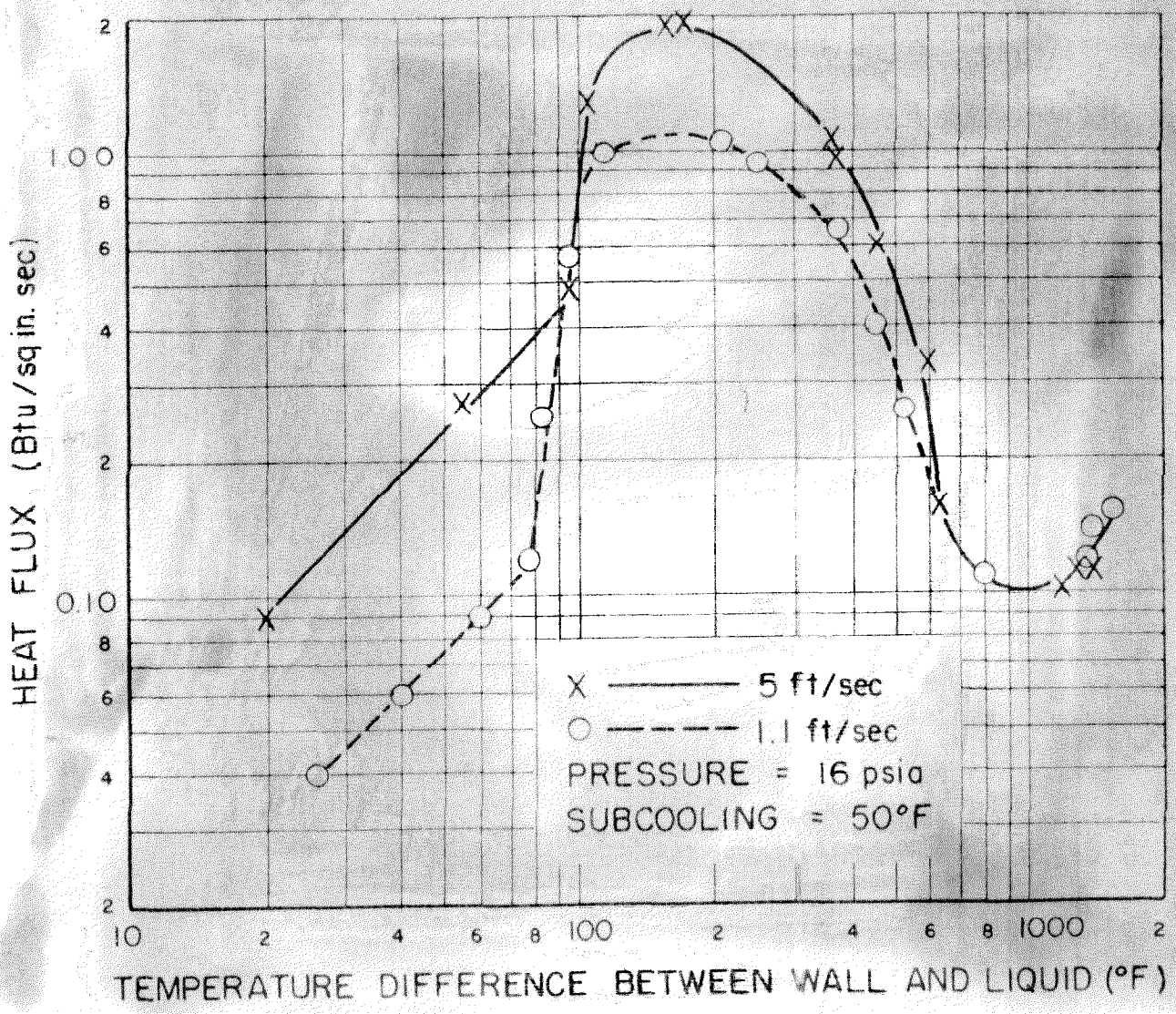

Figure 21. Effect of Velocity on Temperature Difference

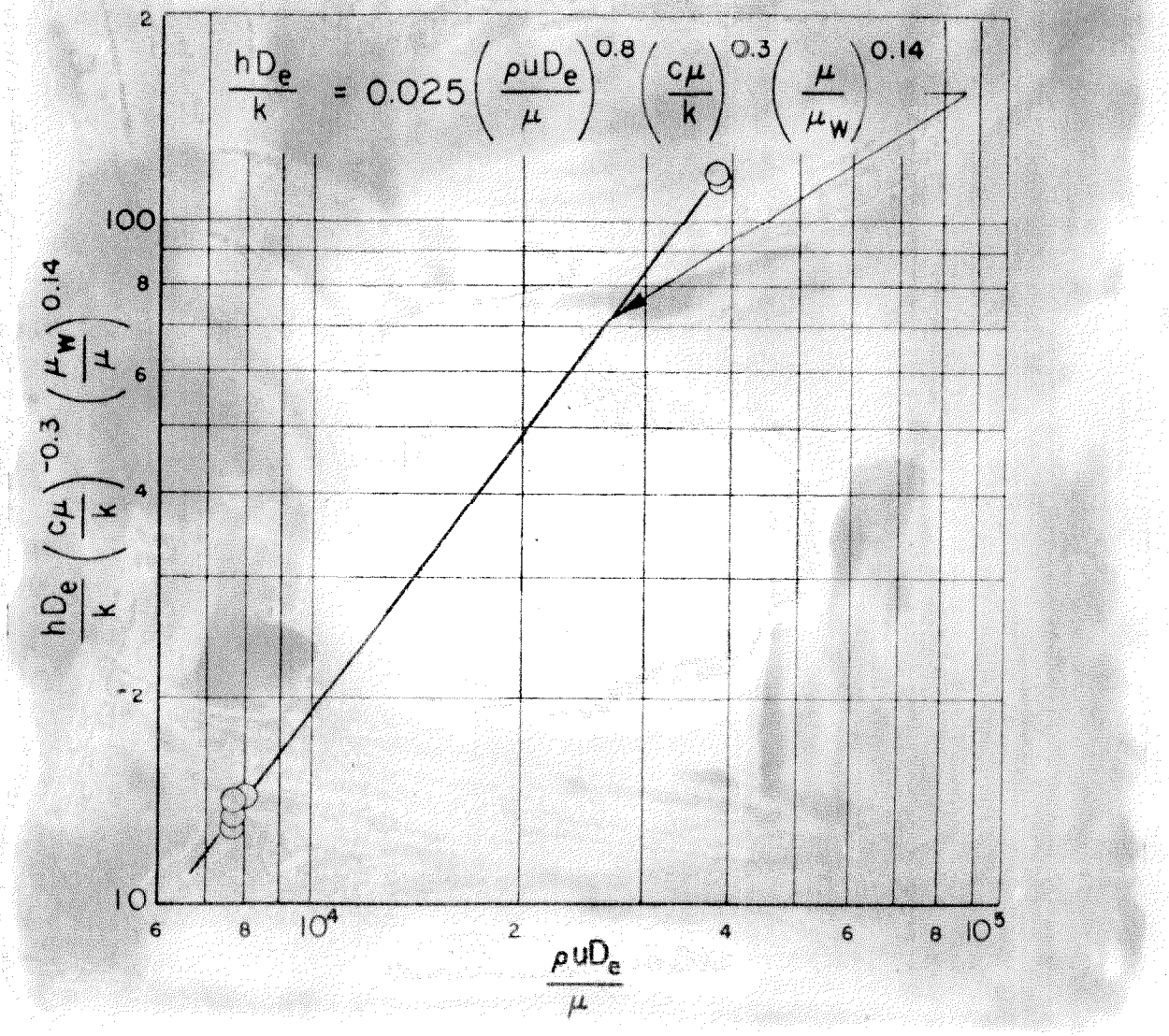

Figure 29. Correlation of Forced Convection Data

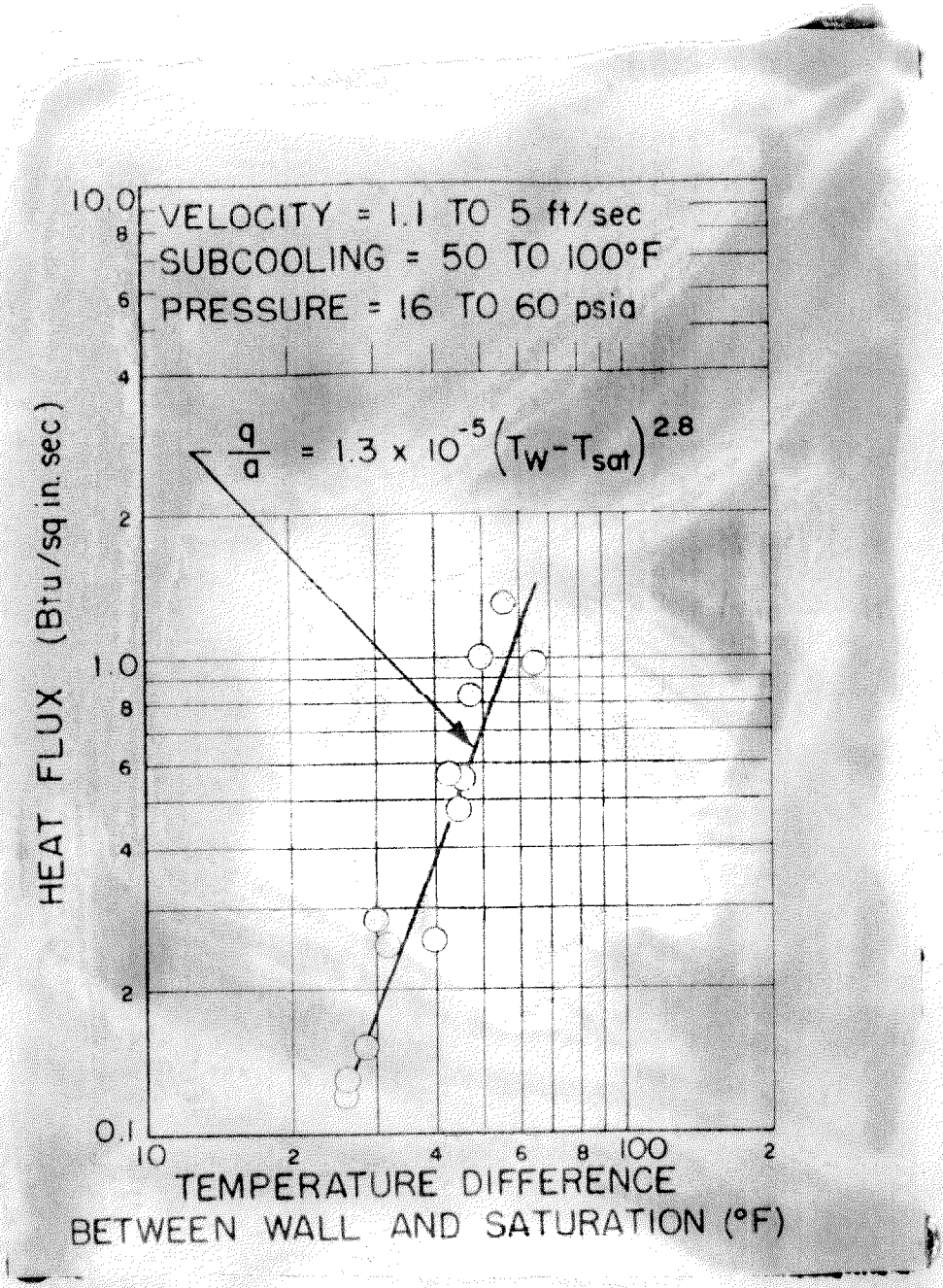

Figure 30. Correlation of Nucleate Boiling Data

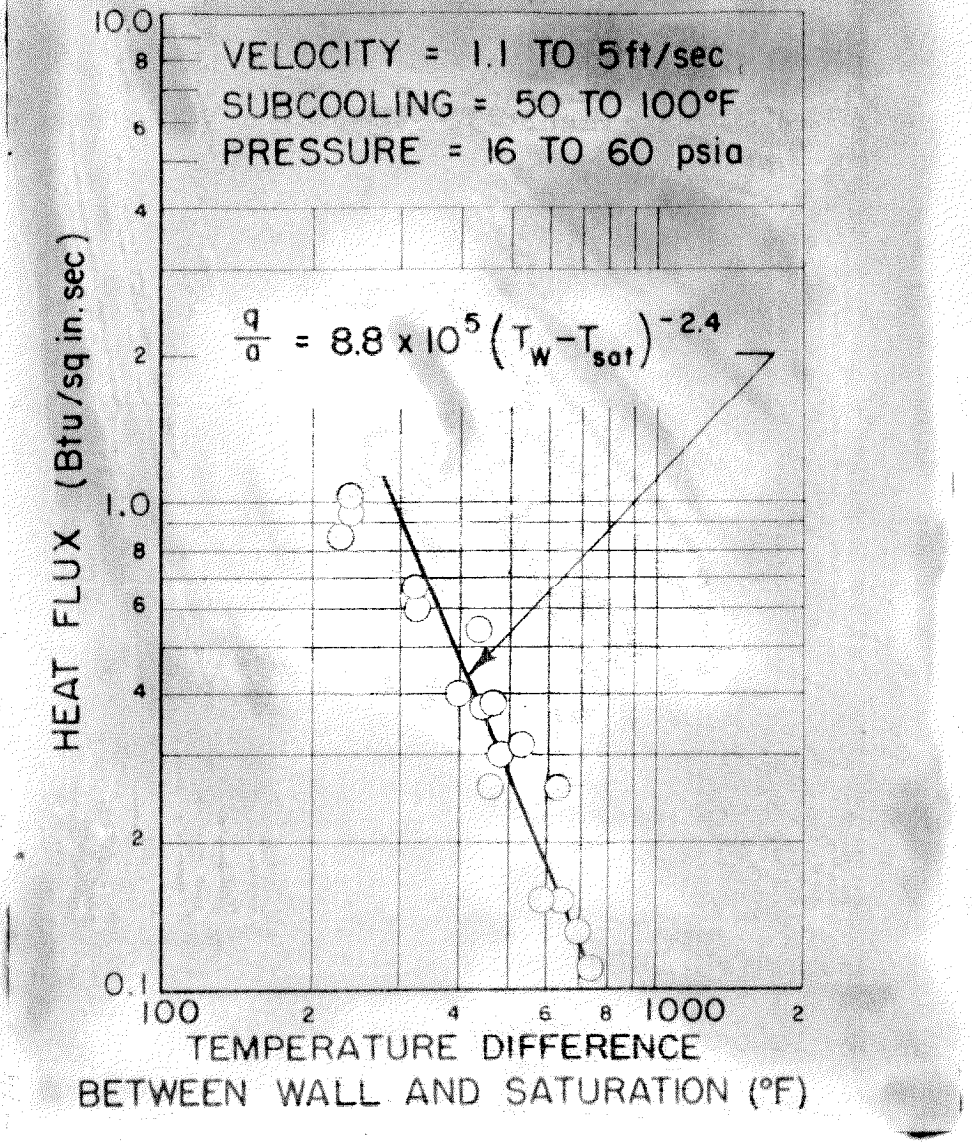

Figure 31. Correlation of Partial Film Boiling Data

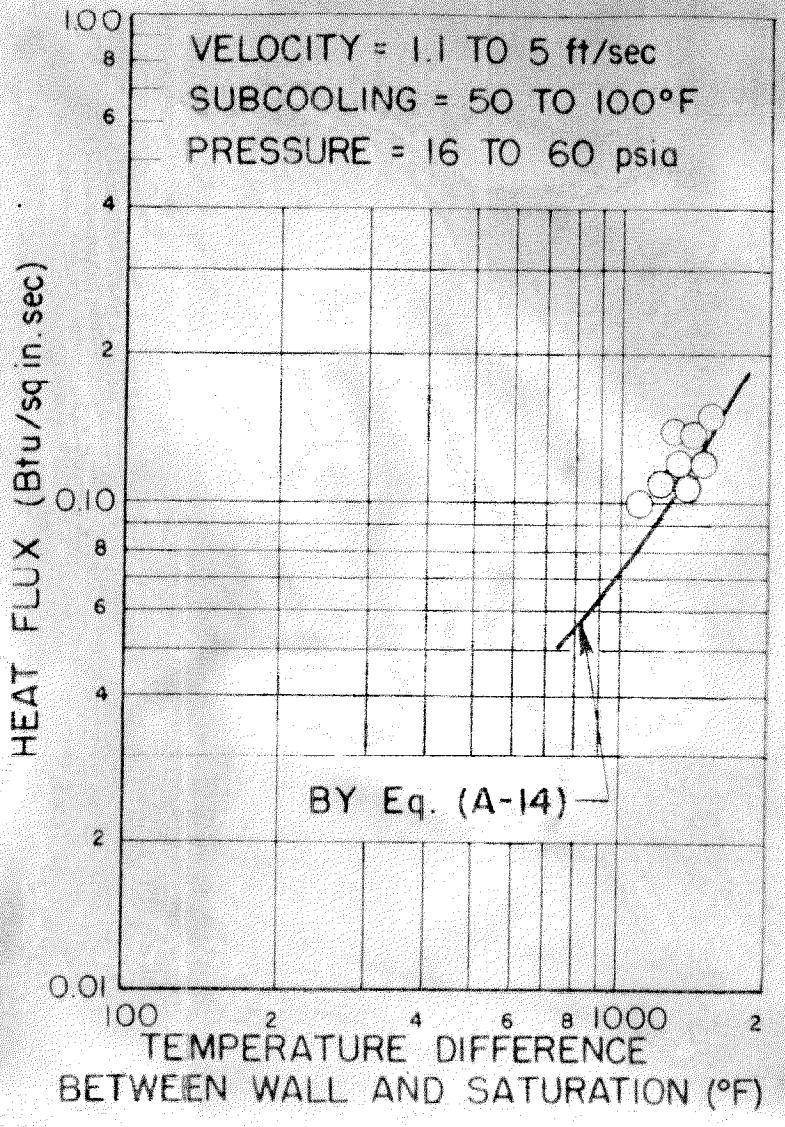

Figure 32a. Correlation of Complete Film Boiling Data

Figure 33a. Types of Heating Tube Failures

Figure 33b. Test-Section Tank for Water

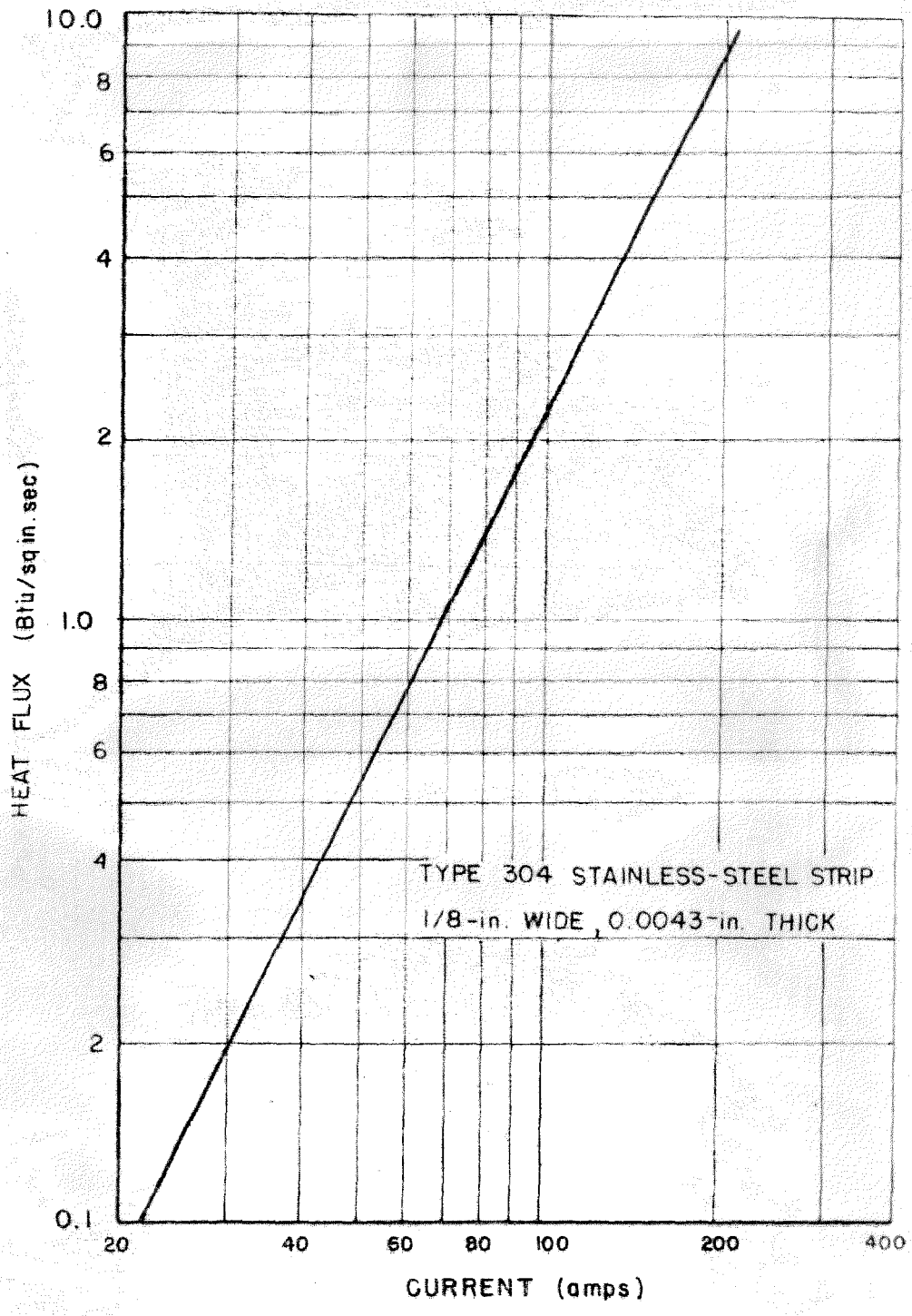

Figure 33b. Heat Flux vs Electrical Current

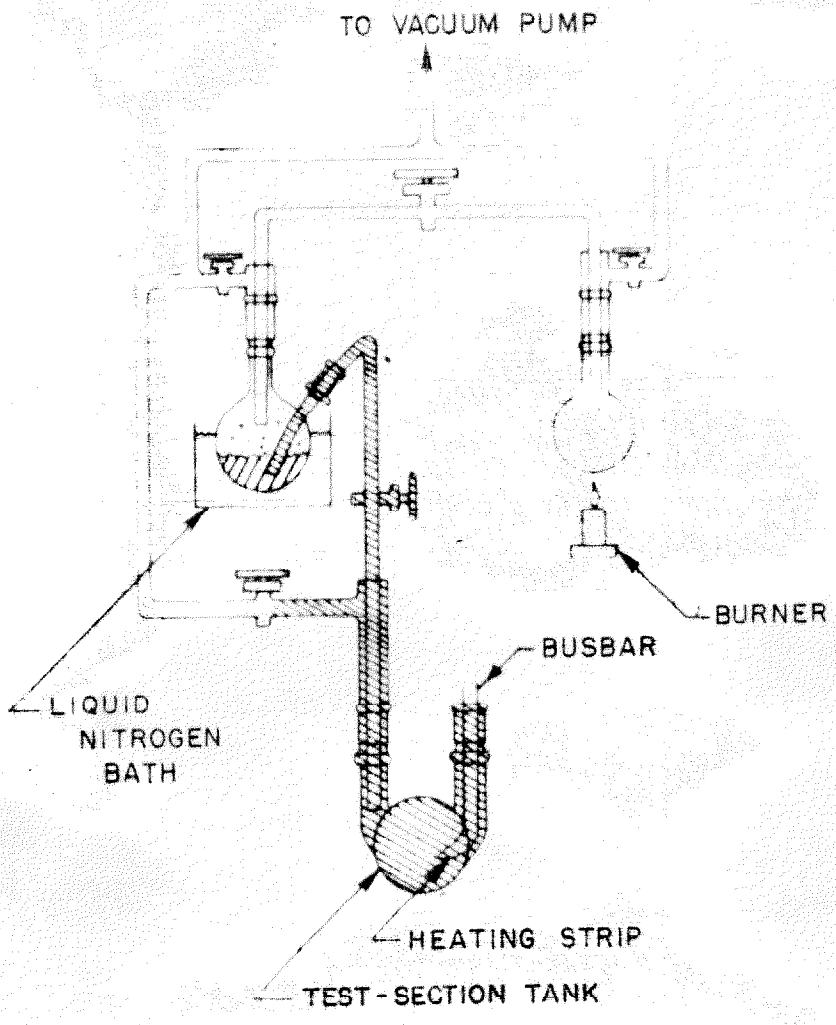

Figure 34. Degassing System for Carbon Tetrachloride

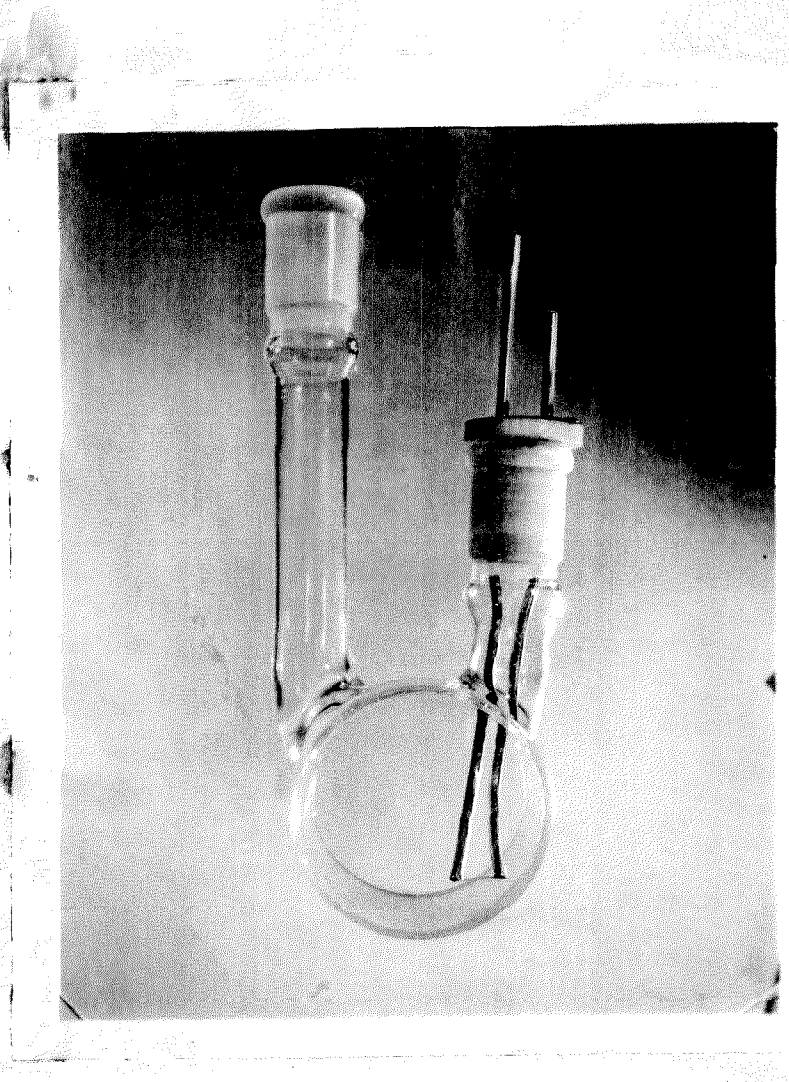

Figure 35. Test-Section Tank for Carbon Tetrachloride

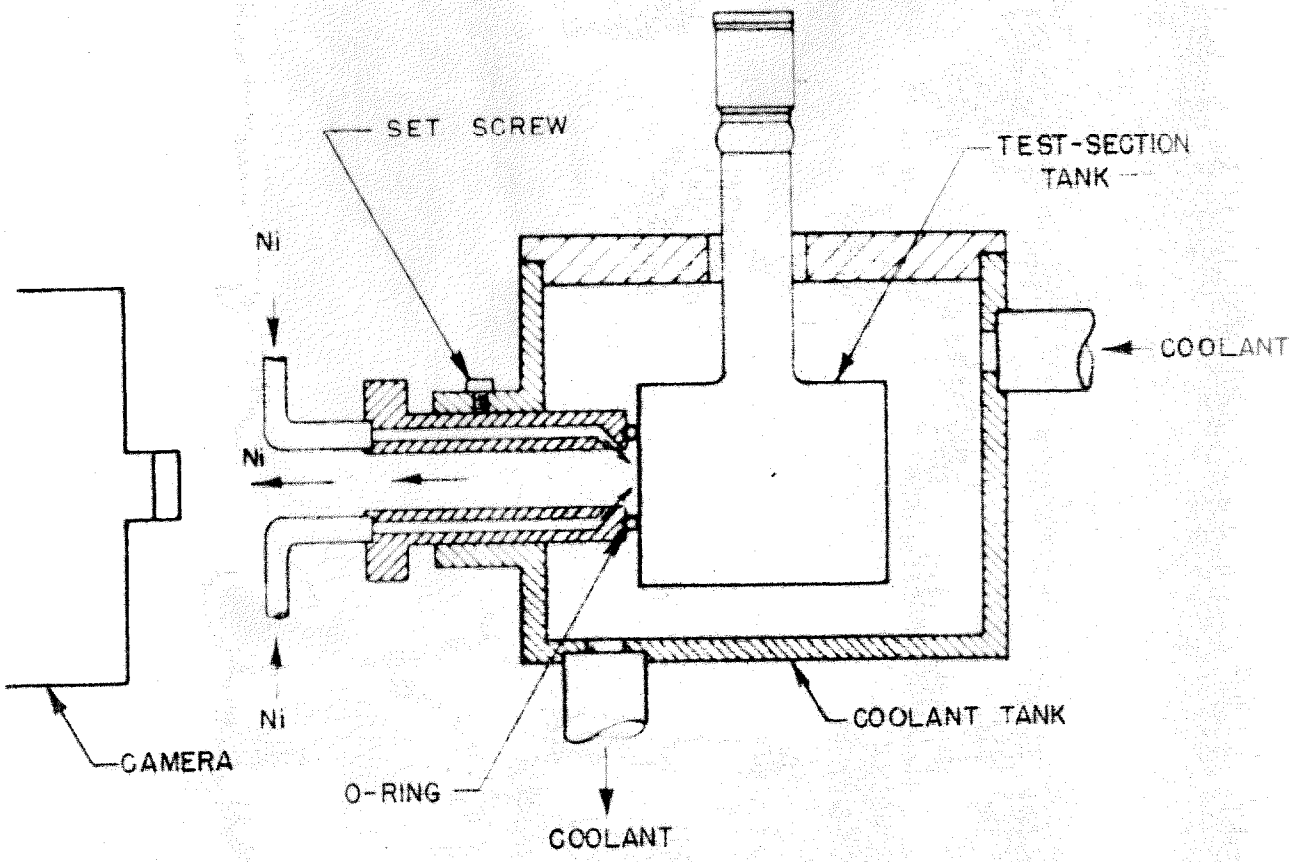

Figure 36. Coolant Tank

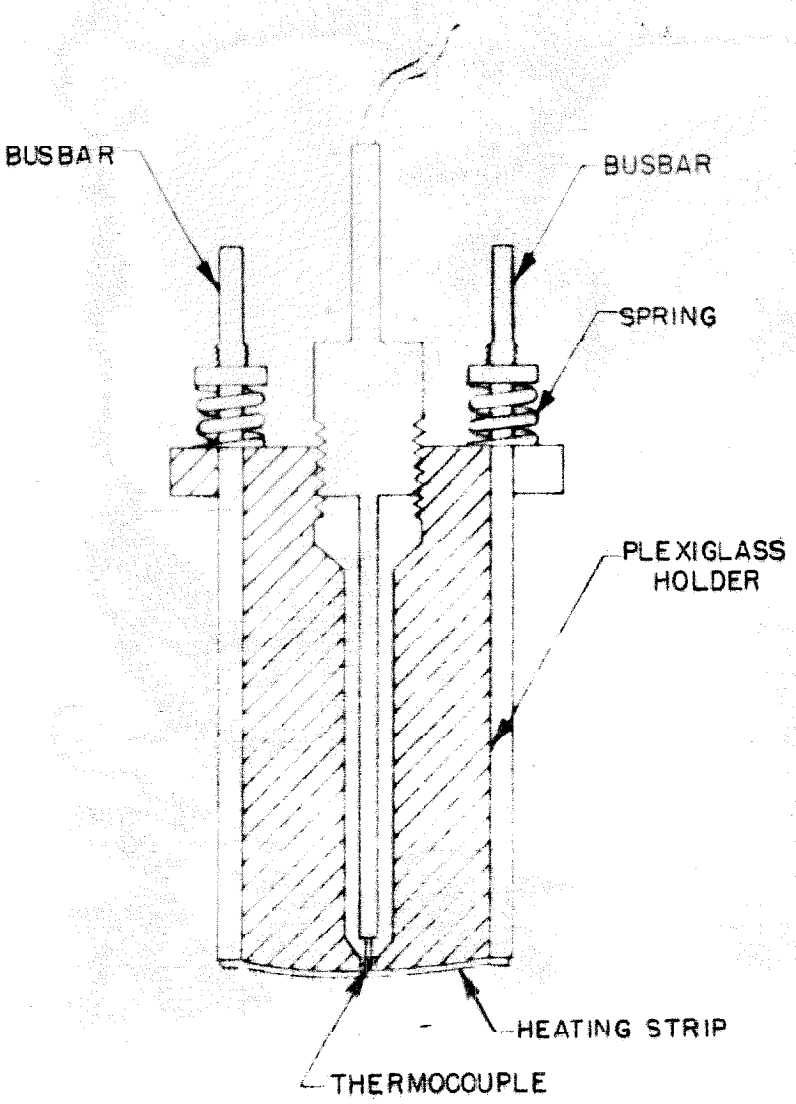

Figure 37. Apparatus for Measuring Wall Temperature

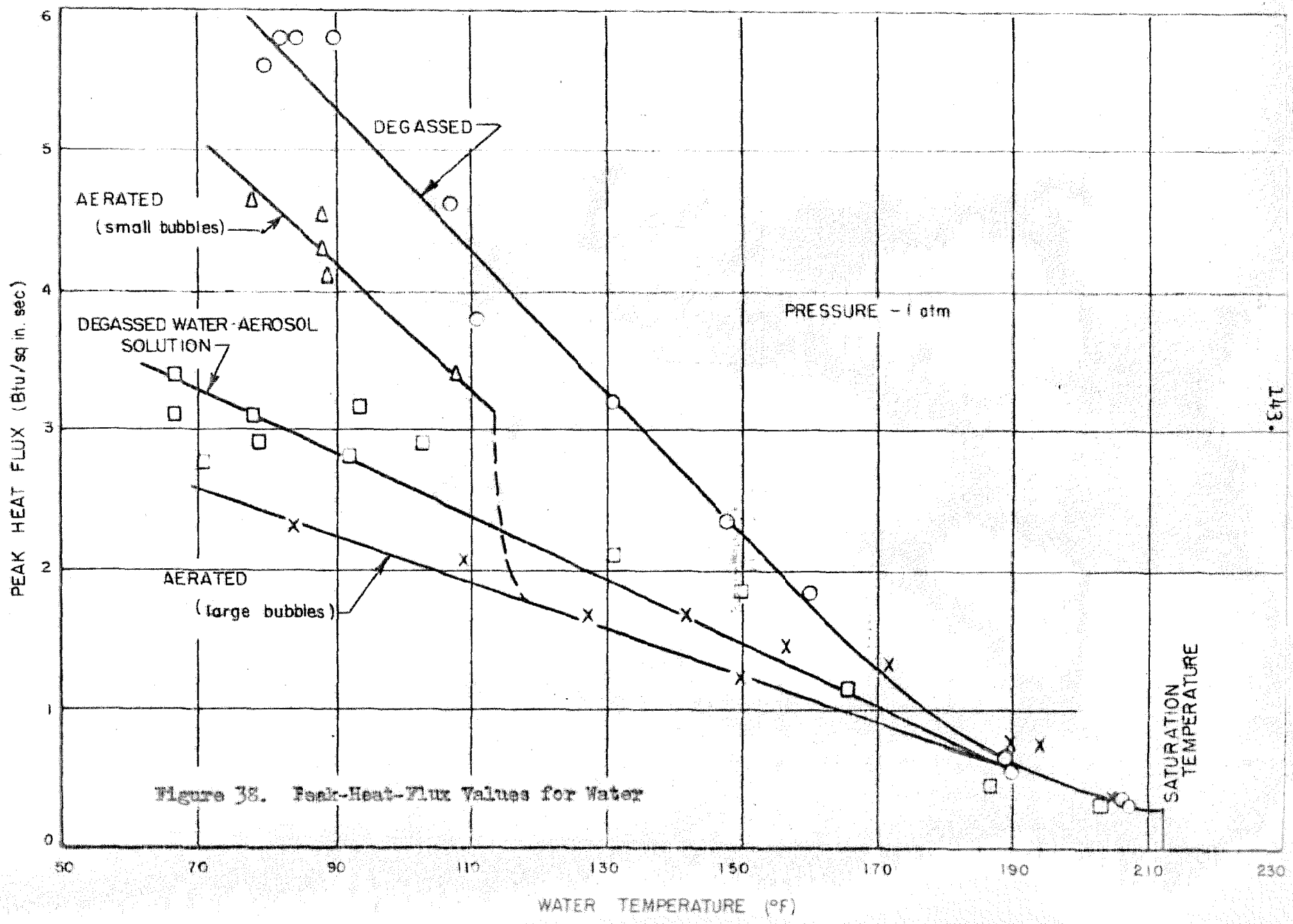

Figure 38. Peak-Heat-Flux Values for Water

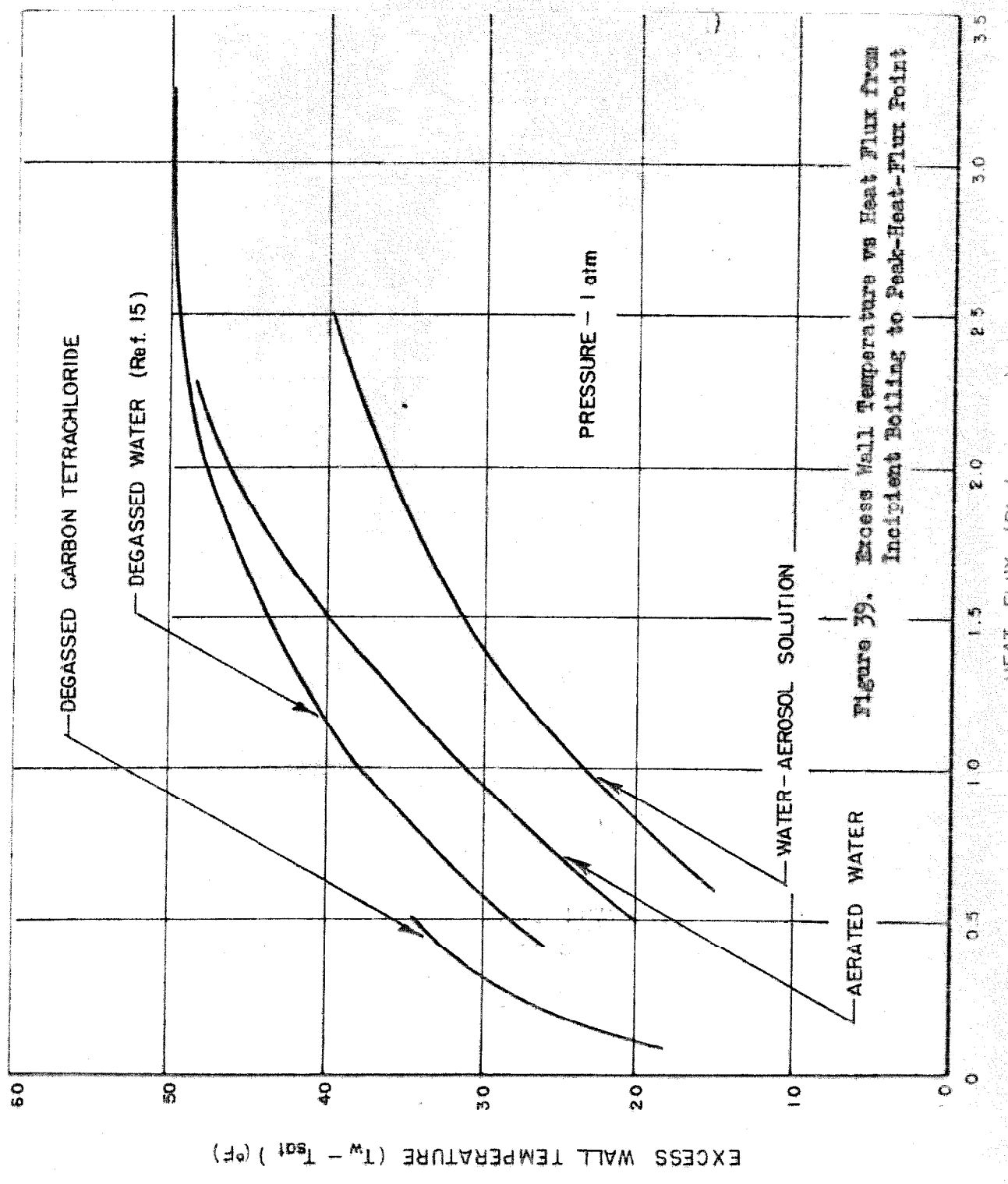

Figure 39. Excess Wall Temperature vs Heat Flux from Incipient Boiling to Peak-Heat-Flux Point

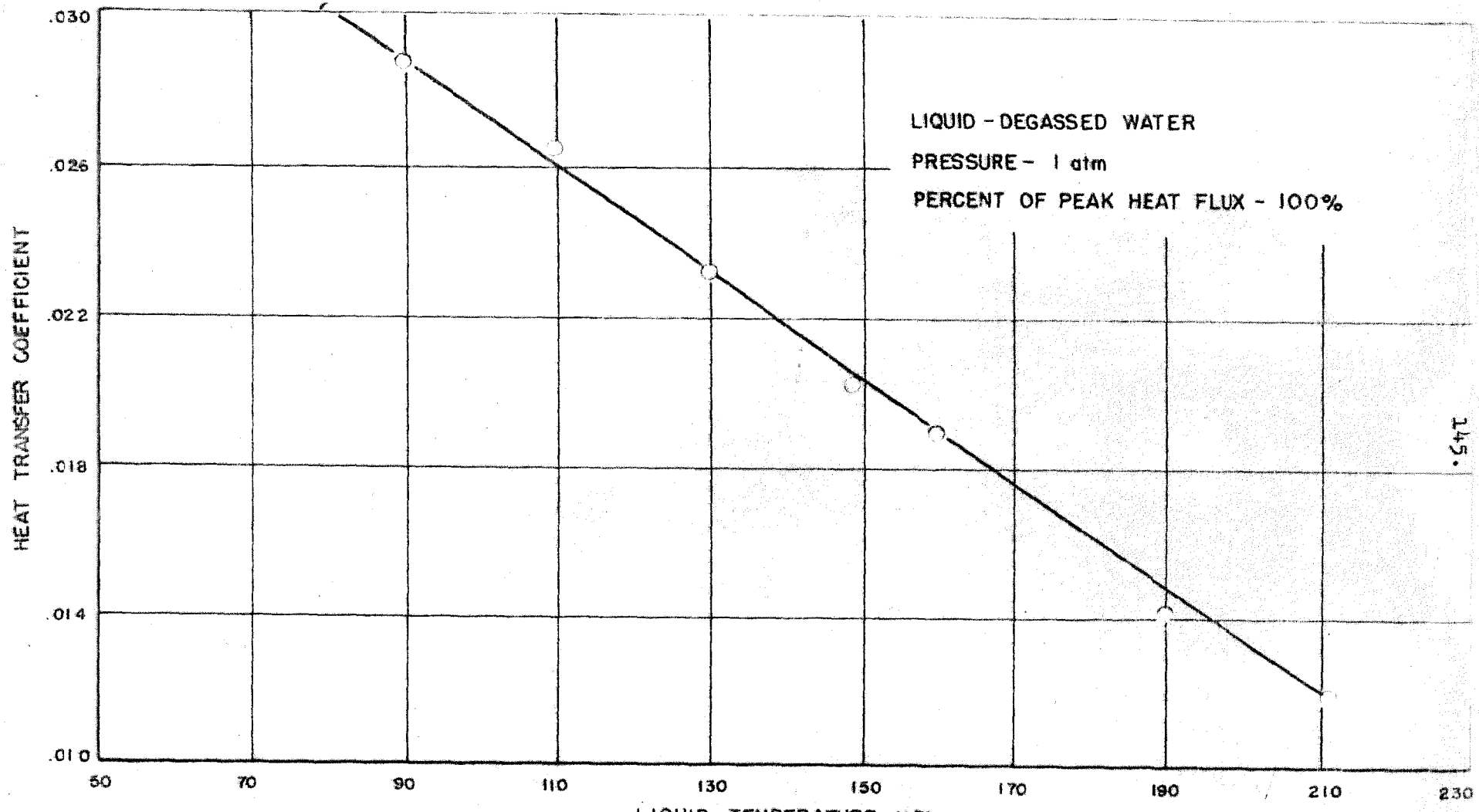

Figure 40. Heat Transfer Coefficient vs Liquid Temperature

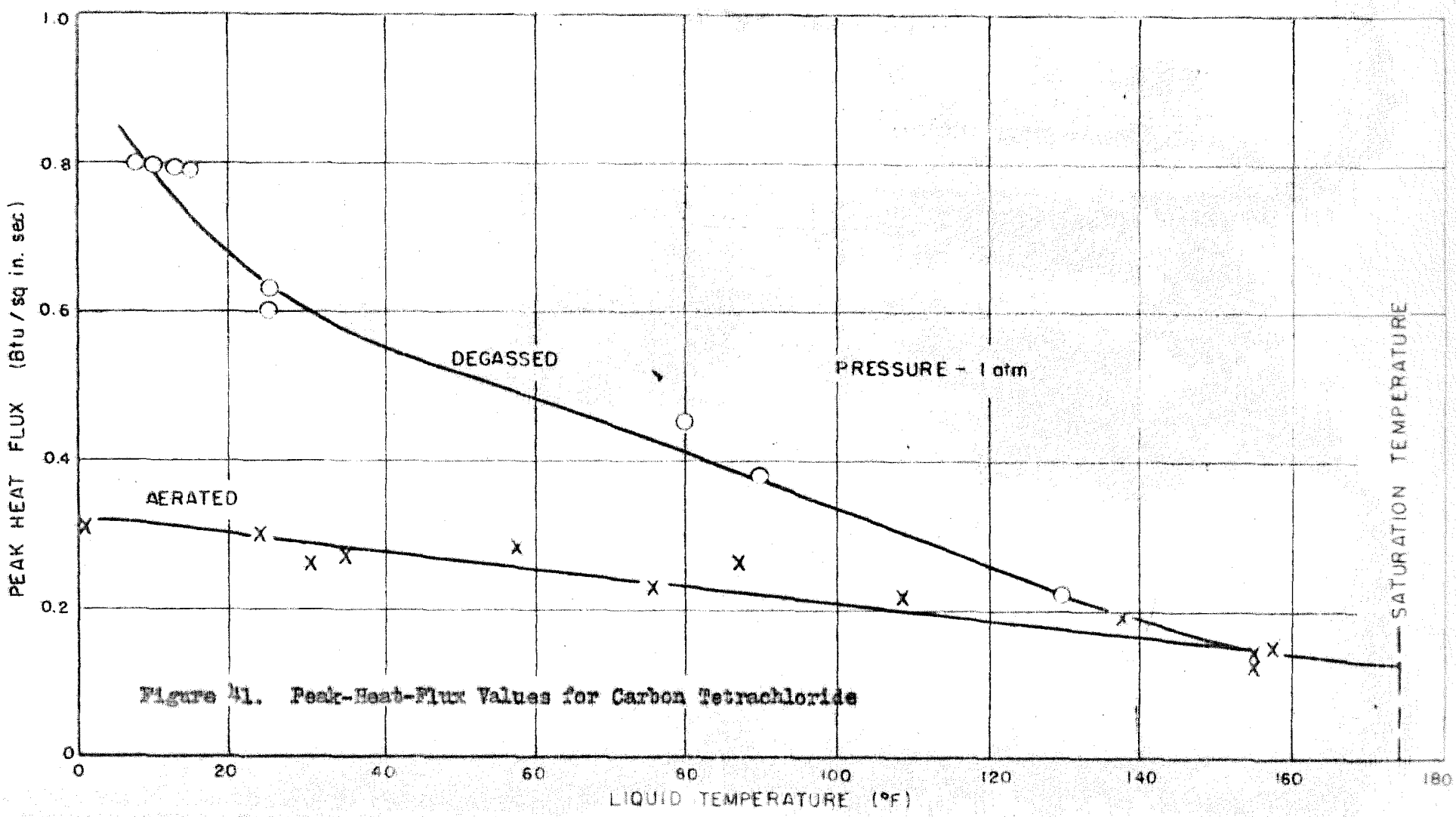

Figure 41. Peak-Heat-Flux Values for Carbon Tetrachloride

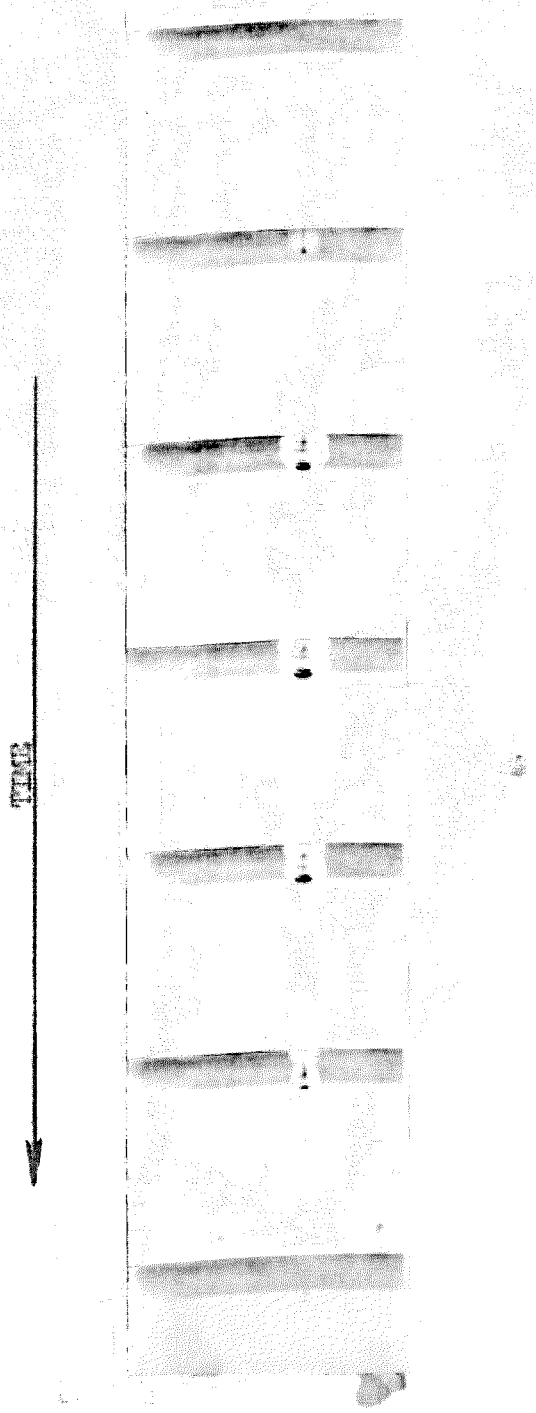

Figure 42. Photographs of typical Nucleate Bubble Forming on Underside of Heating Strip in Water

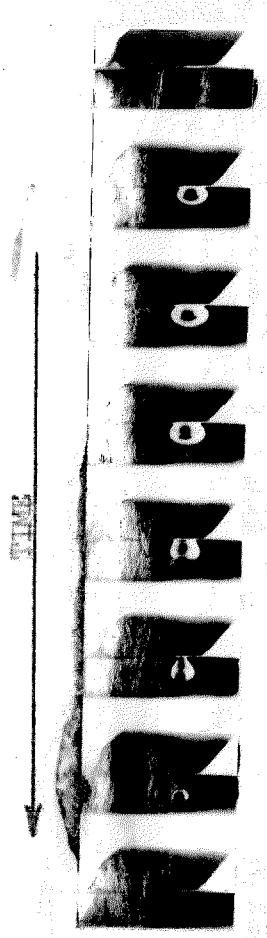

Figure 43. Nucleate Bubble Detaching from Underside of Heating Strip in Water

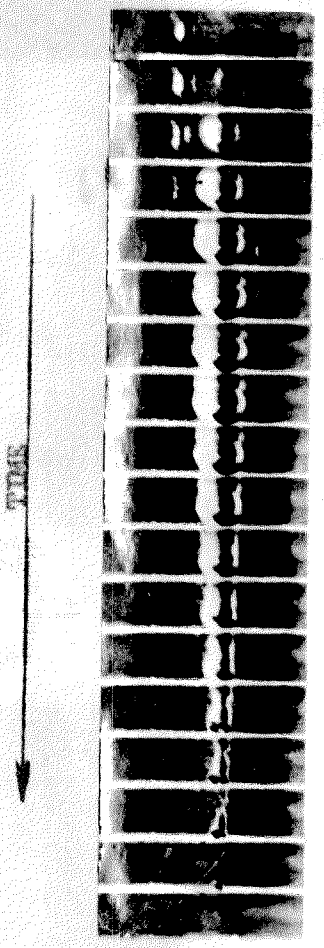

Figure 44. Photographs of Bubble Base Separating from Heating Surface in Water

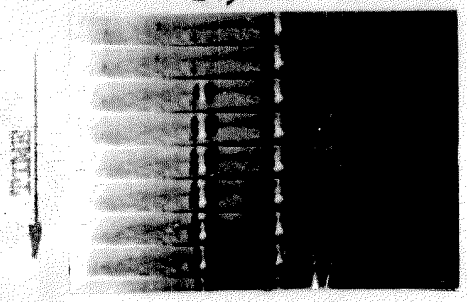

a) 31 per cent of Peak Heat Flux

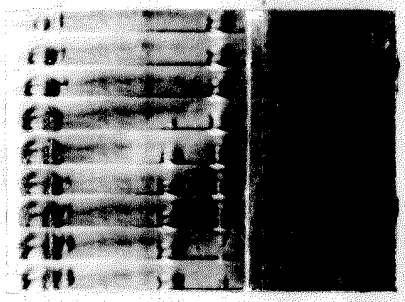

b) 34 per cent of Peak Heat Flux

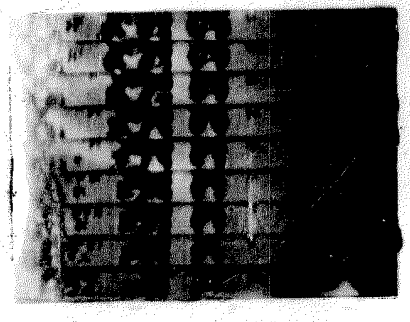

c) 63 per cent of Peak Heat Flux

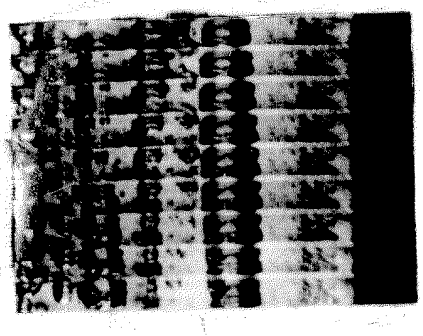

d) 74 per cent of Peak Heat Flux

Figure 45. Photographs of Nucleate Bubbles in Water Showing Influence of Heat Flux

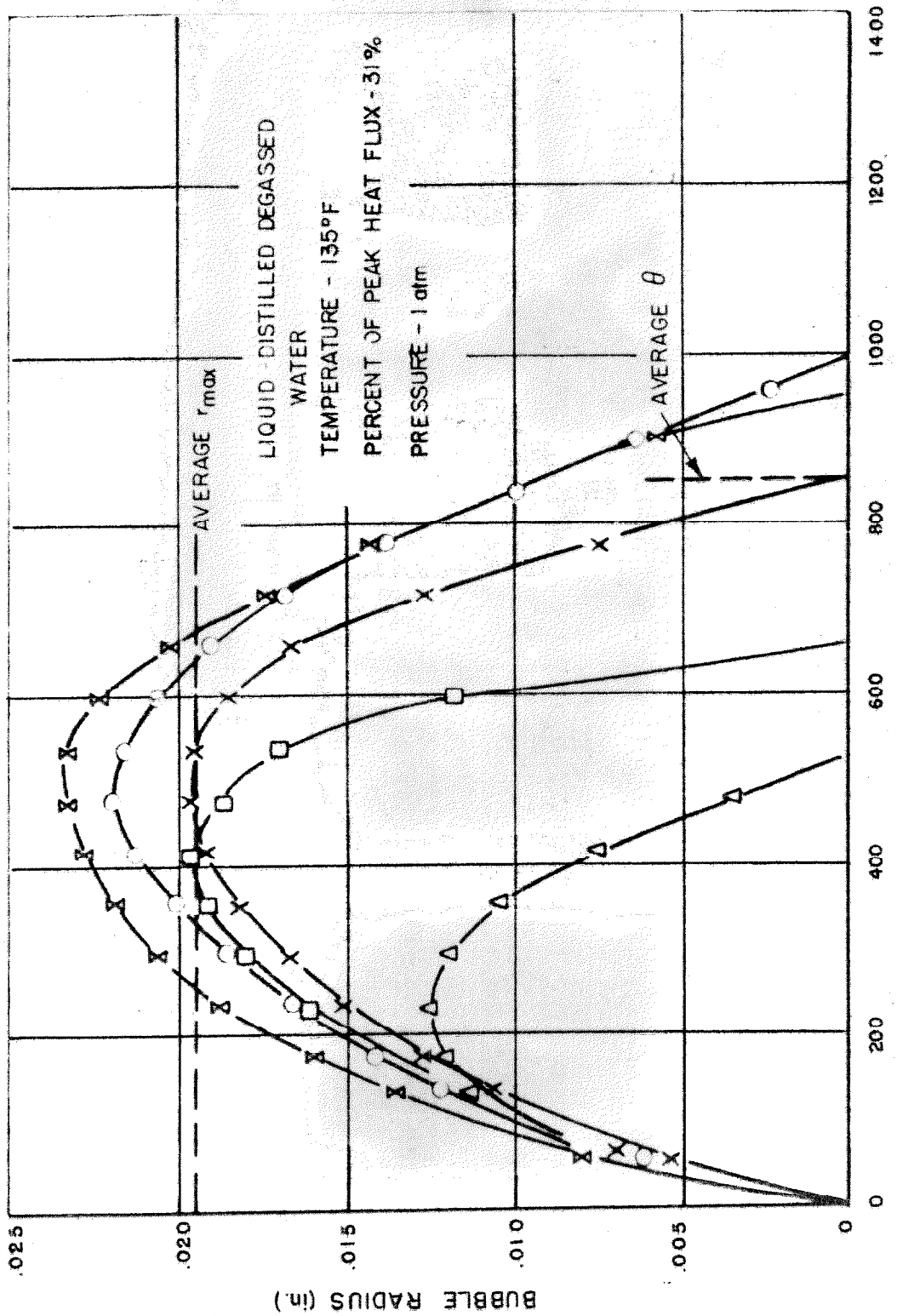

Figure 46. Bubble Radius vs Time

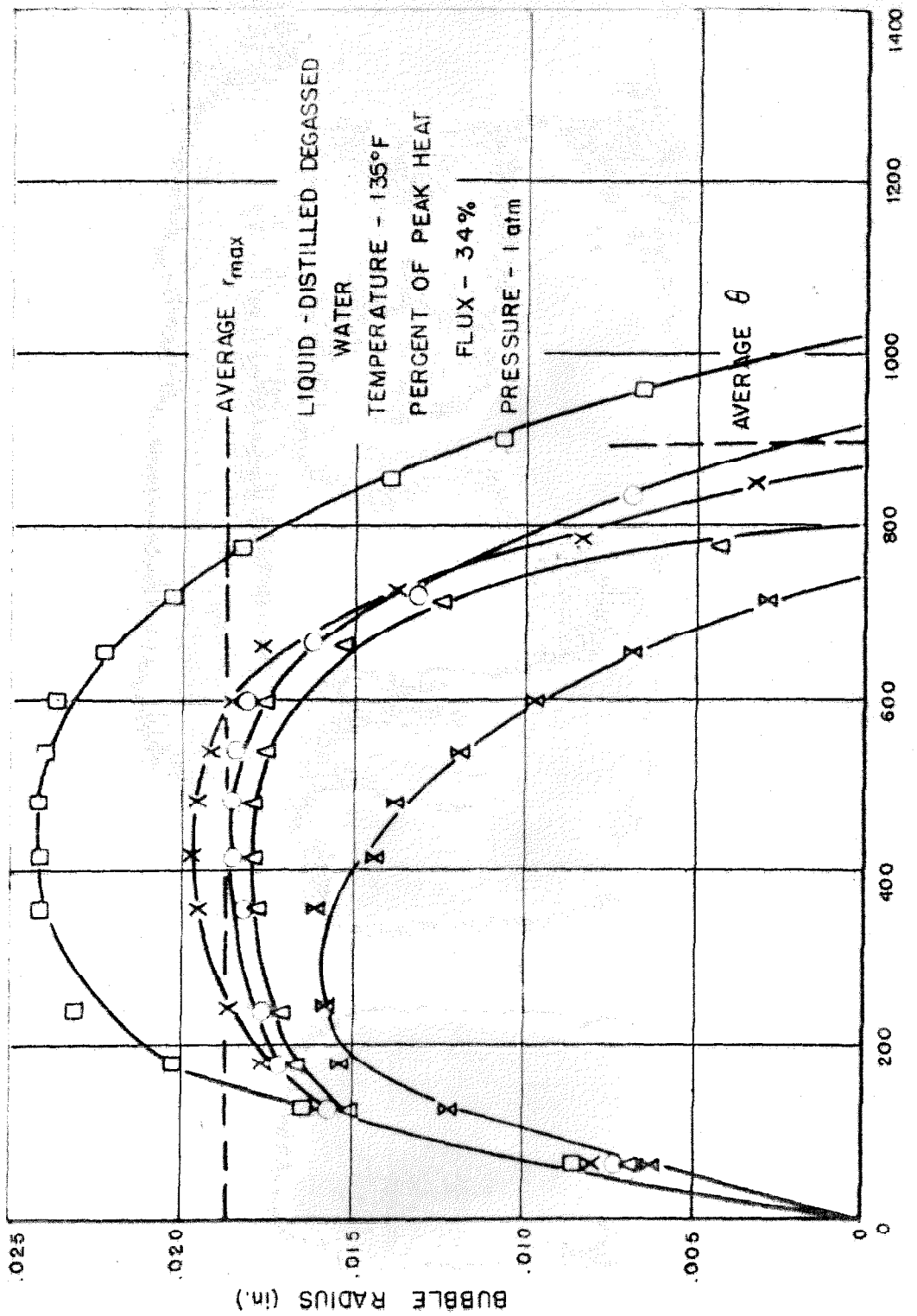

Figure 47. Bubble Radius vs Time

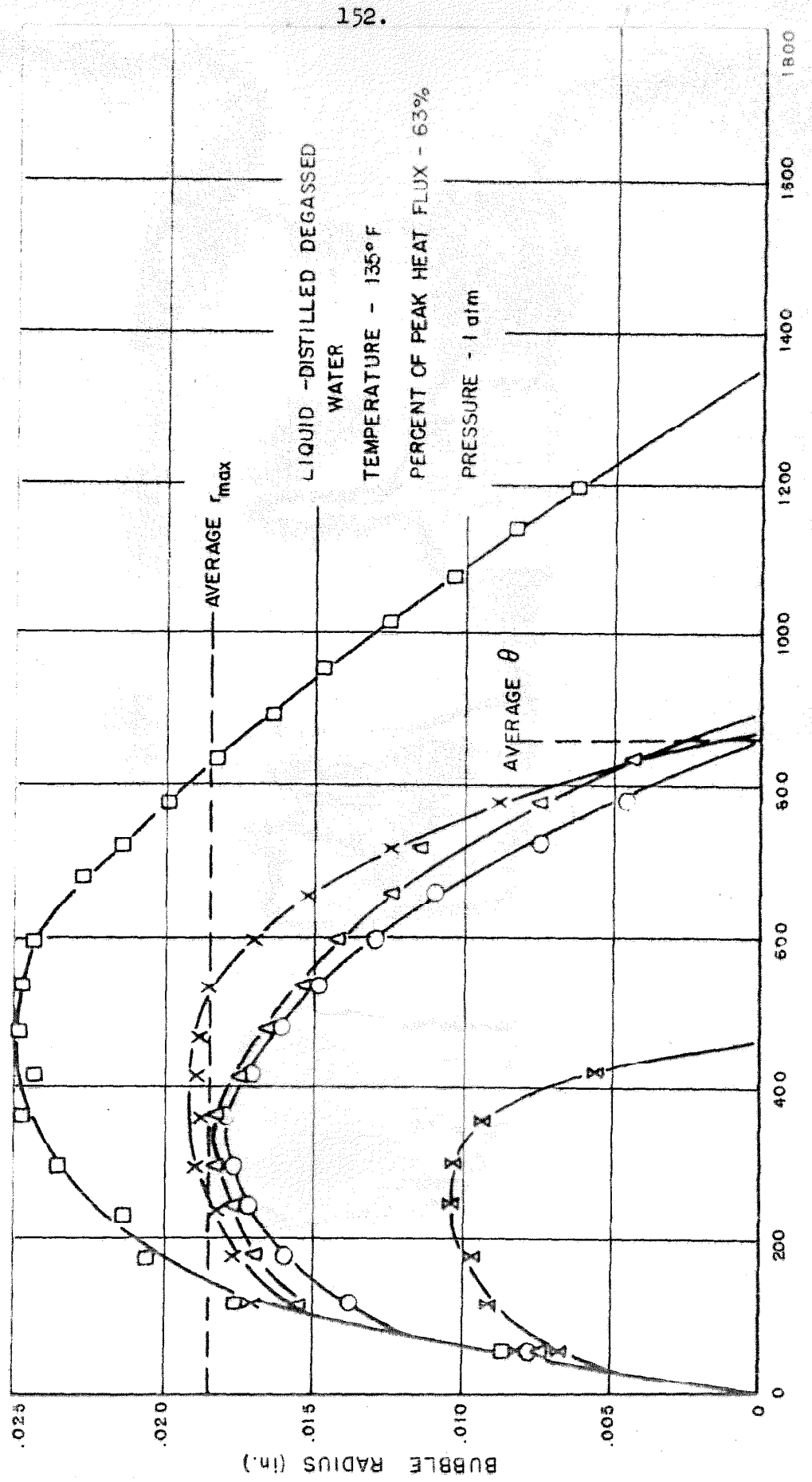

Figure 48. Bubble Radius vs Time

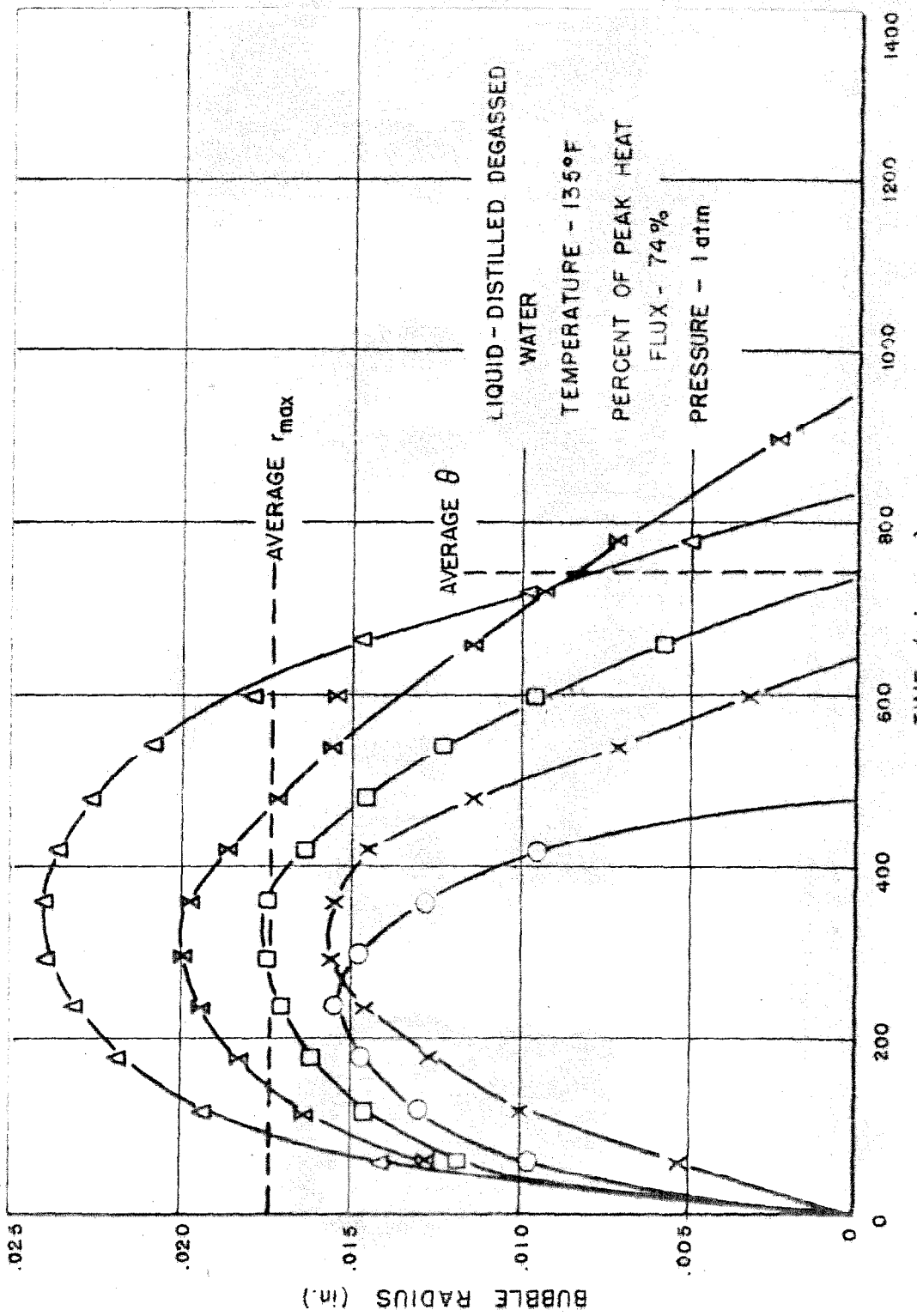

Figure 49. Bubble Radius vs Time

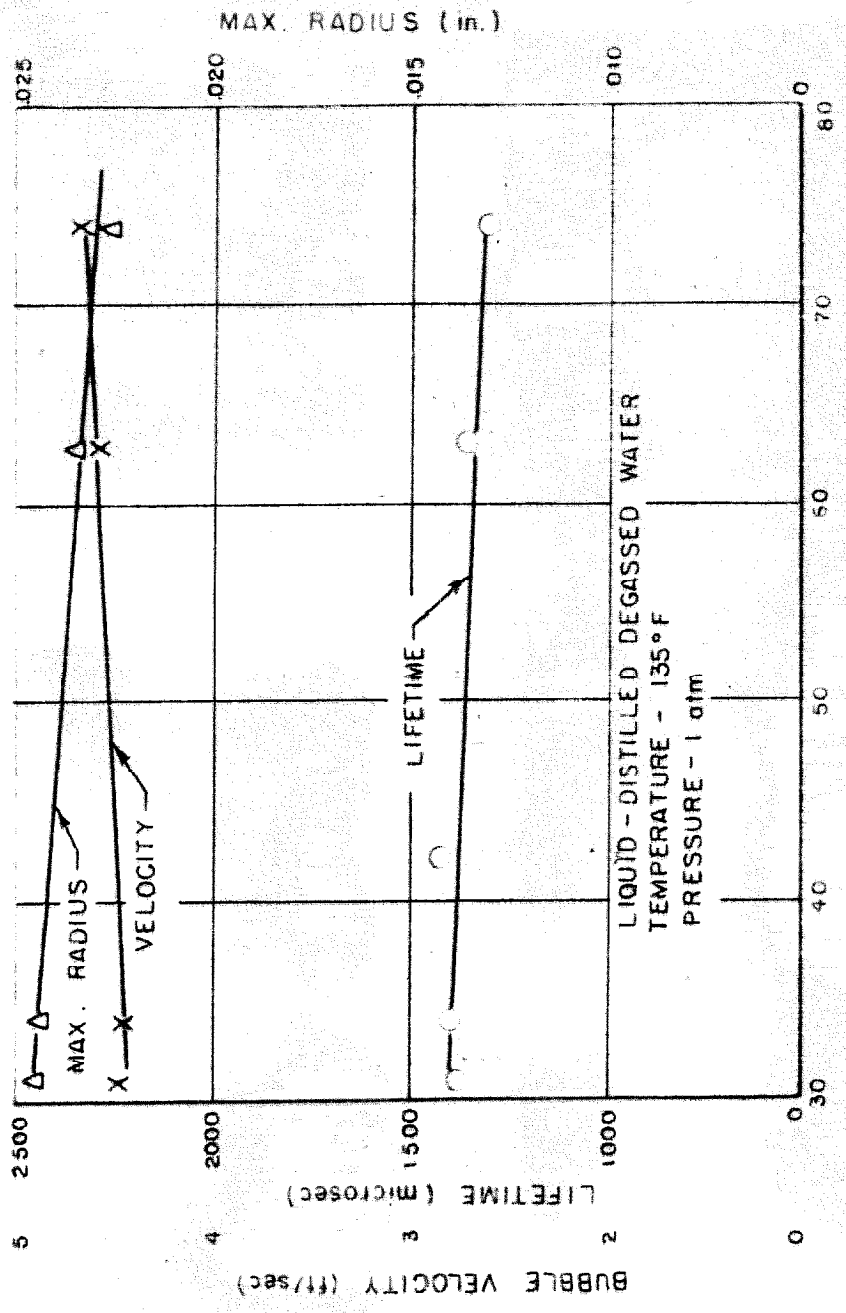

Figure 50. Effect of Heat Flux on Bubble Dynamics

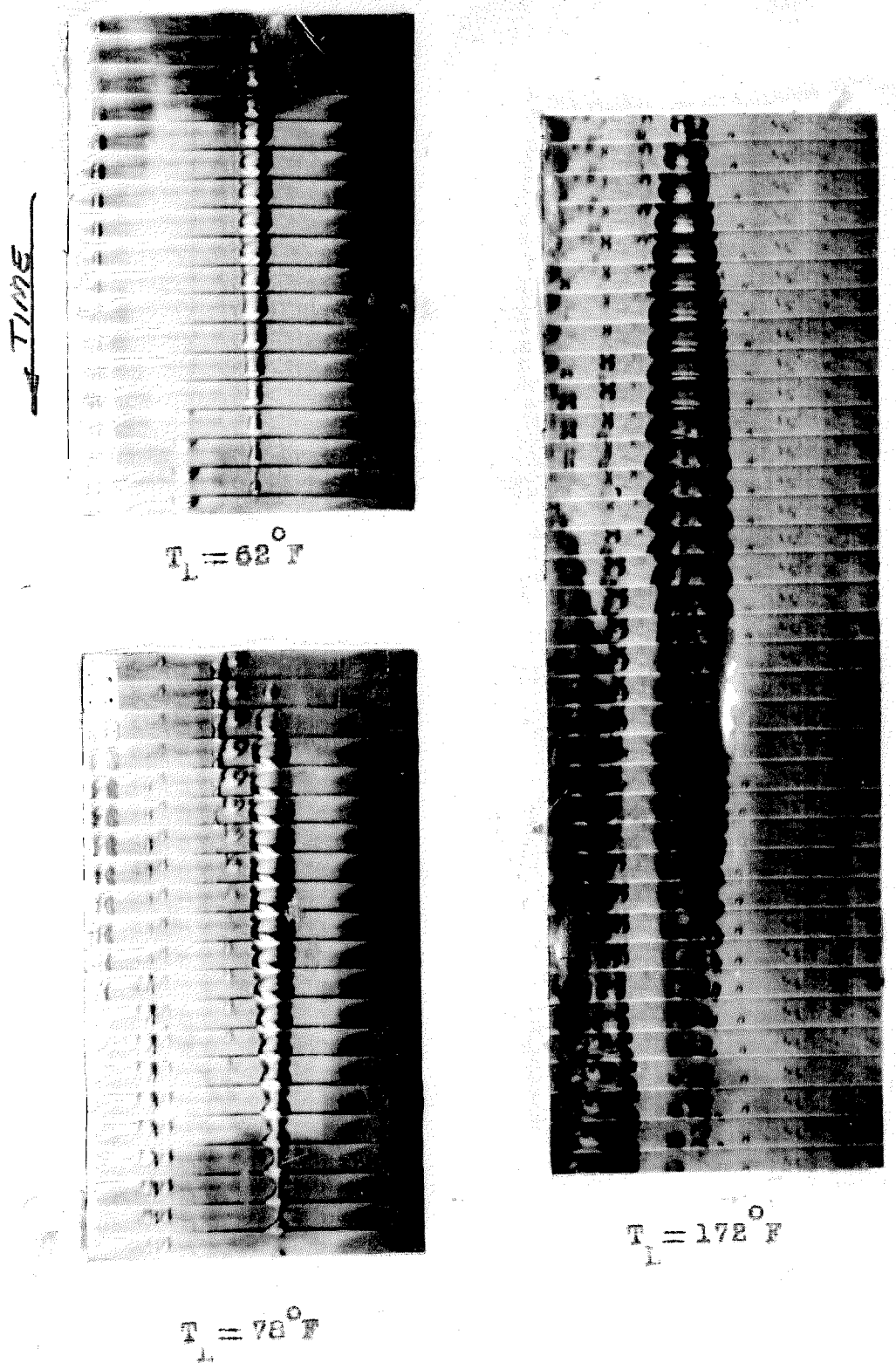

Figure 51. Photographs of Bubbles Showing Influence of Liquid Temperature for Water

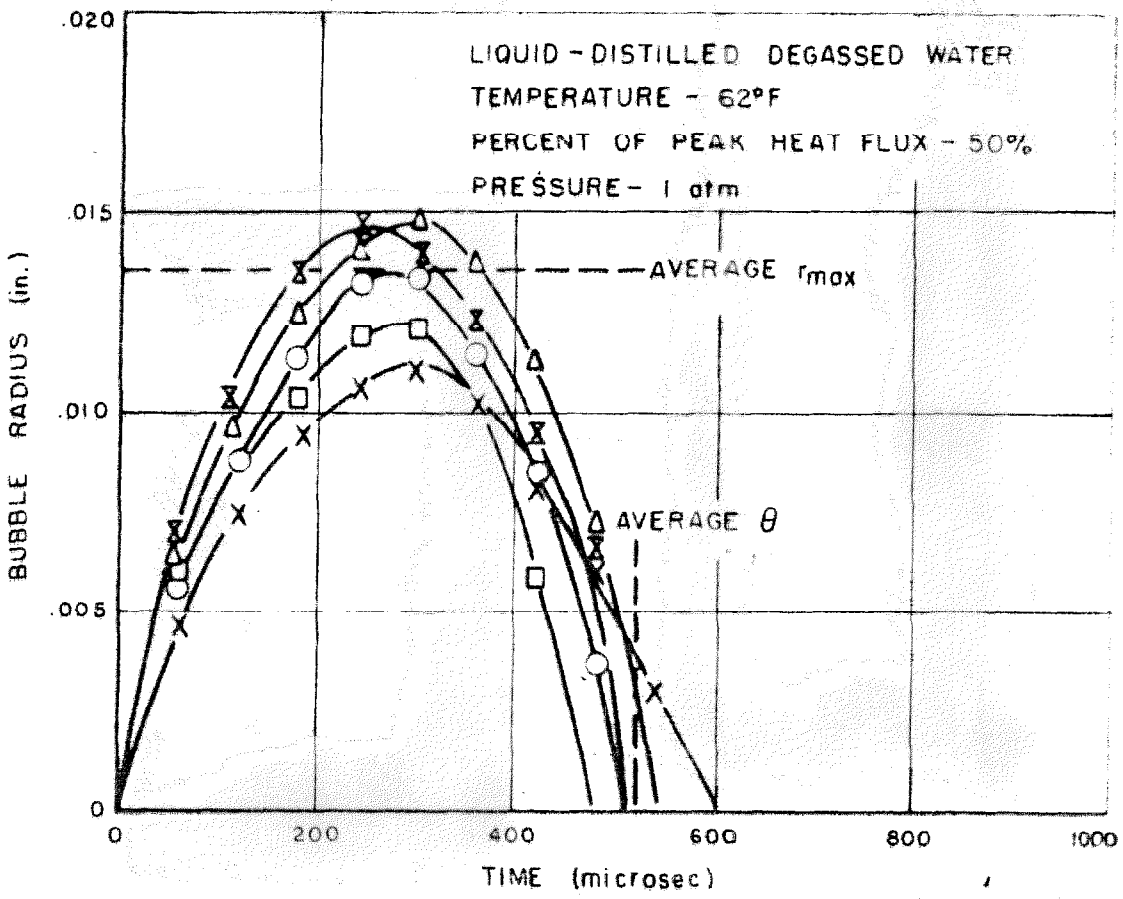

Figure 52. Bubble Radius vs Time

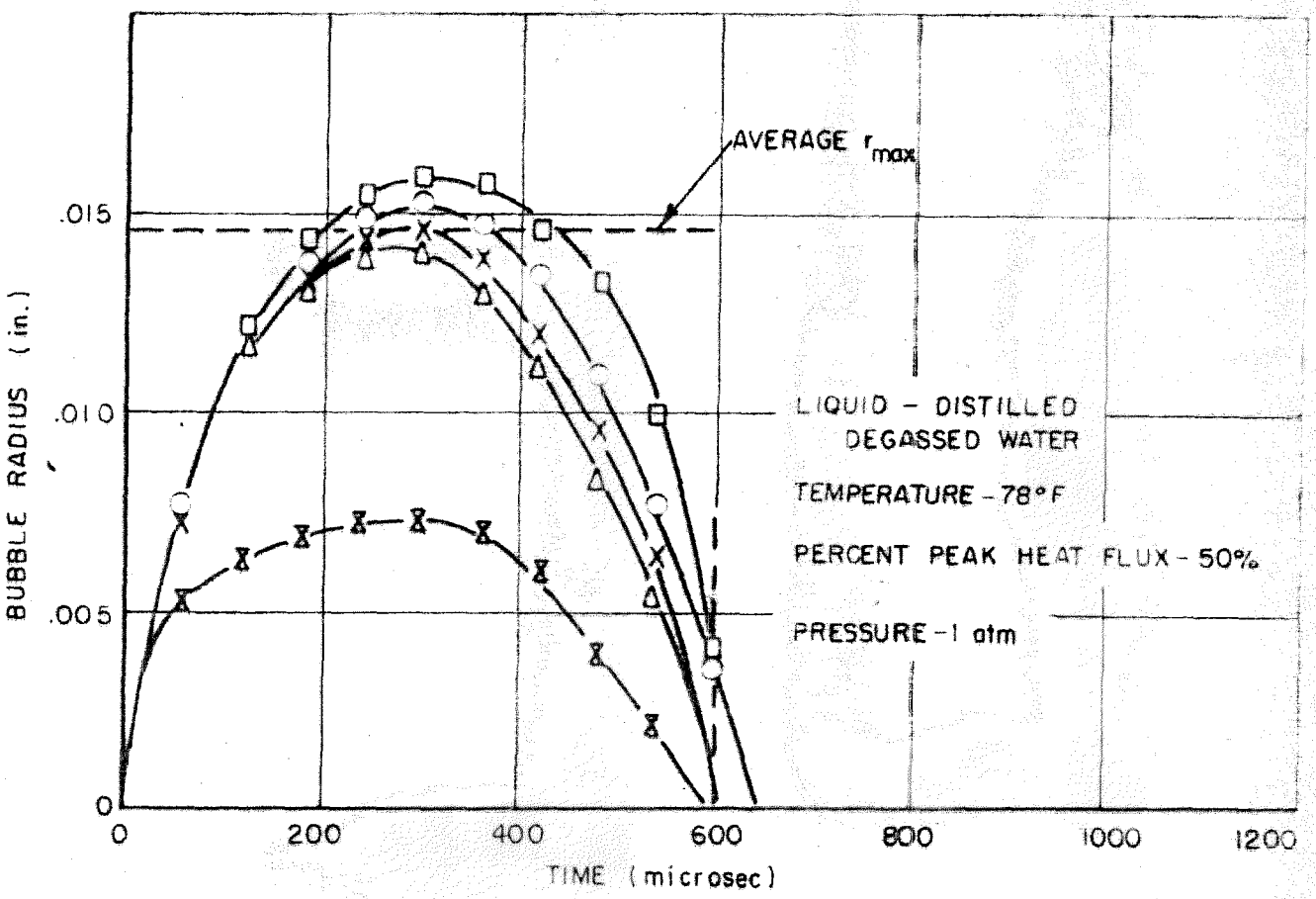

Figure 53. Bubble Radius vs Time

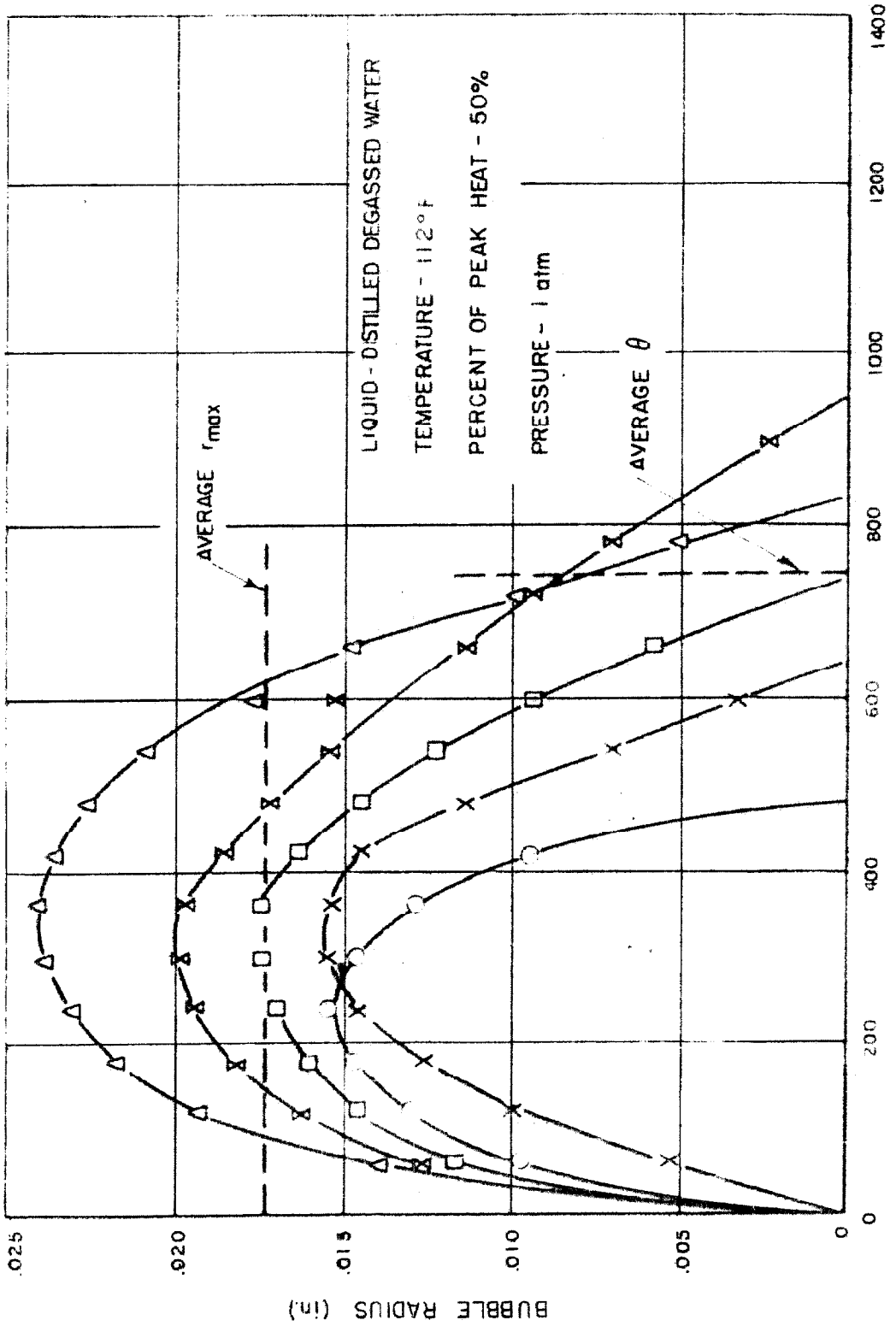

Figure 54. Bubble Radius vs Time

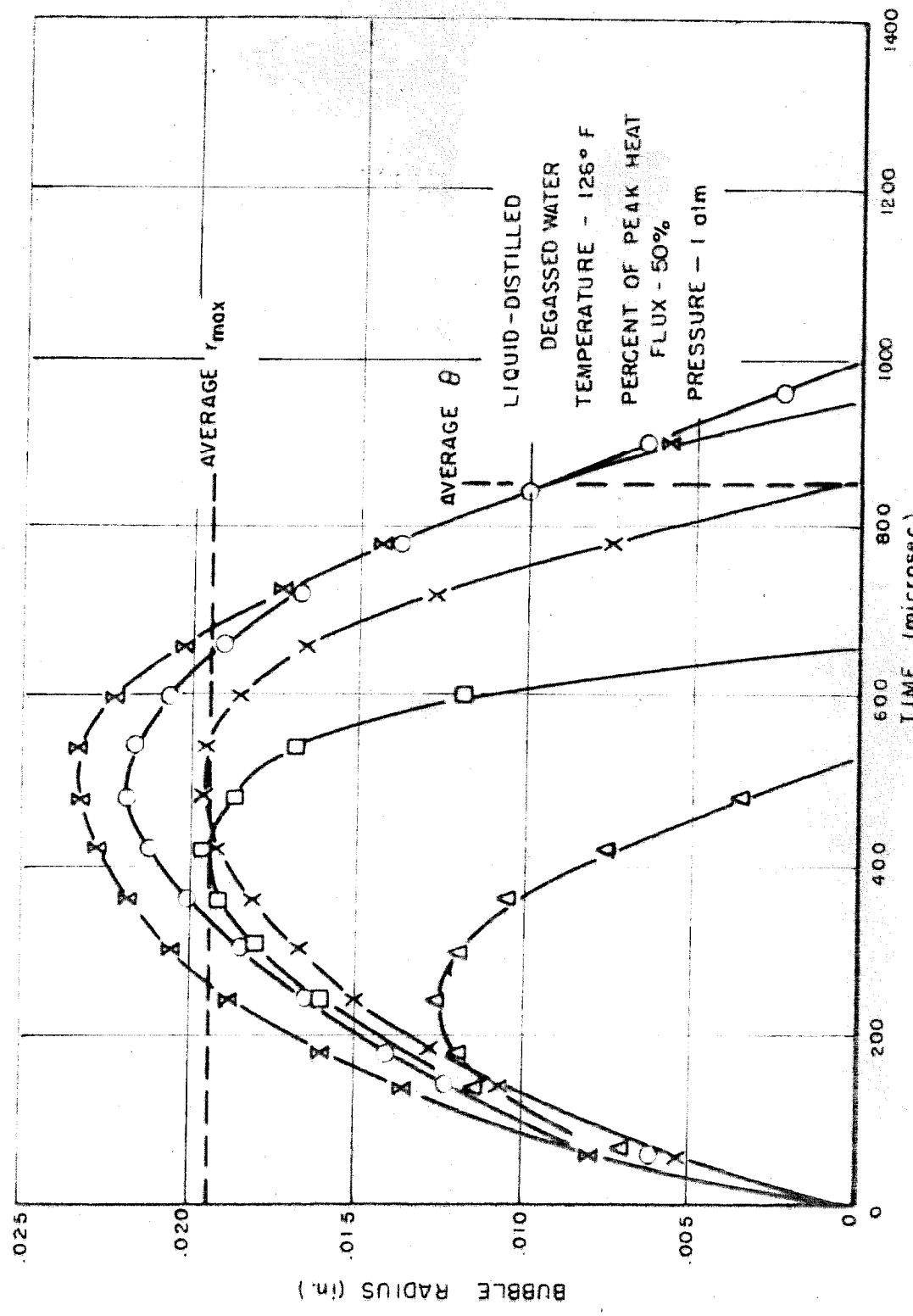

Figure 55. Bubble Radius vs Time

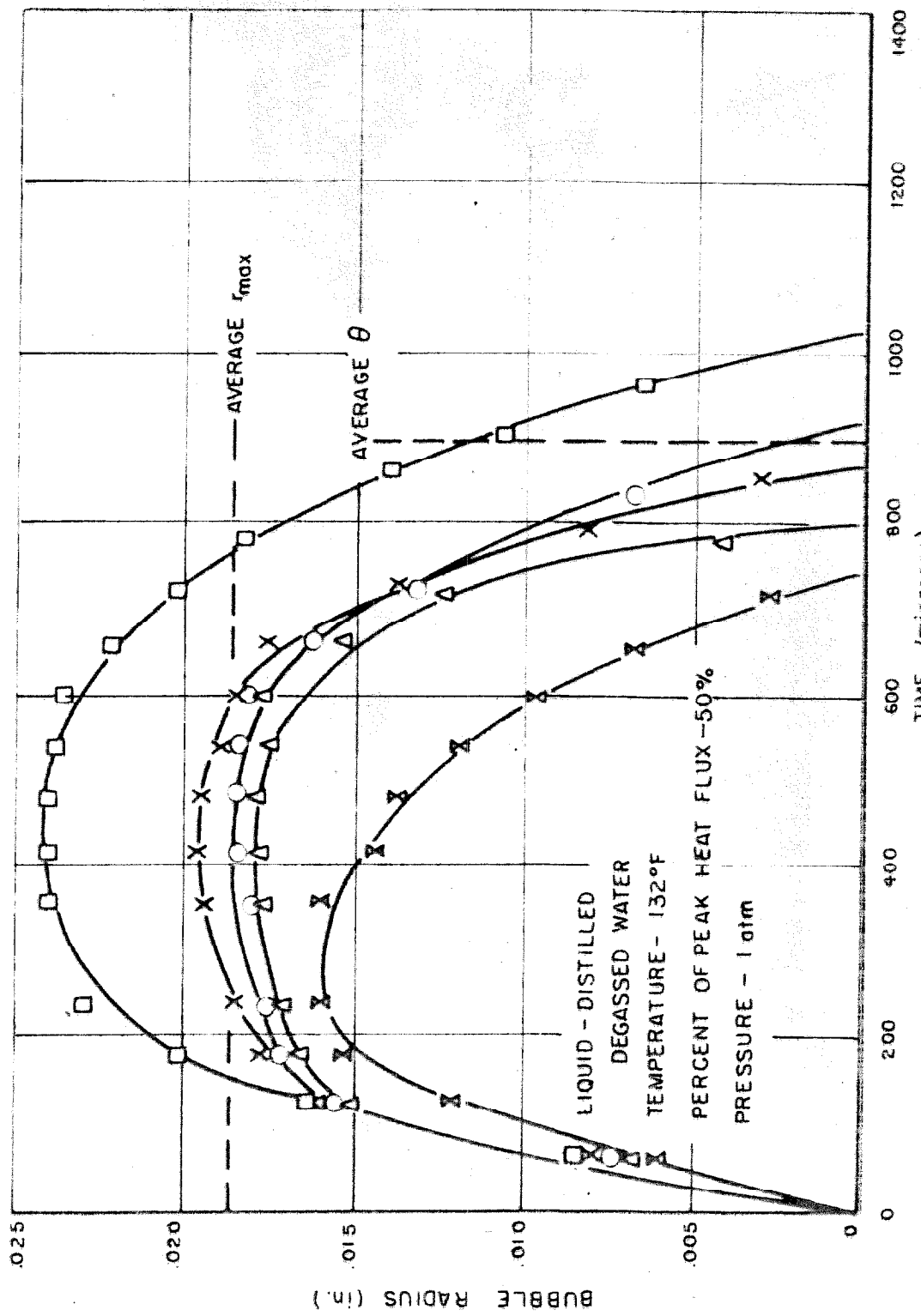

Figure 55. Bubble Radius vs Time

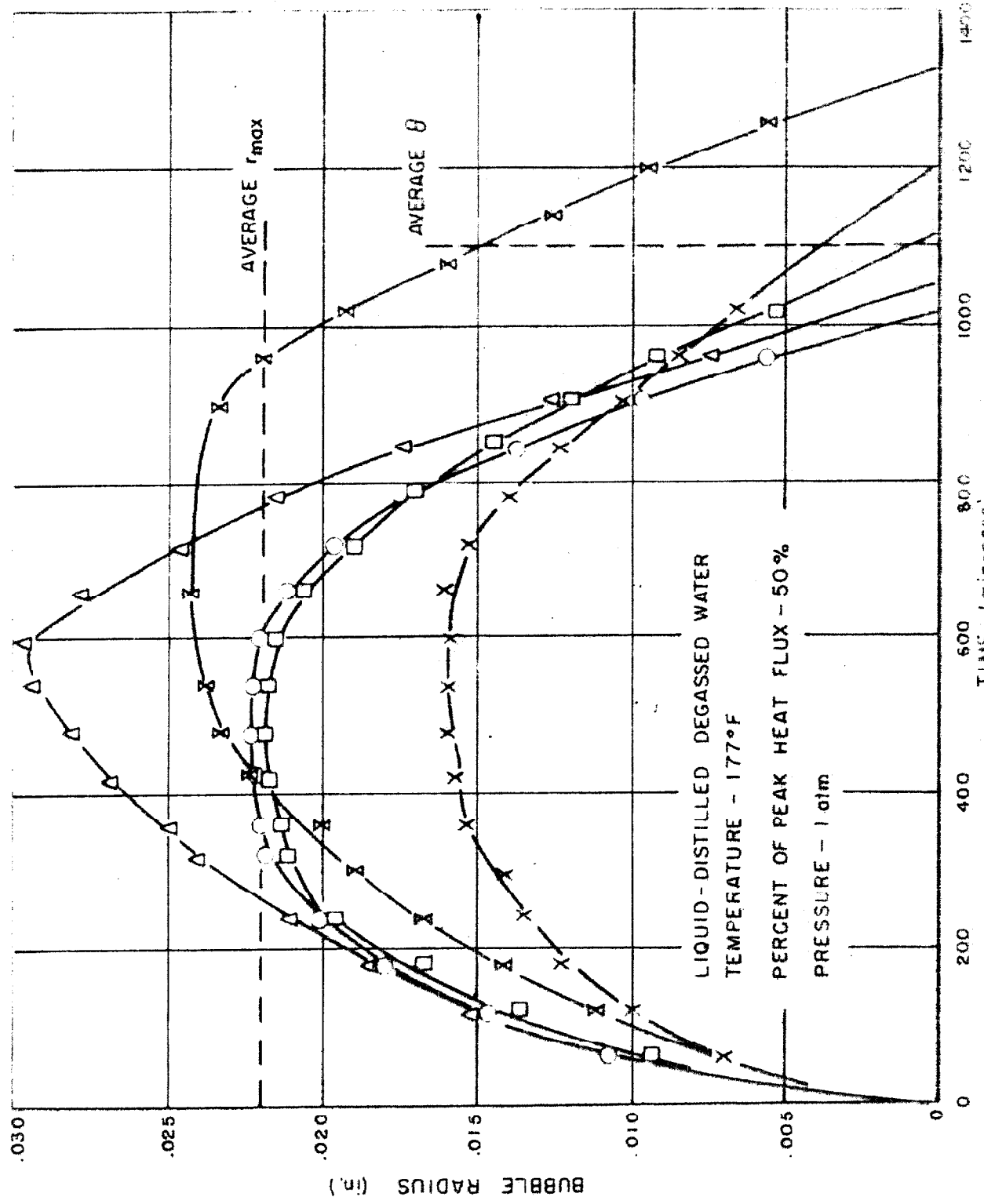

Figure 57. Bubble Radius vs Time

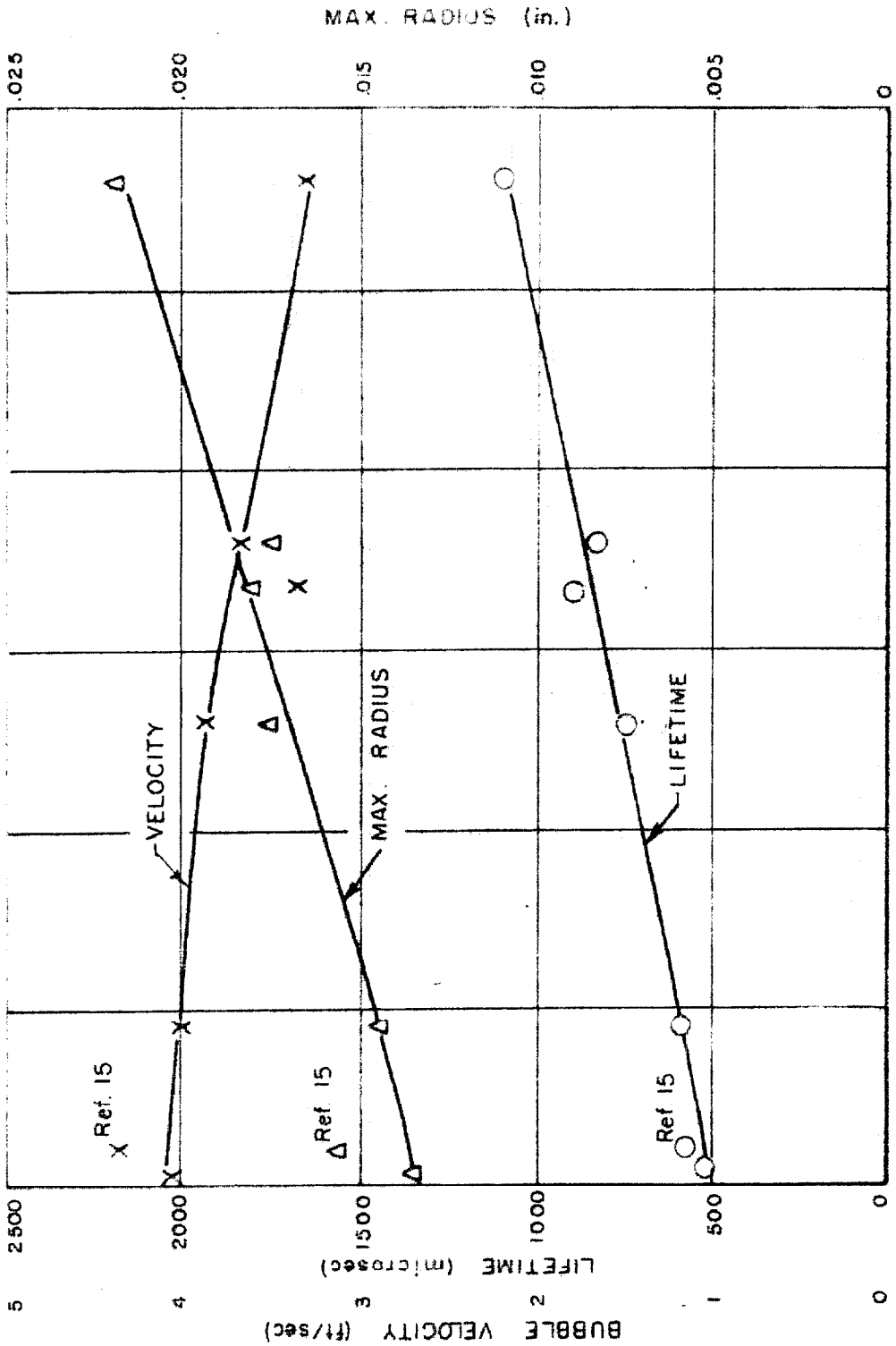

Figure 58. Effect of Liquid Temperature on Bubble Dynamics

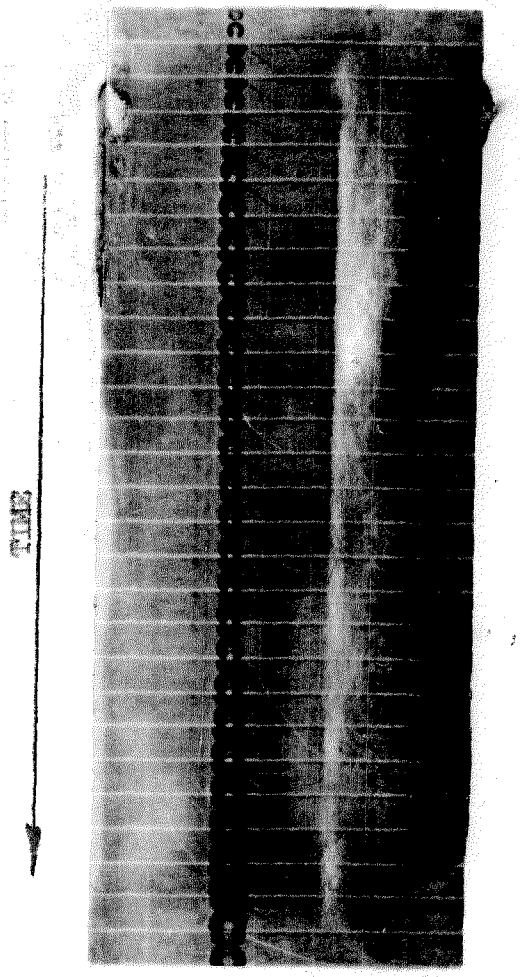

Figure 59. Photographs of Stagnant Gas Bubble in Water

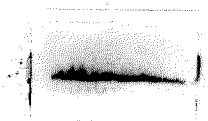

Figure 60. Photograph of Detaching Gas Bubbles in Water

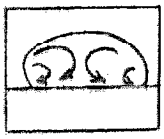

Figure 61. Circulation Pattern for Gas Bubble Liquid Film

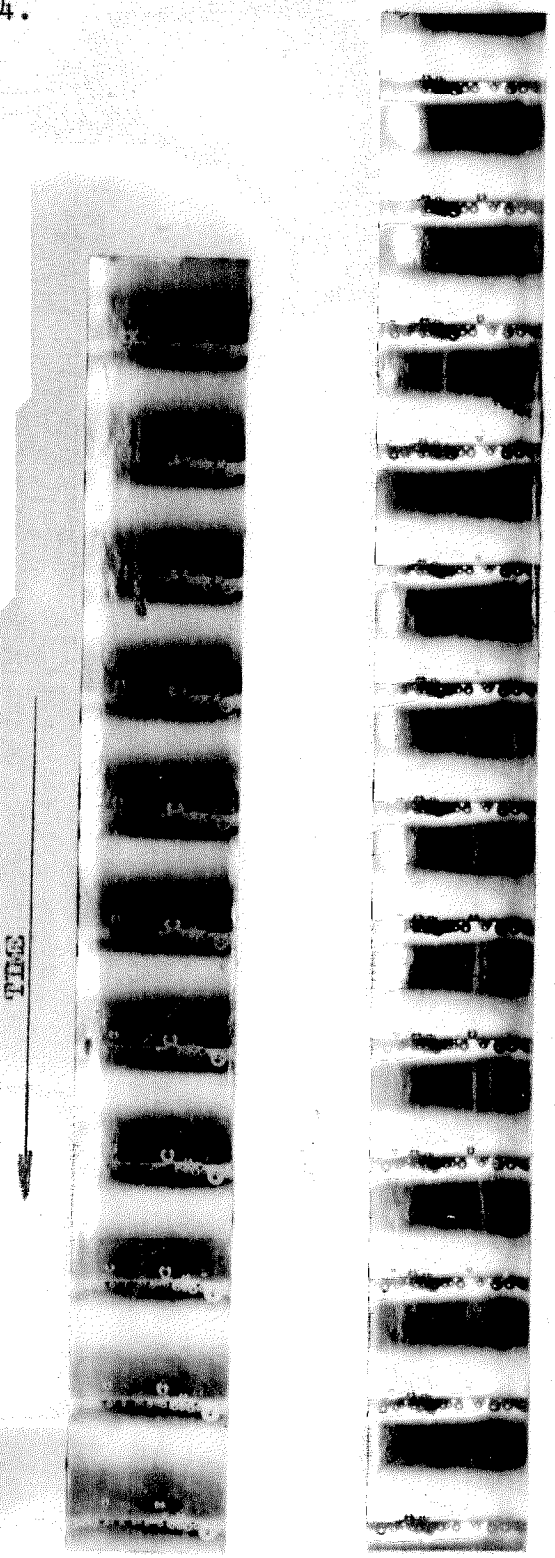

Figure 62. Photographs of Nucleate Bubbles in Water-Aerosol Solution

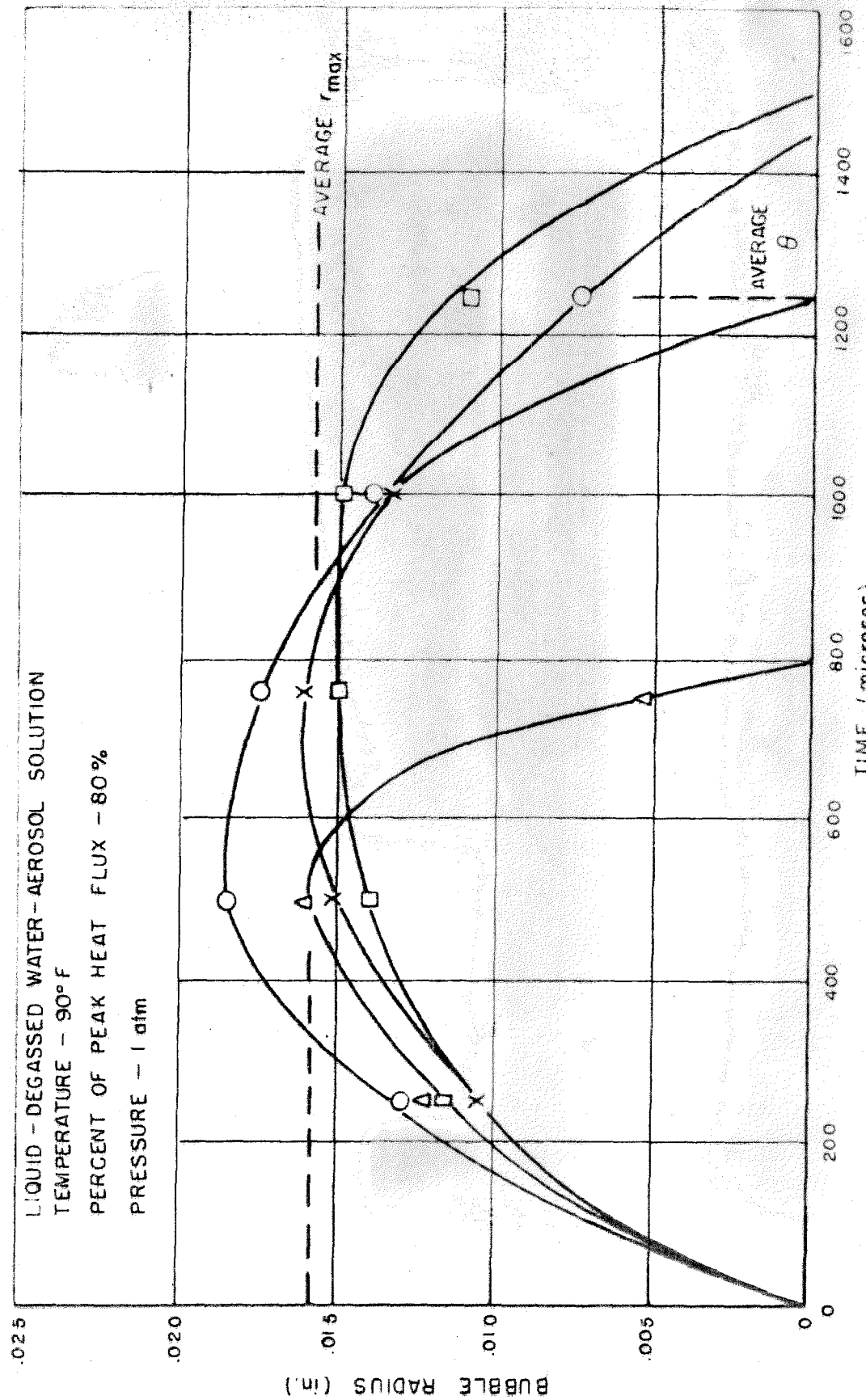

Figure 63. Bubble Radius vs Time

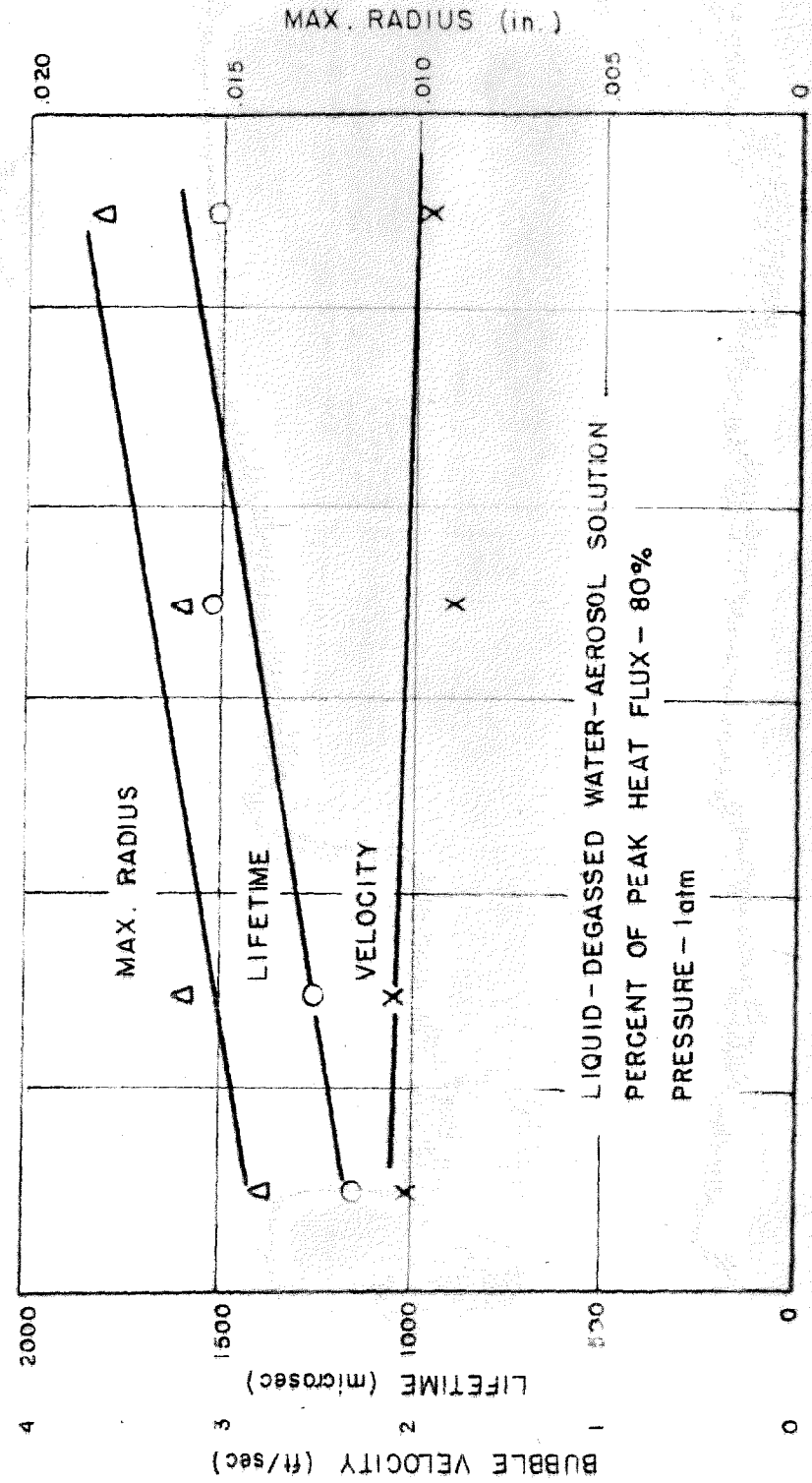

Figure 64. Effect of Liquid Temperature on Bubble Dynamics

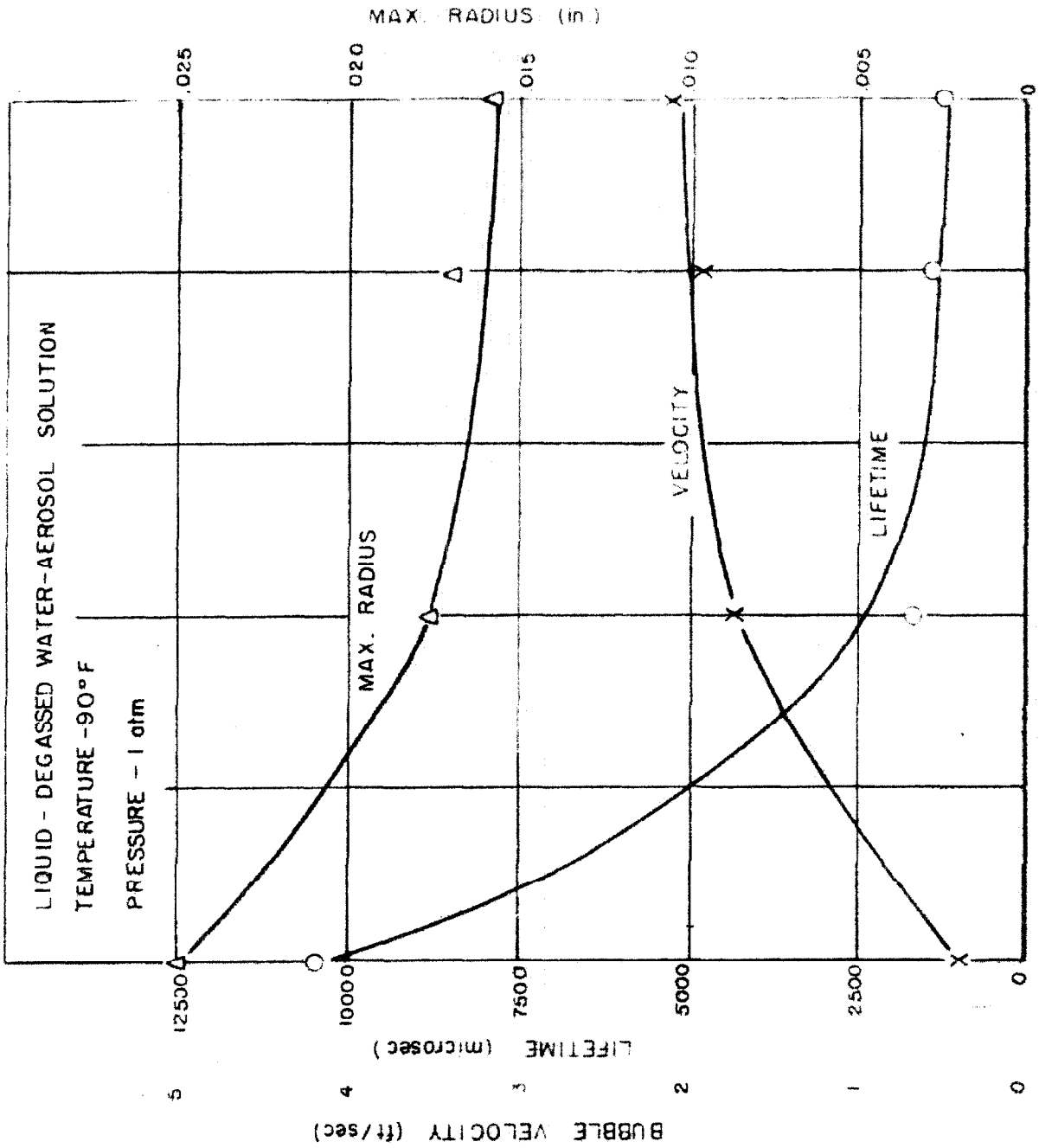

Figure 65. Effect of Heat Flux on Bubble Dynamics

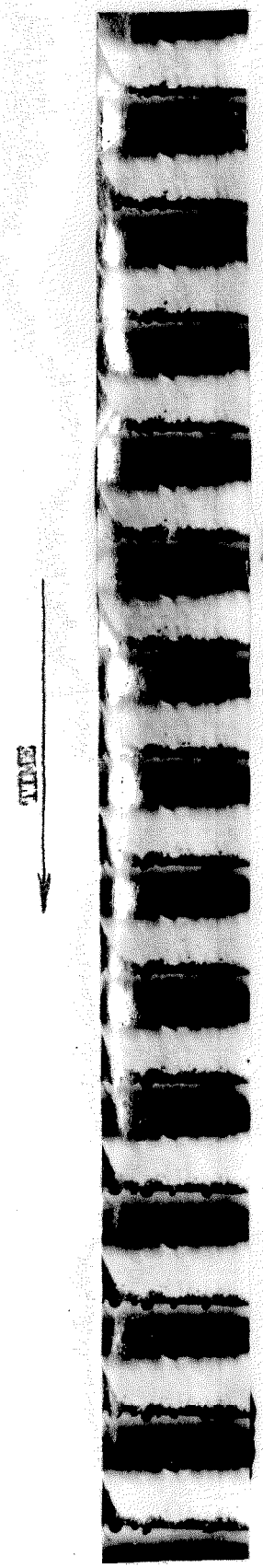

Figure 66. Shadowgraph of Nucleate Bubbles in Carbon Tetrachloride

$T_L = 140^{\circ}F$

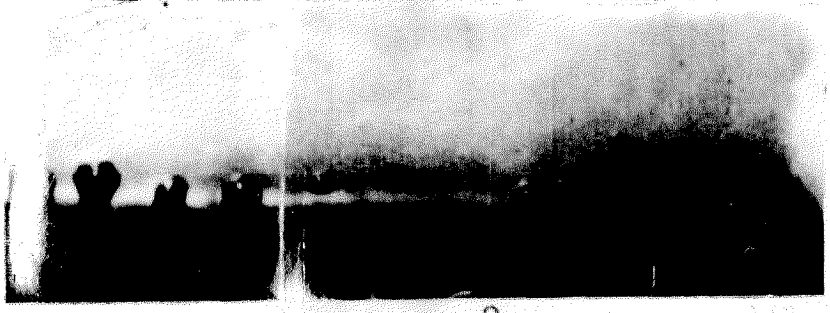

$T_L = 135^{\circ}F$

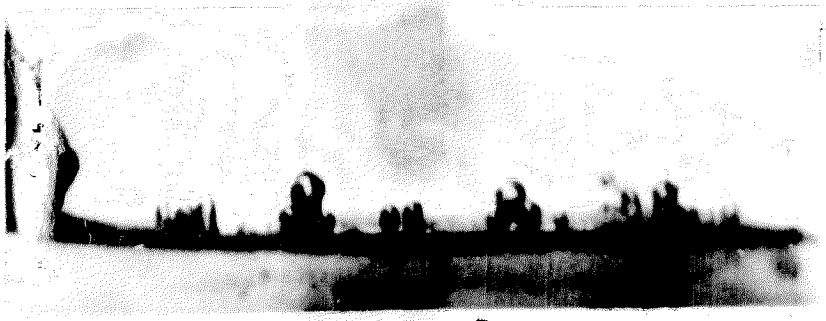

$T_L = 97^{\circ}F$

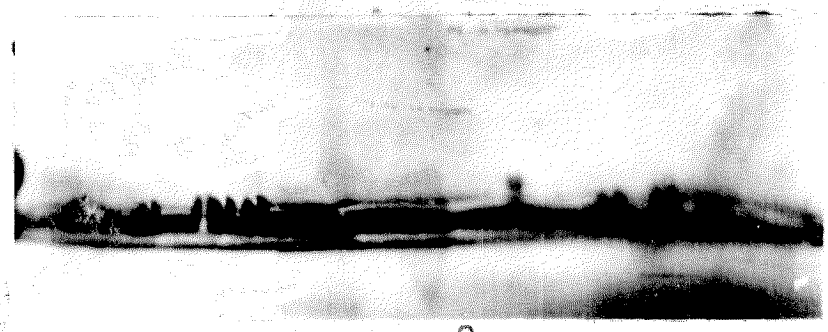

$T_L = 45^{\circ}F$

Figure 87. Photographs of Bubbles Showing Influence of Liquid Temperature for Carbon Tetrachloride

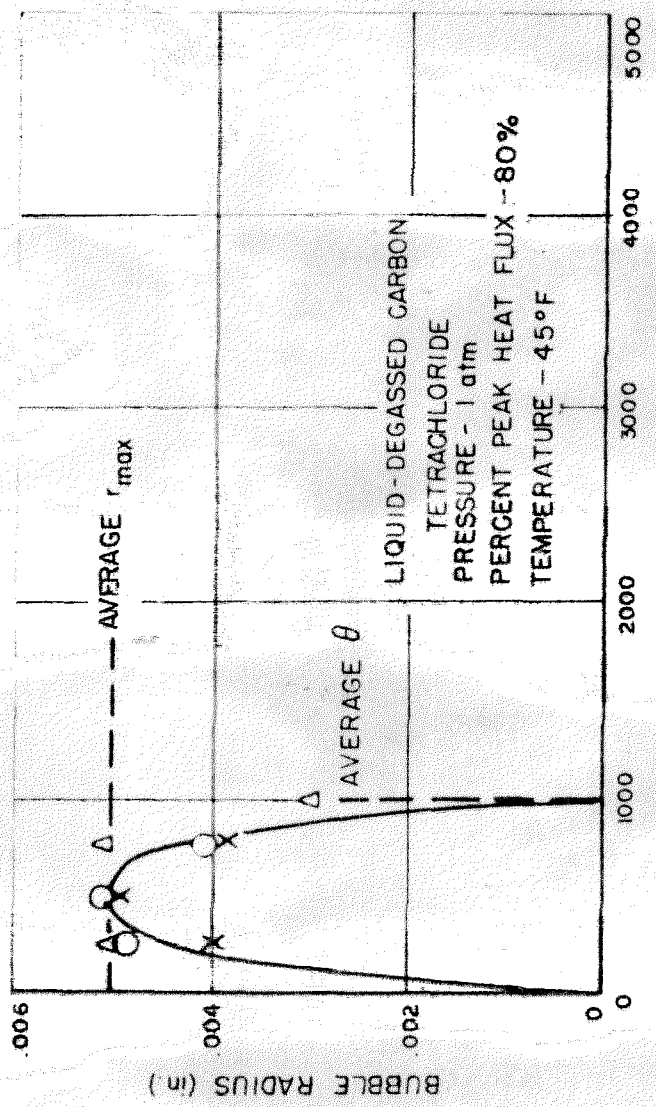

Figure 68. Bubble Radius vs Time

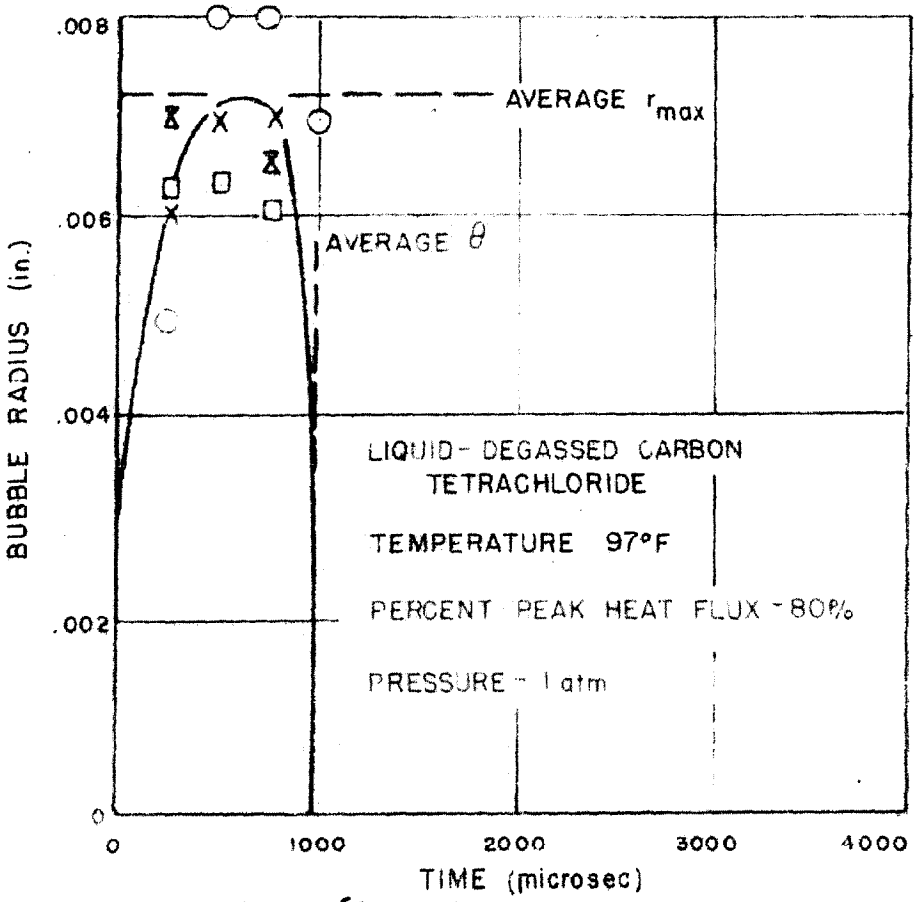

Figure 69. Bubble Radius vs Time

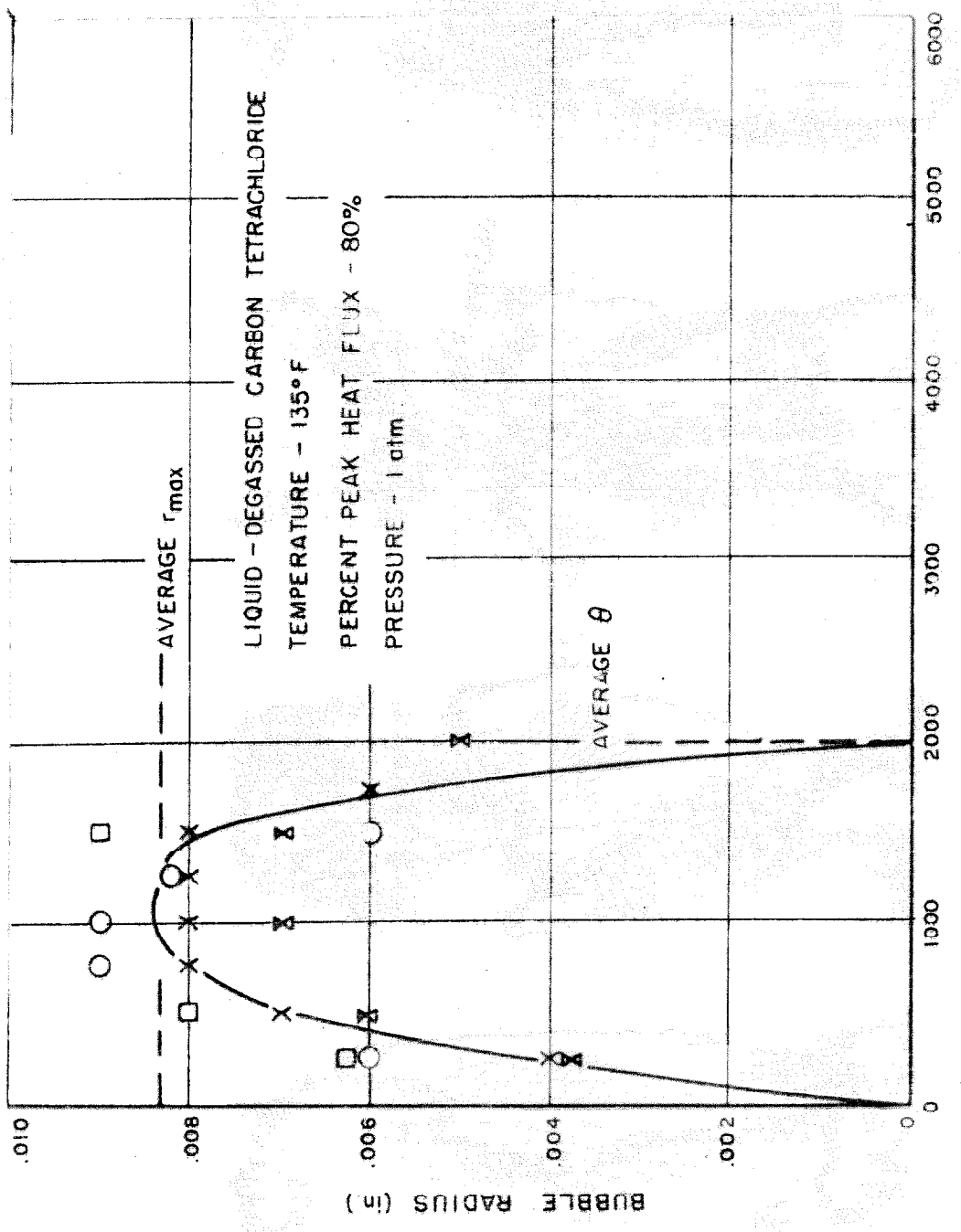

Figure 70. Bubble Radius vs Time

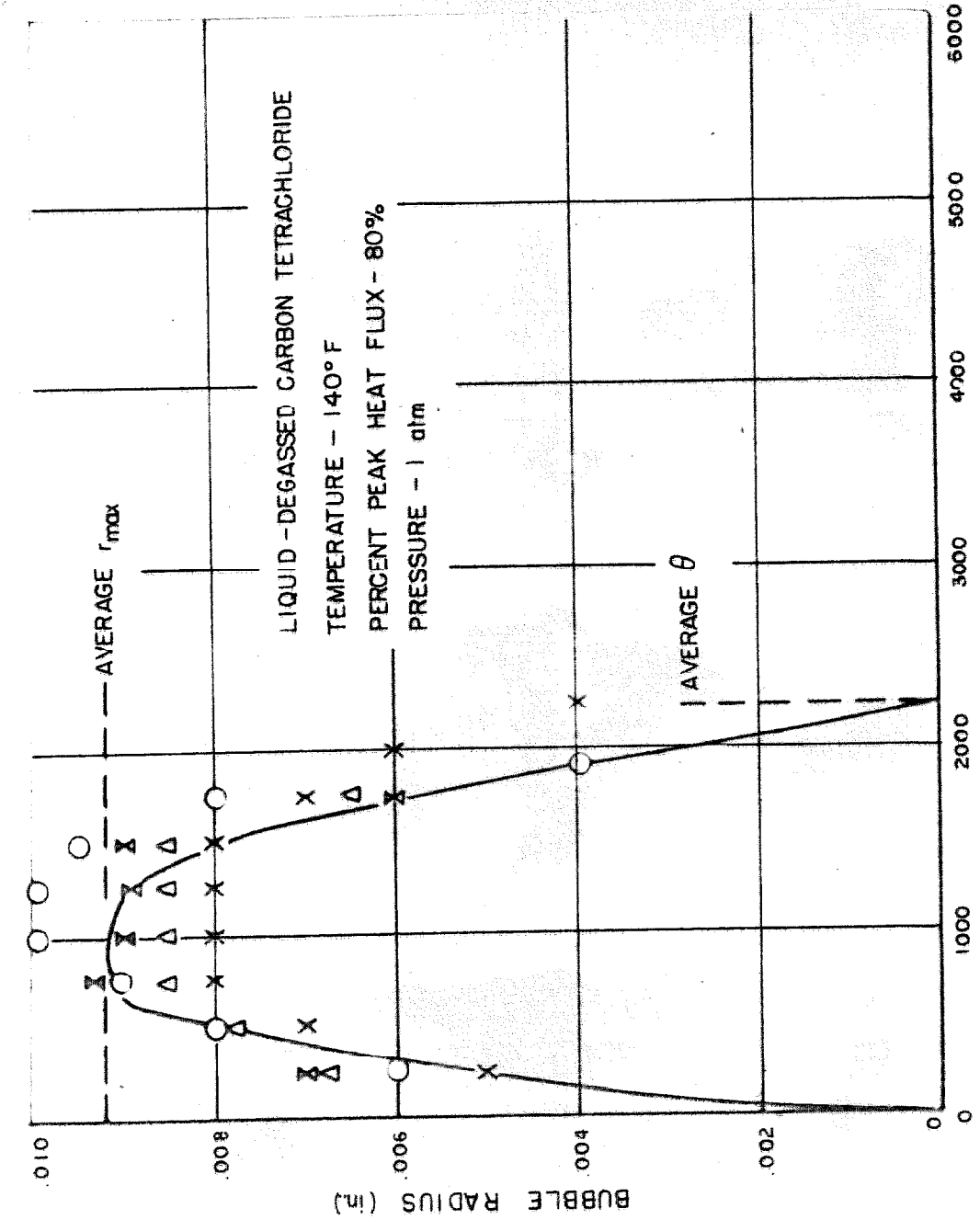

Figure 71. Bubble Radius vs Time

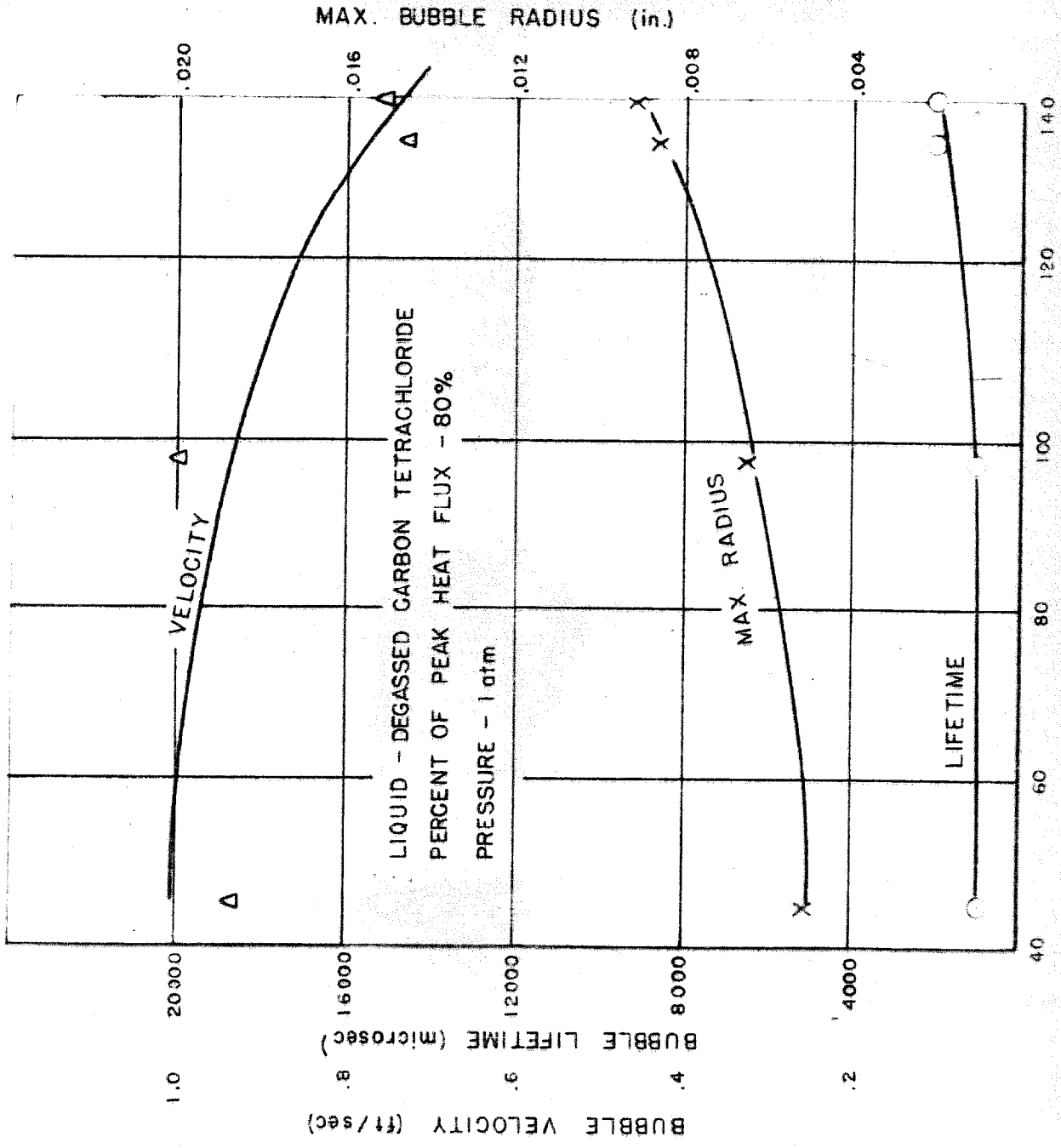

Figure 72. Effect of Liquid Temperature on Bubble Dynamics

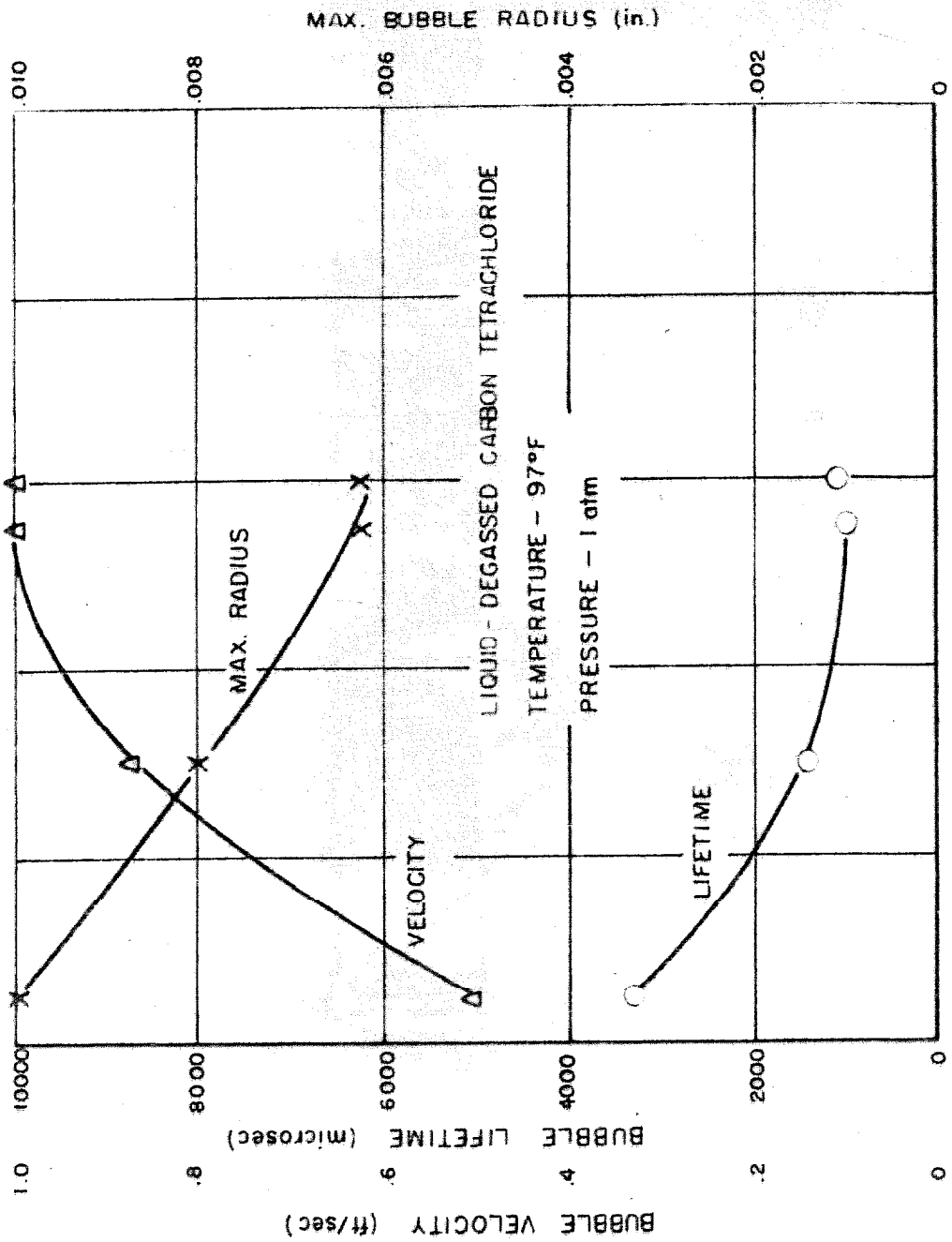

Figure 73. Effect of Heat Flux on Bubble Dynamics

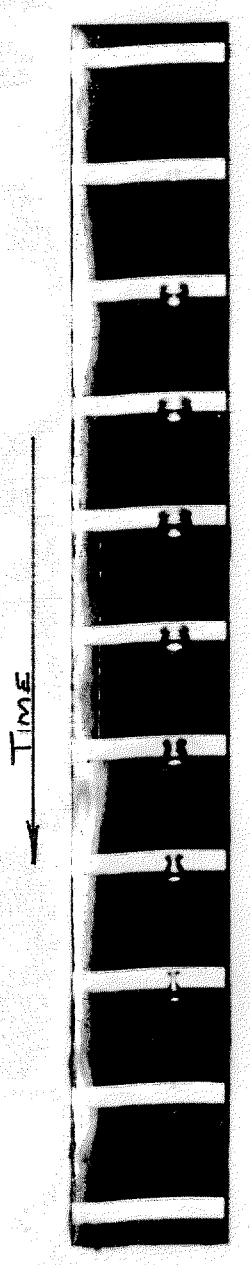

Figure 74. Photographs of Bubble Detaching from Underside of Strip in Water with Low Subcooling

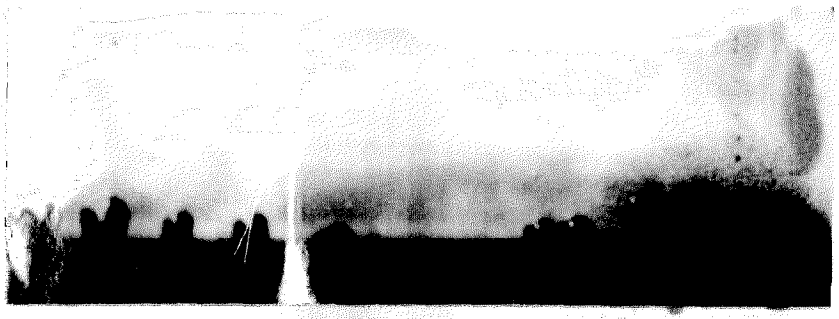

25 per cent of Peak Heat Flux

50 per cent of Peak Heat Flux

75 per cent of Peak Heat Flux

80 per cent of Peak Heat Flux

Figure 75. Photographs of Bubbles Showing Influence of Heat Flux for Carbon Tetrachloride

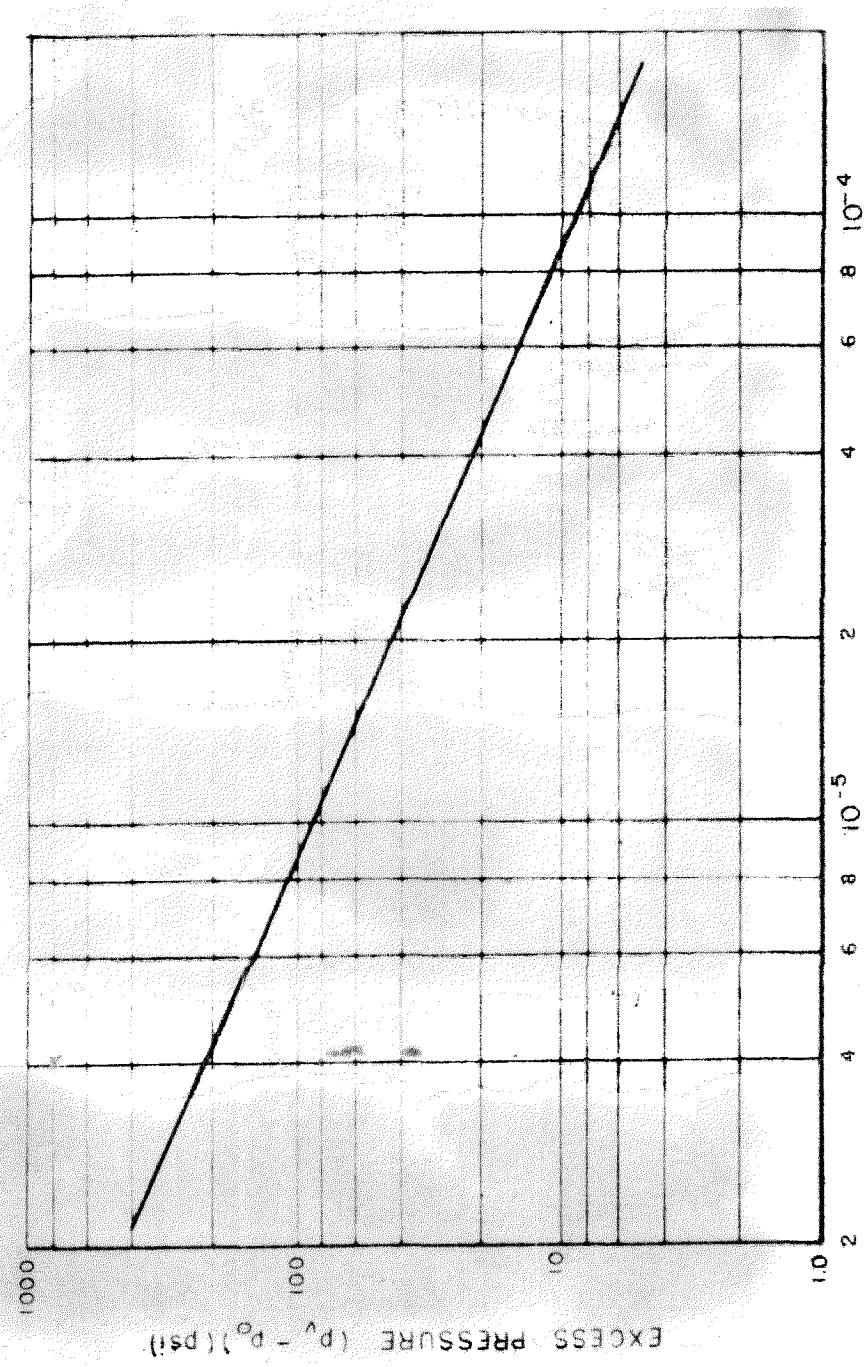

Figure 76. Excess Pressure vs Radius for Water-Vapor Nucleus

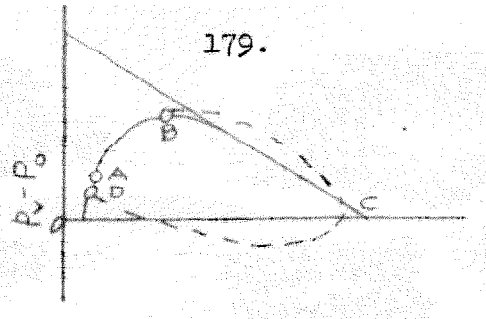

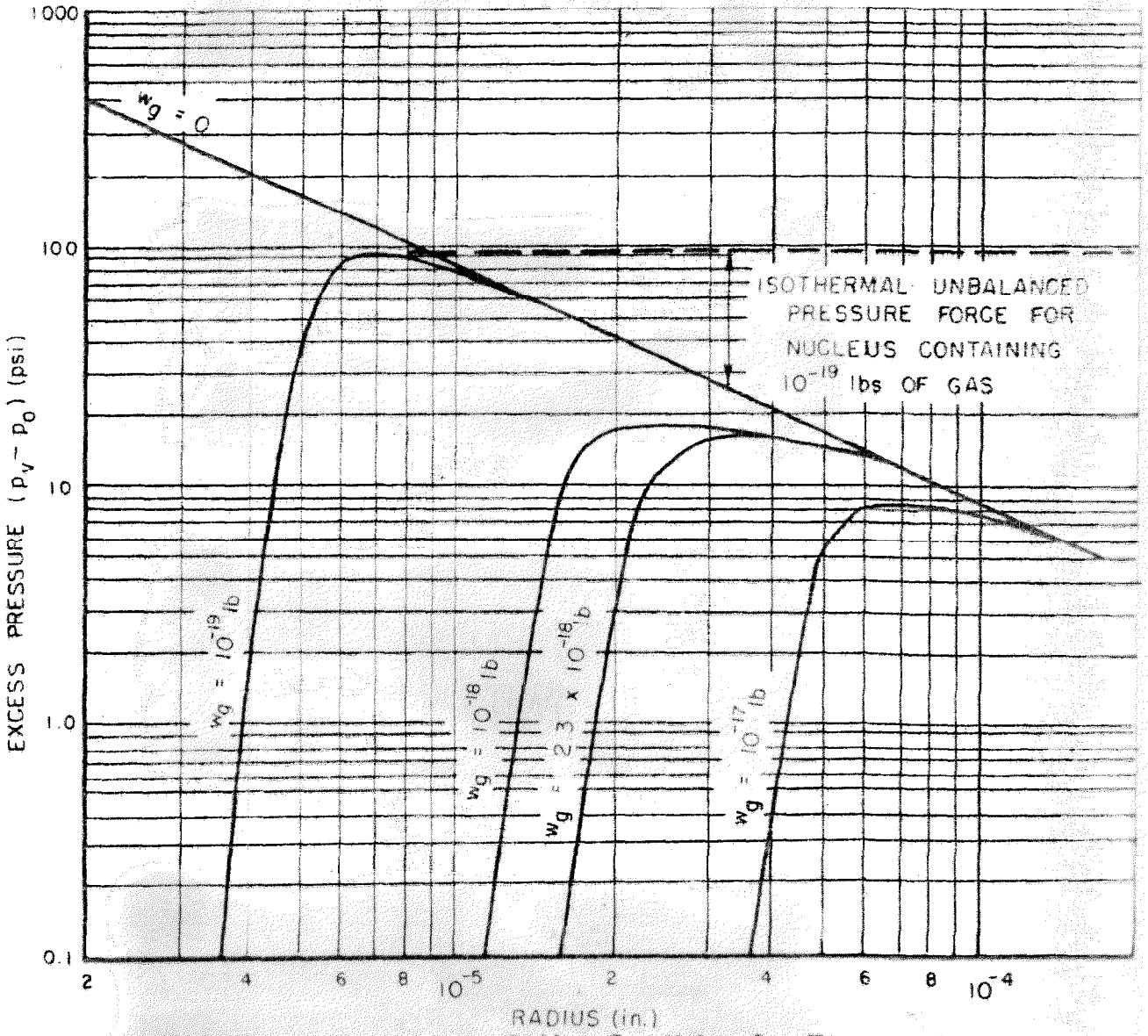

Figure 77. Excess Pressure vs Radius for Water Gas-Vapor Nucleus

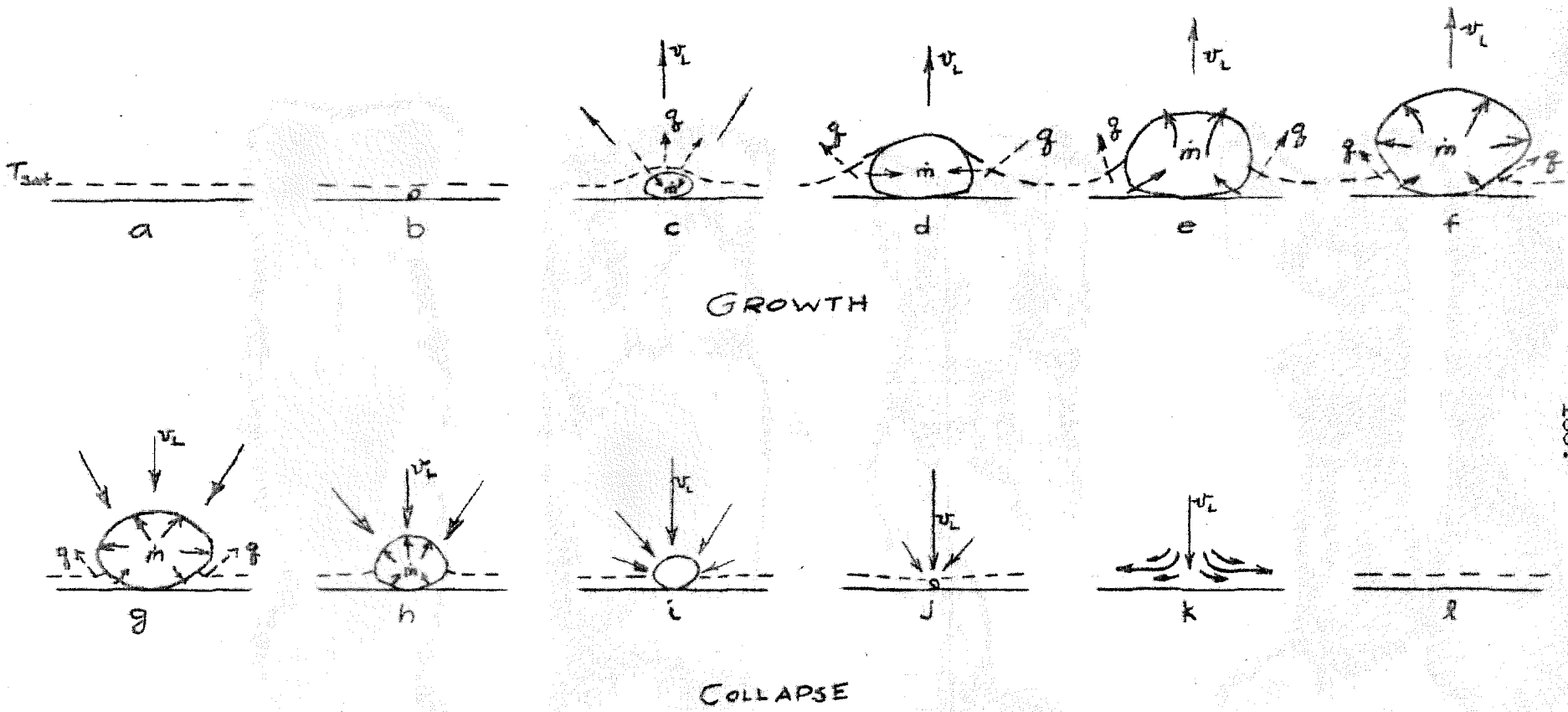

Figure 78. Sketch of Nucleate Bubble in Degassed Water

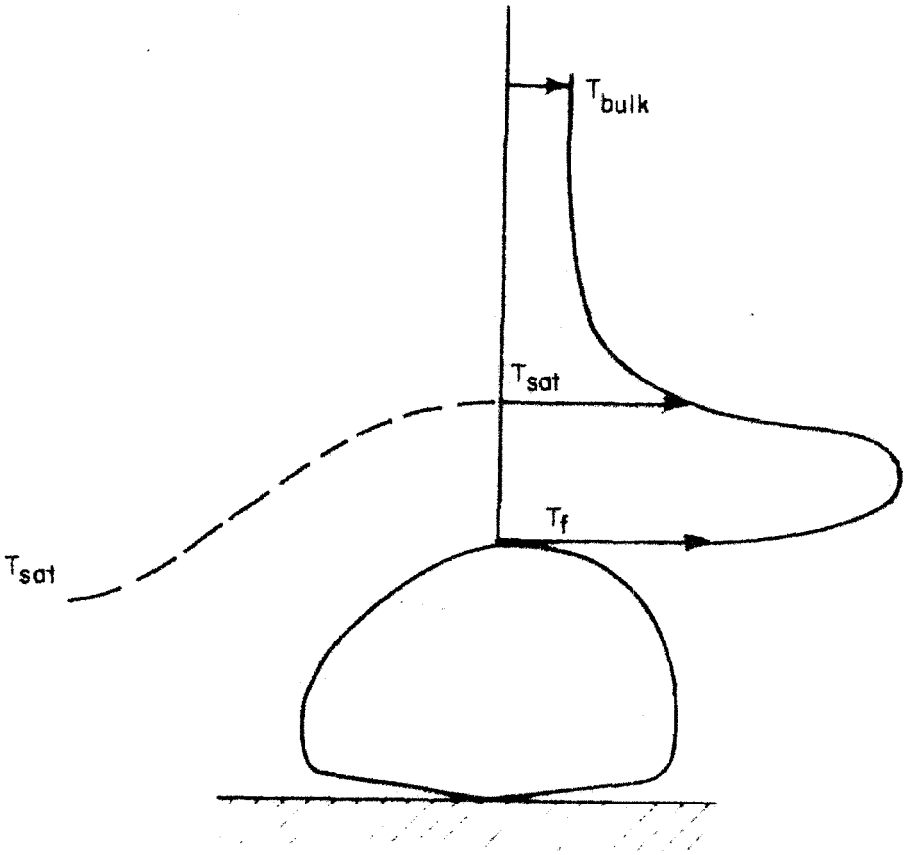

Figure 79. Temperature Profile in Bubble Film During Growth Period

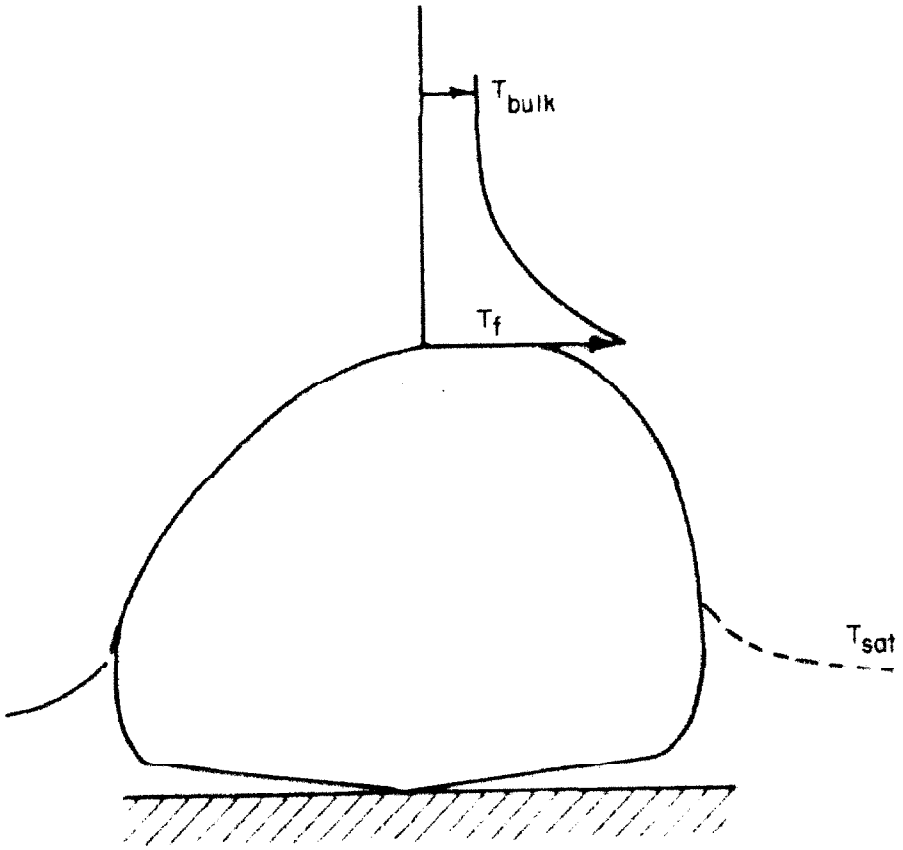

Figure 60. Temperature Profile in Bubble Film at Maximum Radius

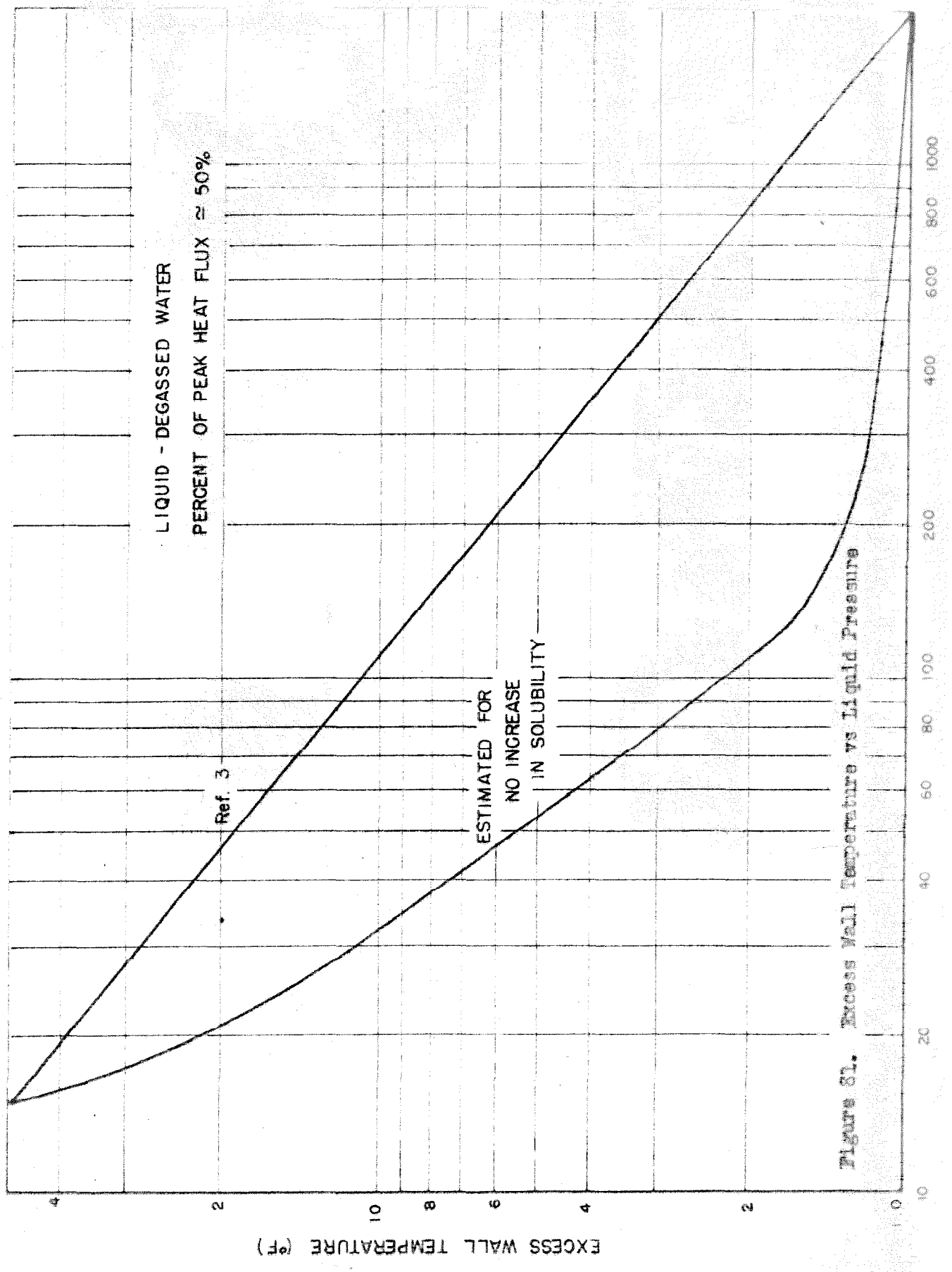

Figure 87. Excess Wall Temperature vs Liquid Pressure

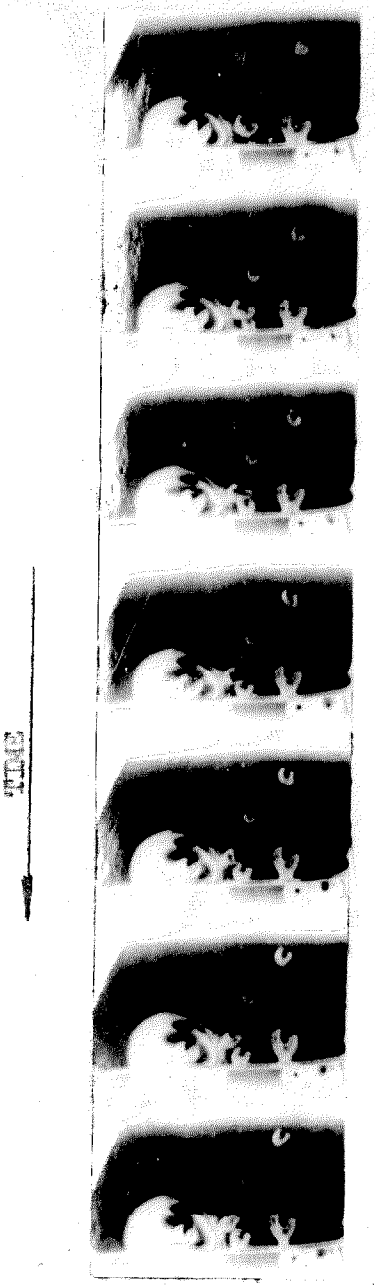

Figure 82. Photograph of Bulk Boiling in Water

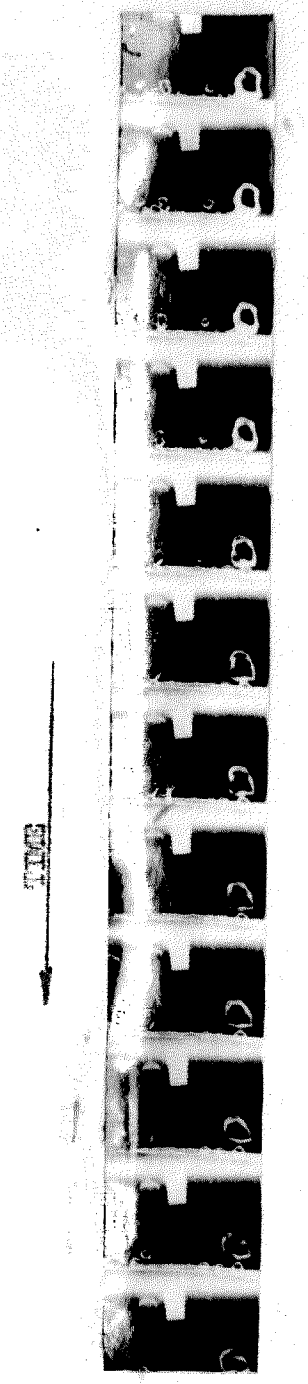

Figure 83. Photograph of Bubbles in Water with Low Subcooling (by Gunther)

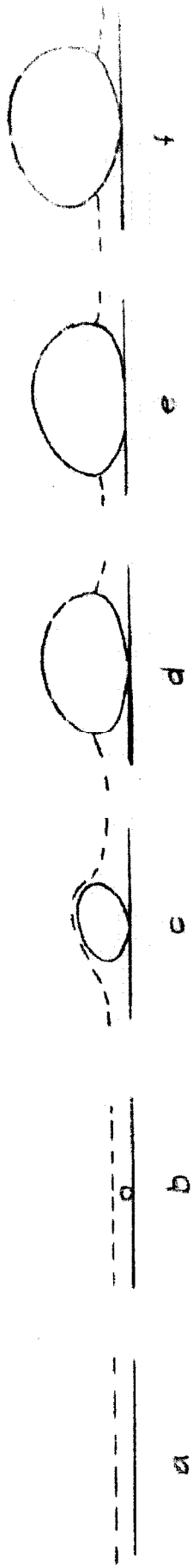

Figure 84. Sketch of Nucleate Bubble in Aerated Water

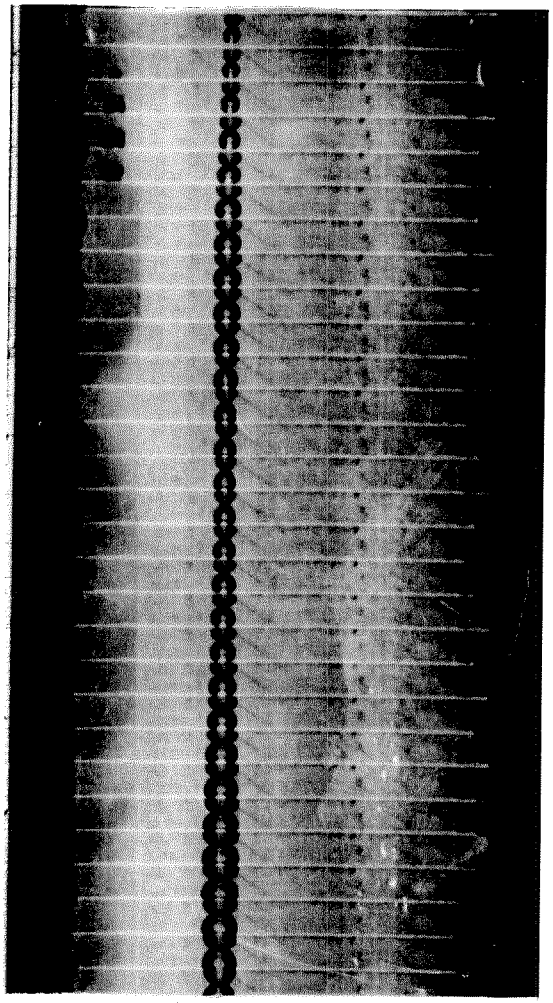

Figure 85. Photograph of Stagnant Gas-Vapor Bubble in Water

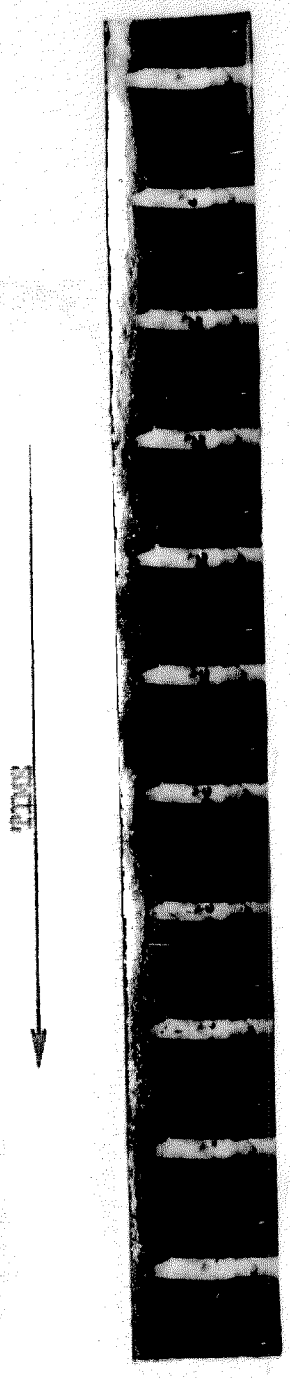

Figure 36a. Photographs of Nucleate Bubble in Degassed Carbon Tetrachloride

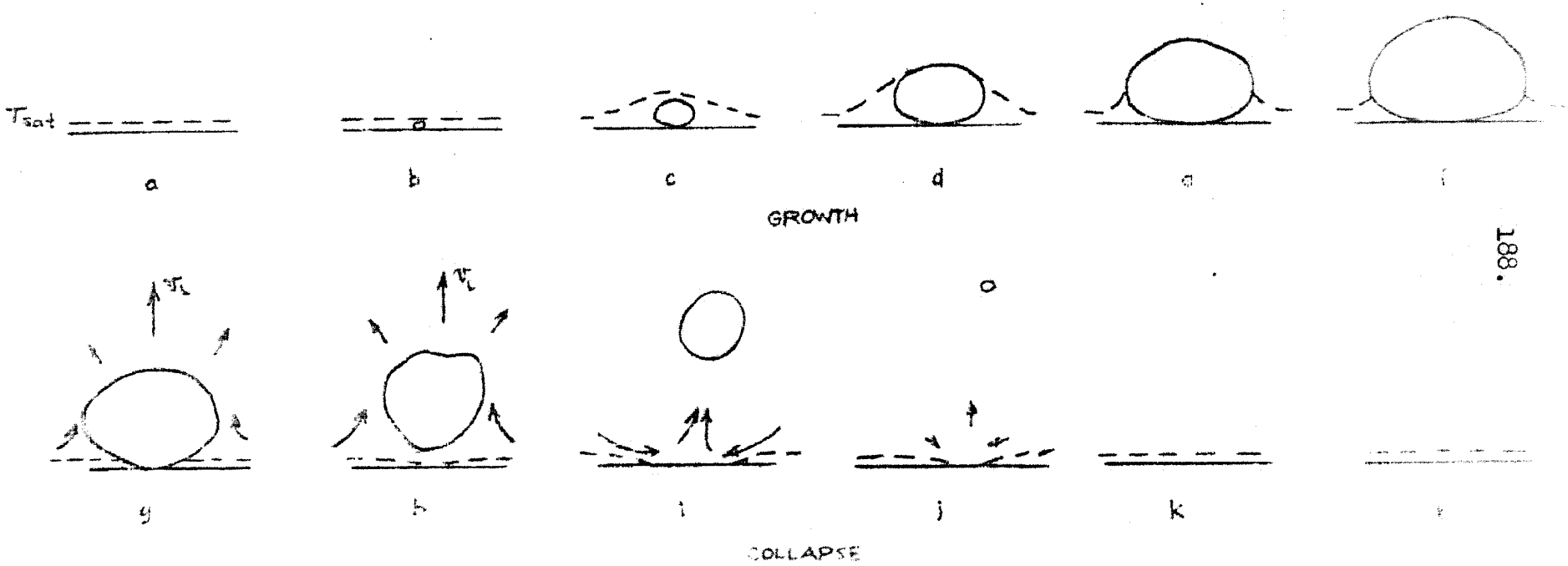

Figure 86b. Sketch of Nucleate Bubble in Degassed Carbon Tetrachloride

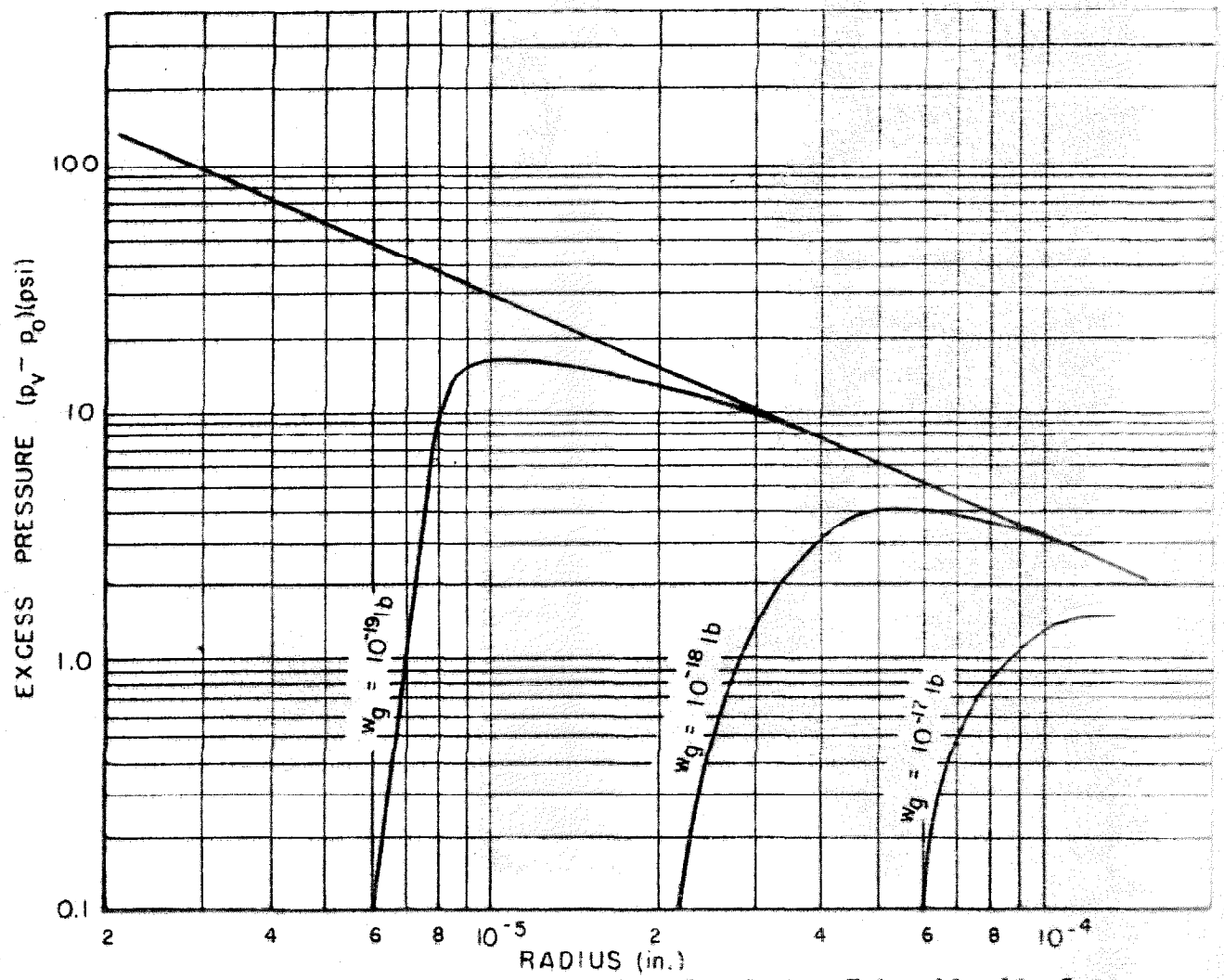

Figure 87. Excess Pressure vs Radius for Carbon Tetrachloride Gas-Vapor Nucleus

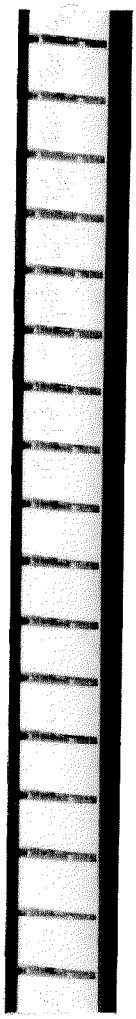

Figure 88. Photograph of Stagnant-Degassed Carbon Tetrachloride Bubble.

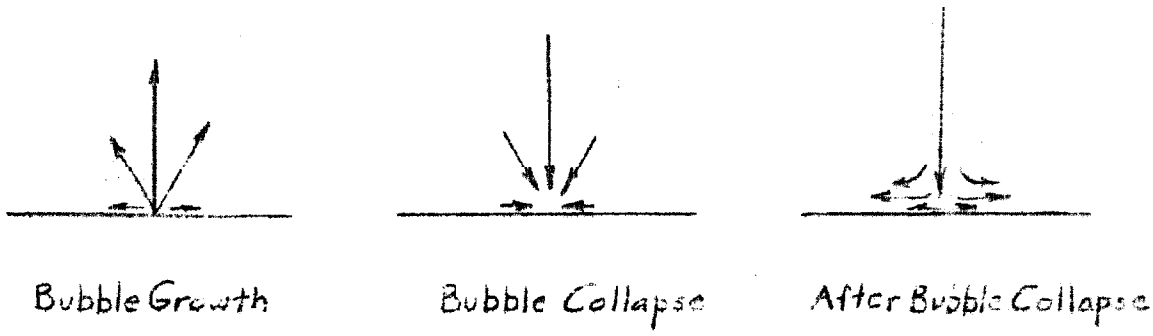

Figure 89a. Induced Liquid Velocity Pattern for Non-detaching Bubble

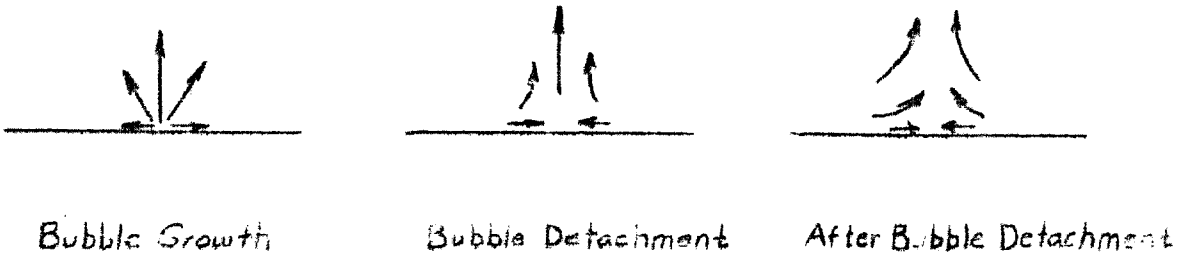

Figure 89b. Induced Liquid Velocity Pattern for Detaching Bubble

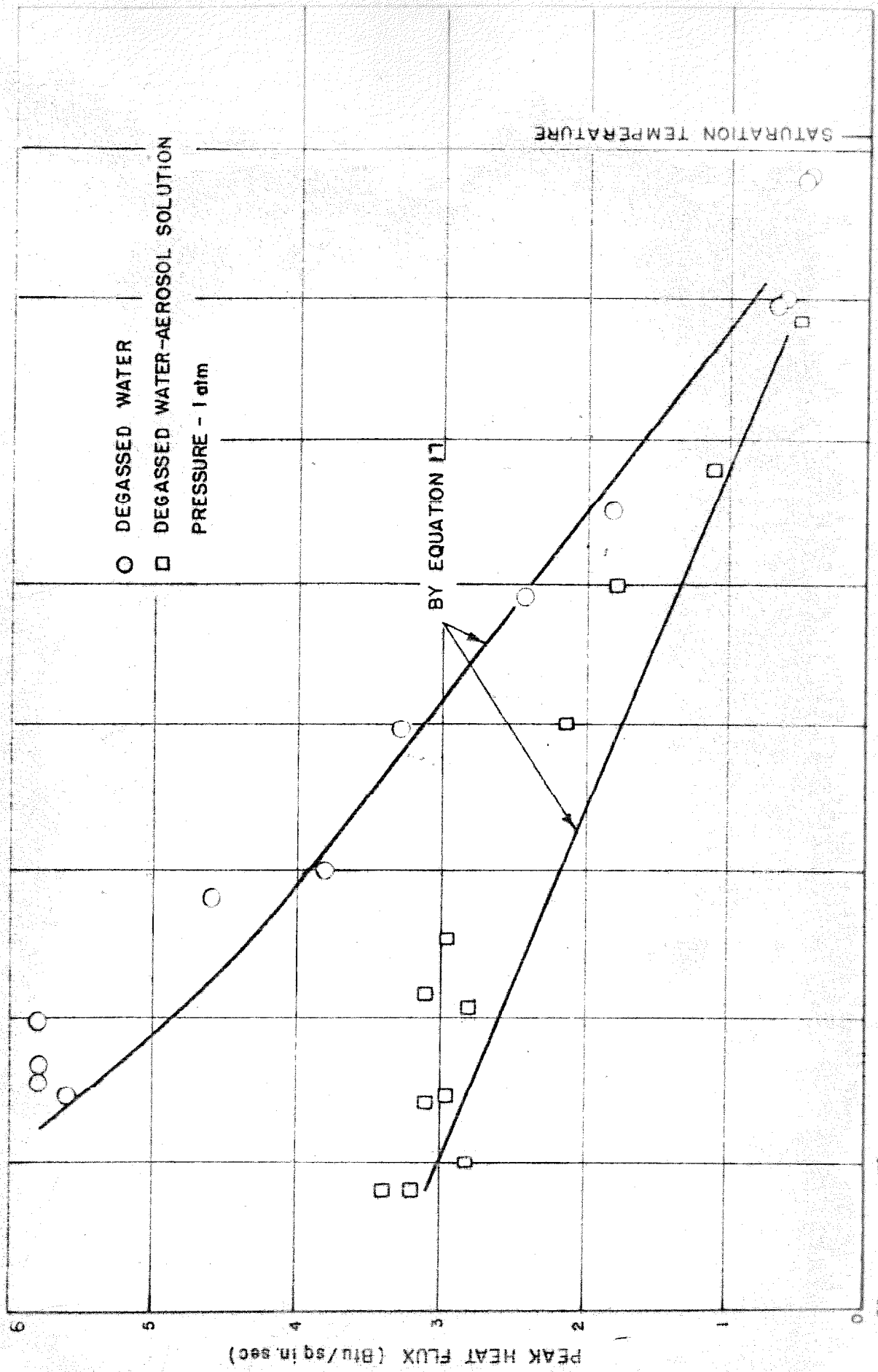

Figure 90. Comparison of Predicted Peak Heat Flux with Experimental Data

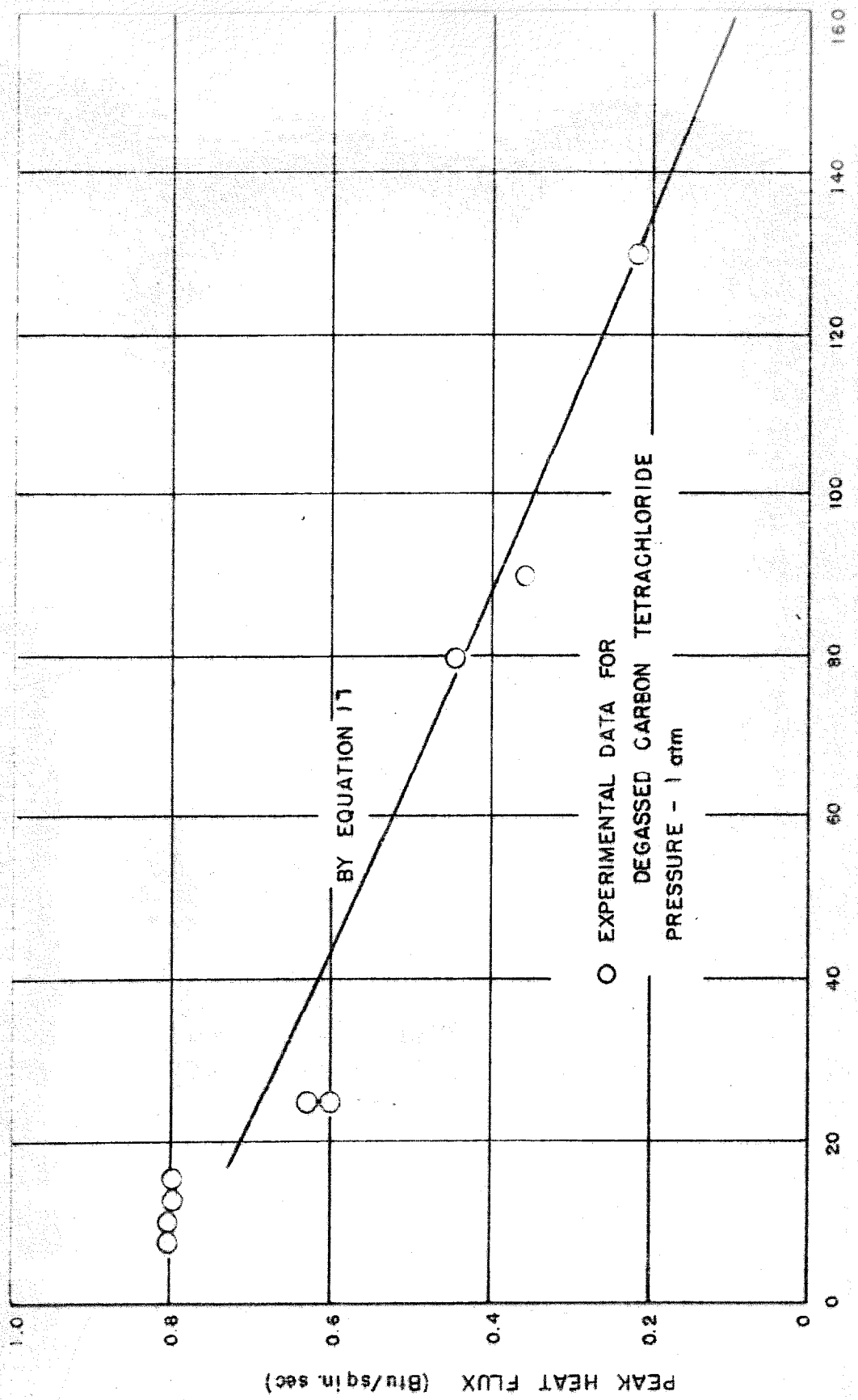

Figure 91. Comparison of Predicted Peak Heat Flux with Experimental Data

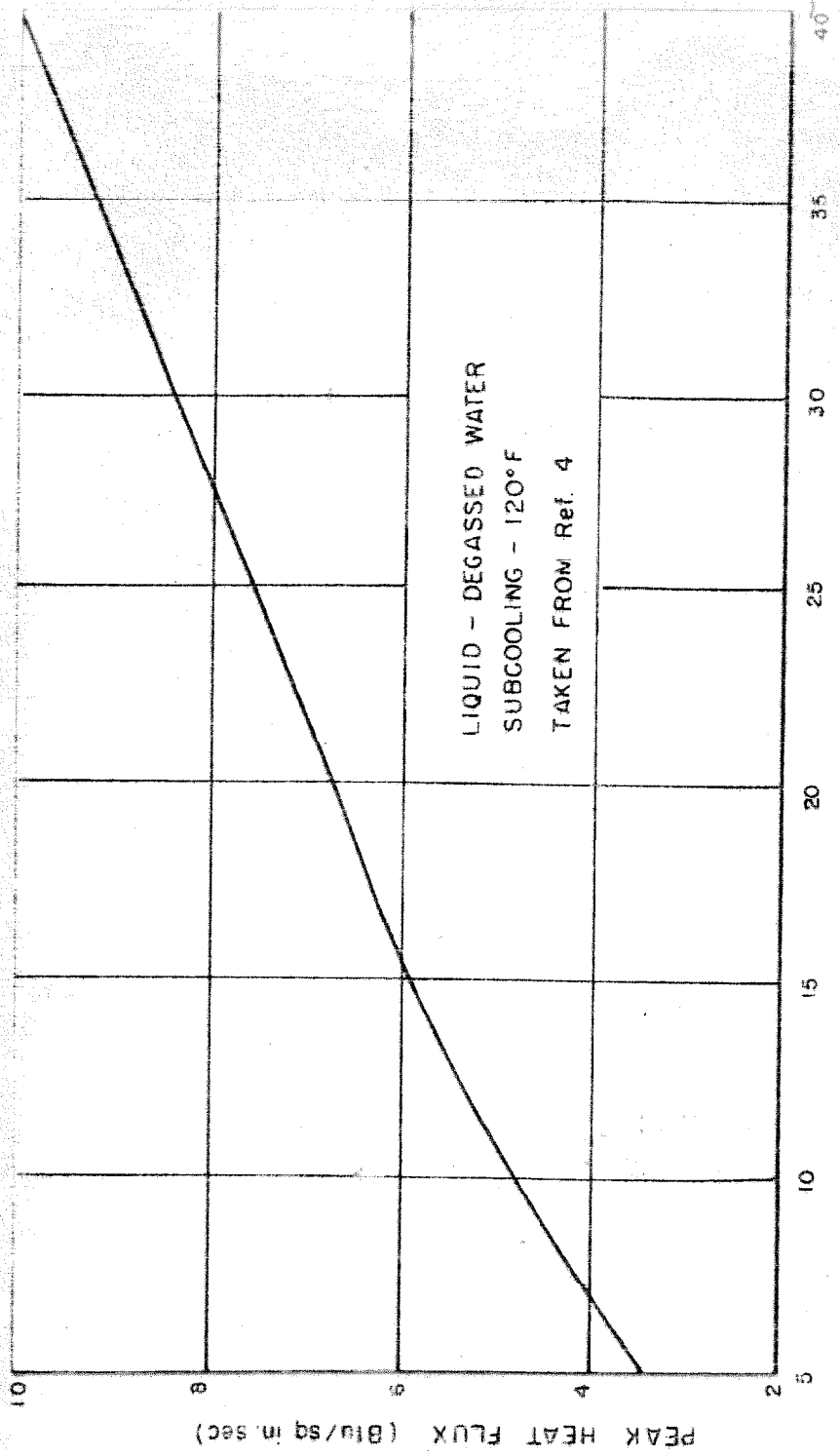

Figure 92. Effect of Free-Stream Velocity on Peak Heat Flux